77-11,453

BOUSEK, Ronald Richard, 1941-
THEORETICAL ANALYSIS FOR THE DEVELOPMENT OF
A CHARGE-EXCHANGE X-RAY LASER.

The University of Arizona, Ph.D., 1976
Physics, general

Xerox University Microfilms, Ann Arbor, Michigan 48106

THEORETICAL ANALYSIS FOR THE DEVELOPMENT OF A CHARGE-EXCHANGE X-RAY LASER

by

Ronald Richard Bousek

A Dissertation Submitted to the Faculty of the

DEPARTMENT OF PHYSICS

In Partial Fulfillment of the Requirements
For the Degree of

DOCTOR OF PHILOSOPHY

In the Graduate College

THE UNIVERSITY OF ARIZONA

1 9 7 6

THE UNIVERSITY OF ARIZONA

GRADUATE COLLEGE

I hereby recommend that this dissertation prepared under my direction by RONALD RICHARD BOUSEK entitled Theoretical Analysis for the Development of a Charge-Exchange X-Ray Laser be accepted as fulfilling the dissertation requirement of the degree of Doctor of Philosophy

Marlan O Scully 10/11/76

Dissertation Director Date

After inspection of the final copy of the dissertation, the following members of the Final Examination Committee concur in its approval and recommend its acceptance:*

Frederic A Hopf	10/11/76
Theodore Bowen	10/24/76
John D McCullen	10/24/76
Jon-Wei Nee	10/25/76

*This approval and acceptance is contingent on the candidate's adequate performance and defense of this dissertation at the final oral examination. The inclusion of this sheet bound into the library copy of the dissertation is evidence of satisfactory performance at the final examination.

STATEMENT BY AUTHOR

This dissertation has been submitted in partial fulfillment of requirements for an advanced degree at The University of Arizona and is deposited in the University Library to be made available to borrowers under rules of the Library.

Brief quotations from this dissertation are allowable without special permission, provided that accurate acknowledgment of source is made. Requests for permission for extended quotation from or reproduction of this manuscript in whole or in part may be granted by the head of the major department or the Dean of the Graduate College when in his judgment the proposed use of the material is in the interests of scholarship. In all other instances, however, permission must be obtained from the author.

SIGNED: Ronald R. Bowsel

TABLE OF CONTENTS

TABLE OF CONTENTS--Continued.

LIST OF ILLUSTRATIONS

LIST OF TABLES

ABSTRACT

Theoretical gain calculations are presented for a soft x-ray laser whose upper level is pumped by charge transfer. Six different reactions are considered. The laser scheme involves simultaneously focusing and sweeping an ion beam along a target. Because of the short rise time of the population inversion, the pumping can be described by a delta function; but, the presence of doppler broadening allows the gain to be roughly approximated by the steady-state gain formula. Planar and cylindrical ion beam focusing systems are evaluated in terms of a) ideal lens behavior, b) space charge, and c) transverse thermal velocities. The cylindrical geometry is shown to have better focusing properties against space charge. It is estimated that order-of-magnitude larger focused current densities may be obtained with the cylindrical geometry than with the planar geometry. Gains are calculated for the six reactions, and the high gain for the case of Hg^{+} + Cs suggests that this reaction could be used to experimentally test the cylindrical focusing laser scheme.

Some other pertinent results of the present calculations are: a) there is a limiting target atom density

beyond which there is a diminishing advantage to further increasing the density, b) there is an optimum ion beam current in the cylindrical geometry for each reaction, and c) since space charge can theoretically be overcome by going to short enough focal lengths, emittance is the ultimate theoretical limit.

CHAPTER 1

INTRODUCTION

The use of a charge-transfer reaction for pumping a soft x-ray laser has been proposed by Scully, Louisell, and McKnight (1973). They consider the reaction

$$He^{++} + H \longrightarrow He^{+}(2p) + H^{+}$$

in which a collimated He^{++} ion beam is swept across either a solid or gaseous hydrogen target, and an electron is preferentially transferred from an H atom to the 2p excited state of He^{+}. The excited state decays with a 10^{-10} sec mean lifetime with the emission of 304Å radiation. By sweeping the beam along the target with the velocity of light, amplification of stimulated emission can occur over the length of the target, in spite of the short radiative life-time. A further development of this scheme was presented by Louisell, Scully, and McKnight (1975).

We extend this previous work by taking into account the effects which space charge and ion thermal velocities play in limiting the focusing of the ion beam on the target. We also expand the number of potential soft x-ray charge-transfer reactions to six and calculate a gain for each reaction.

A brief outline of the dissertation is presented below.

The semiclassical laser theory of Lamb is used in Chapter 2 to develop gain expressions for the cases of a) steady state population inversion, b) step-function population inversion, and c) delta-function pumping. The treatment in the case of delta-function pumping is introductory rather than rigorous and does not discuss the many details found in the recent literature. Although the delta-function pump theory is appropriate for the type of swept-excitation pumping proposed for the charge-transfer laser, we shall use the simpler steady-state gain expression when calculating gains. This approximation is somewhat justified due to the presence of a non-negligible amount of doppler broadening (10^{10}-10^{11} sec^{-1}): The difference between the steady-state gain and the delta-function pump gain is most pronounced when the inhomogeneous broadening is negligible. In any case, the use of the simpler gain expression is valuable as a tool to find promising laser candidates, in a first approximation.

The six particular charge-transfer reactions of interest are presented in Chapter 3 along with pertinent data from the recent literature. In light of the parameters necessary to estimate gain, the steady-state gain expression is separated into convenient factors. Calculations for the population inversions and the Doppler broadening from scattering are presented. The results are assembled in the form of a gain per unit current density for the focused ion beam. In this way, a gain can be calculated for a given current density. Estimates of reasonable current densities are then the subject of investigation for the remainder of the dissertation.

Chapter 4 addresses the general problem of focusing against space charge and the thermal velocities of the ions. A method is introduced for comparing these two effects in terms of the equivalent optical focal length of the lens system. Liouville's theorem is used to show how the presence of thermal velocities leads to a fundamental theoretical limitation on the focused current density. The concepts of beam emittance and brightness are reviewed.

The parallel-plate ion-beam sweeping system proposed by Scully, Louisell, and McKnight is investigated in Chapter 5 for its focusing capability. Deviation from ideal lens behavior, space charge, and thermal velocities are taken into account. A parallel, but mathematically more complicated analysis is presented in Chapter 6 for a cylindrical focusing geometry. The cylindrical geometry is shown to have much better focusing properties than the planar geometry.

In the final chapter, the results of the preceding chapters are combined, and laser gains are calculated for each of the six charge transfer reactions. For two of the reactions, $Ne^+ + K$ and $Hg^+ + Cs$, the calculated gains are large enough to suggest that these two reactions could be used to experimentally test the feasibility of swept excitation in the cylindrical geometry.

We do not discuss the problem of a practical ion source except to note here that the duoplasmatron promises to be a good candidate, since it is characterized by a high beam brightness and is an excellent source of inert gases at high current densities (Wilson and Brewer, 1973, p. 404). Tabulations of duoplasmatron beam characteristics have been made by Wilson and Brewer (1973, p. 100), and Van Steenbergen (1965). Space charge neutralization to prevent beam expansion prior to focusing should be achievable (Brewer, 1970, p. 93).

CHAPTER 2

DEVELOPMENT OF GAIN FORMULAS

In this chapter we use semiclassical laser theory to calculate expressions for linear gains for three types of time-dependent population inversions: 1) steady-state population inversion, 2) step-function population inversion, and 3) delta-function pumping. The basic development of the electric field equations follows that in the text by Sargent, Scully, and Lamb (1974, Chapter 8). The treatment of step-function population inversion is an extention of the steady-state case. The treatment of delta-function pumping is similar to that of Louisell, Scully, and McKnight (1975) and Seely (1974).

The case of delta-function pumping is of primary interest in the swept-excitation charge-transfer laser and has received detailed attention in several recent papers. (Hopf, Meystre, Scully, and Seely, 1975; Hopf and Meystre, 1975; Bonifacio, Hopf, Meystre, and Scully, 1975; Hopf, Meystre, and McLaughlin, 1976). The physical conditions for delta-function pumping arise as follows: In the proposed laser scheme an ion beam is deflected dynamically so that the intersection of the beam with a target moves with the velocity of light. As the deflected ions travel into the target and capture electrons, a population inversion will build up which will be followed in time by a rise in the macroscopic polarization. If the population rise time is much shorter than the rise time of the polarization, then the pumping rate can be described with a delta function.

Our presentation of delta-function pumping is very simplified, hence incomplete, and is meant to serve only as an introduction to the more detailed theory. In fact, in the following chapters we shall not use the results of the delta-function pump theory to calculate gains. We shall use the simpler steady-state gain expression, since our primary purpose is to examine the problem of ion beam focusing. The relationship between the conventional steady-state gain and the gain in the case of delta-function pumping is examined in the paper by Hopf and Meystre (1975) where the use of the steady state gain expression is shown to lead to an over-estimate of the gain.

Equation of Motion for the Electric Field

The electromagnetic field is described by Maxwell's equations

(MKS units)

$$\nabla \times \vec{E} = -\frac{\partial \vec{B}}{\partial t} \tag{1a}$$

$$\nabla \times \vec{H} = \vec{J} + \frac{\partial \vec{D}}{\partial t} \tag{1b}$$

$$\nabla \cdot \vec{D} = 0 \tag{1c}$$

$$\nabla \cdot \vec{B} = 0 \tag{1d}$$

and by the constitutive relations

$$\vec{D} = \epsilon_0 \vec{E} + \vec{P} \tag{2a}$$

$$\vec{B} = \mu_0 \vec{H} \tag{2b}$$

$$\vec{J} = \sigma \vec{E} \tag{2c}$$

Starting with the curl of (1a) we develop the equation for the electric field:

$$\begin{aligned}
\nabla \times \nabla \times \vec{E} &= -\frac{\partial}{\partial t}\left(\nabla \times \vec{B}\right) \\
&= -\mu_0 \frac{\partial}{\partial t}\left(\nabla \times \vec{H}\right) \\
&= -\mu_0 \frac{\partial}{\partial t}\left(\vec{J} + \frac{\partial \vec{D}}{\partial t}\right) \\
&= -\mu_0 \sigma \frac{\partial \vec{E}}{\partial t} - \mu_0 \frac{\partial^2}{\partial t^2}\left(\epsilon_0 \vec{E} + \vec{P}\right)
\end{aligned}$$

Then $$\nabla \times \nabla \times \vec{E} + \mu_0 \sigma \frac{\partial \vec{E}}{\partial t} + \mu_0 \epsilon_0 \frac{\partial^2 \vec{E}}{\partial t^2} = -\mu_0 \frac{\partial^2 \vec{P}}{\partial t^2} \tag{3}$$

To simplify (3) we use

$$\begin{aligned}\nabla\times\nabla\times\vec{E} &= -\nabla^2\vec{E}+\nabla(\nabla\cdot\vec{E})\\ &= -\nabla^2\vec{E}+\frac{1}{\epsilon_0}\nabla(\nabla\cdot\vec{D}-\nabla\cdot\vec{P})\\ &= -\nabla^2\vec{E}\end{aligned} \tag{4}$$

where $\nabla\cdot D=0$ from Maxwell's equation, and $\nabla\cdot P$ is assumed to be negligible. The equation describing the electric field now becomes

$$\nabla^2\vec{E}-\mu_0\sigma\frac{\partial\vec{E}}{\partial t}-\mu_0\epsilon_0\frac{\partial^2\vec{E}}{\partial t^2}=\mu_0\frac{\partial^2 P}{\partial t^2} \tag{5}$$

For a plane-polarized field propagating in the z-direction,

$$\frac{\partial^2 E}{\partial z^2}-\mu_0\sigma\frac{\partial E}{\partial t}-\frac{1}{c^2}\frac{\partial^2 E}{\partial t^2}=\mu_0\frac{\partial^2 P}{\partial t^2} \tag{6}$$

We look for a real ("zero-phase") solution of the form

$$\begin{aligned}E(z,t) &= \mathcal{E}(z,t)\cos\theta\\ P(z,t) &= S(z,t)\sin\theta\end{aligned} \tag{7}$$

where

$$\begin{aligned}\theta &= kz-\nu t\\ &= \nu\left(\frac{z}{c}-t\right)\end{aligned} \tag{8}$$

We make the usual slowly varying amplitude and phase approximation in which

$$\begin{aligned}&\frac{\partial\mathcal{E}}{\partial z}\ll k\mathcal{E} &\qquad &\frac{\partial S}{\partial z}\ll kS\\ &\frac{\partial\mathcal{E}}{\partial t}\ll \nu\mathcal{E} &\qquad &\frac{\partial S}{\partial t}\ll \nu S\end{aligned} \tag{9}$$

Then (6) reduces to

$$\frac{\partial \mathcal{E}}{\partial z} + \frac{1}{c}\frac{\partial \mathcal{E}}{\partial t} + K\mathcal{E} = \frac{\nu}{2\epsilon_0 c} S(z,t) \tag{10}$$

where K denotes the loss per unit length.

Equation (10) describes how the electric field is driven by the polarization. We now use the population matrix of the atoms in the amplifying medium to develop an expression for the polarization of the medium.

We consider a two-level atom with upper level a and lower level b. The population matrix obeys the equations of motion,

$$\frac{\partial \rho_{aa}}{\partial t} = \lambda_a - \gamma_a \rho_{aa} - \frac{i}{\hbar}\wp E(\rho_{ab} - \rho_{ba}) \tag{11}$$

$$\frac{\partial \rho_{bb}}{\partial t} = \lambda_b - \gamma_b \rho_{bb} + \frac{i}{\hbar}\wp E(\rho_{ab} - \rho_{ba}) \tag{12}$$

$$\frac{\partial \rho_{ab}}{\partial t} = -(i\omega + \Gamma)\rho_{ab} - \frac{i}{\hbar}\wp E(\rho_{aa} - \rho_{bb}) \tag{13}$$

$$\rho_{ba} = \rho_{ab}^* \tag{14}$$

(For example see Sargent, Scully and Lamb, 1974, Chap. 8.) λ_a and λ_b are the pumping rates into levels a and b, γ_a and γ_b are the decay rates of the two levels, and is the dipole matrix element between the two levels. For example, for light polarized in the x-direction, $\wp = e|\langle a|x|b\rangle|$. The energy separation between the states is given by $\hbar\omega$, and $\Gamma = \frac{1}{2}(\gamma_a + \gamma_b) + \gamma_{ph}$, where γ_{ph} is the decay rate due to elastic collisions.

The macroscopic polarization is given by

$$P(z,t) = N\wp \int_{-\infty}^{\infty} d\omega\, \sigma(\omega) \left[\rho_{ab} + \rho_{ba} \right] \tag{15}$$

where N is the number of atoms per unit volume, and $\sigma(\omega)$ is the atomic distribution. For Doppler broadening we assume the Gaussian form

$$\sigma(\omega) = \frac{2}{\Delta\omega_D} \left(\frac{\ln 2}{\pi} \right)^{1/2} e^{-\frac{4 \ln 2 (\omega-\nu)^2}{(\Delta\omega_D)^2}} \tag{16}$$

where $\Delta\omega_D$ is the full Doppler linewidth at half maximum.

We integrate (13) to obtain

$$\begin{aligned} \rho_{ab} &= \frac{-i\wp}{\hbar} \int_{-\infty}^{t} dt' E \left(\rho_{aa} - \rho_{bb} \right) e^{-(i\omega - \Gamma)(t-t')} \\ &= \frac{-i\wp}{\hbar} \int_{-\infty}^{t} dt' \mathcal{E}(z,t') \left(\rho_{aa} - \rho_{bb} \right) \\ &\qquad \times \cos(kz - \nu t') e^{-(i\omega - \Gamma)(t-t')} \end{aligned} \tag{17}$$

which, under the rotating wave approximation, becomes

$$\begin{aligned} \rho_{ab}(t) = \frac{-i\wp}{2\hbar} e^{i\theta} \int_{-\infty}^{t} dt' \mathcal{E}(t') \left[\rho_{aa}(t') - \rho_{bb}(t') \right] \\ \times e^{-[i(\omega-\nu) + \Gamma](t-t')} \end{aligned} \tag{18}$$

The substitution of (18) and its conjugate into (15) gives

$$\begin{aligned} P(z,t) = \frac{N\wp^2}{\hbar} \int_{-\infty}^{\infty} d\omega\, \sigma(\omega) \int_{-\infty}^{t} dt' e^{-\Gamma(t-t')} \mathcal{E}(t') \\ \times \left[\rho_{aa}(t') - \rho_{bb}(t') \right] \left[\sin\theta \cdot \cos(\omega-\nu)(t-t') \right. \\ \left. - \cos\theta \cdot \sin(\omega-\nu)(t-t') \right] \end{aligned} \tag{19}$$

Now σ, ρ_{aa}, and ρ_{bb} are even functions of $(\omega-\nu)$, while $\sin(\omega-\nu)(t-t')$ is odd, so the last integral vanishes. Comparison of (19) and (7) shows that

$$S(z,t) = \frac{N\wp}{\hbar}\int_{-\infty}^{\infty} d\omega\, \sigma(\omega) \int_{-\infty}^{t} dt'\, e^{-\Gamma(t-t')}\, \mathcal{E}(t') \times \left[\rho_{aa}(t') - \rho_{bb}(t')\right] \cos(\omega-\nu)(t-t') \tag{20}$$

Equation (20) is the expression we want to use as the driving term in the equation of motion for the electric field (10). This gives

$$\frac{\partial \mathcal{E}}{\partial z} + \frac{1}{c}\frac{\partial \mathcal{E}}{\partial t} + K\mathcal{E} = \frac{N\nu\wp^2}{2\epsilon_0 c\hbar}\int_{-\infty}^{\infty} d\omega\, \sigma(\omega)\int_{-\infty}^{t} dt'\, e^{-\Gamma(t-t')} \times \mathcal{E}(t')\left[\rho_{aa}(t') - \rho_{bb}(t')\right] \times \cos(\omega-\nu)(t-t') \tag{21}$$

We next make the following simplifying assumptions: a) The medium is lossless, K=0. b) The population densities, ρ_{aa} and ρ_{bb}, do not depend upon ω, so the integral over ω can be evaluated. c) The electric field envelope varies slowly enough so that $\mathcal{E}$ can be taken outside of the time integration. We shall comment on this last assumption at the conclusion of this chapter.

Under the above assumptions, (21) becomes

$$\frac{\partial \mathcal{E}}{\partial z} + \frac{1}{c}\frac{\partial \mathcal{E}}{\partial t} = \frac{1}{2}\mathcal{R}\,\mathcal{E}(t)\int_{-\infty}^{t} dt'\, e^{-\alpha^2(t-t')^2 - \Gamma(t-t')} \times \left[\rho_{aa}(t') - \rho_{bb}(t')\right] \tag{22}$$

with

$$\mathcal{R} \equiv \frac{N\nu\wp^2}{\epsilon_0 c \hbar} \tag{23}$$

$$\alpha \equiv \frac{\Delta\omega_D}{4\sqrt{\ln 2}} \tag{24}$$

Consider a traveling wave whose intensity $\mathcal{E}^2$ grows exponentially with distance traveled, i.e.,

$$\mathcal{E}^2 = \mathcal{E}_0^2\, e^{gz} \tag{25}$$

where g is the linear gain. From (25)

$$\frac{d}{dz}\mathcal{E}^2 = g\,\mathcal{E}^2 \tag{26}$$

or

$$\frac{d\mathcal{E}}{dz} = \frac{1}{2} g\,\mathcal{E} \tag{27}$$

Since

$$\frac{d\mathcal{E}}{dz} = \frac{\partial \mathcal{E}}{\partial z} + \frac{1}{c}\frac{\partial \mathcal{E}}{\partial t}$$

we can compare (27) with (22) to see that the linear gain is given by

$$g = \mathcal{R}\, I(z,t) \tag{28}$$

where

$$I(z,t) \equiv \int_{-\infty}^{t} dt' e^{-\alpha^2(t-t')^2 - \Gamma(t-t')}$$
$$\times \left[\rho_{aa}(z,t') - \rho_{bb}(z,t') \right] \tag{29}$$

Calculating the gain via (28) involves evaluating the integral (29). In the next sections we calculate the gain for three different cases: 1) constant population inversion, 2) step-function inversion, and 3) delta-function pumping.

Constant Population Inversion

We shall assume that the fractional population difference is maintained at a constant value ΔF, i.e.,

$$\rho_{aa} - \rho_{bb} = \Delta F \tag{30}$$

We put (30) into (29) to obtain

$$I = \Delta F \int_{-\infty}^{t} dt' e^{-\alpha^2(t-t')^2 - \Gamma(t-t')} \tag{31}$$

We complete the square in the exponent to obtain

$$I = \Delta F e^{\beta^2} \int_{-\infty}^{t} dt' e^{-[\alpha(t-t')+\beta]^2} \tag{32}$$

where

$$\beta \equiv \frac{\Gamma}{2\alpha} \tag{33}$$

With the substitution, $\tau \equiv t-t'$ (32) becomes

$$I = \Delta F e^{\beta^2} \int_0^\infty d\tau \, e^{-(\alpha\tau+\beta)^2} \tag{34}$$

Finally we define a new variable, $x \equiv \alpha\tau + \beta$, so that

$$I = \frac{\Delta F e^{\beta^2}}{\alpha} \int_\beta^\infty dx \, e^{-x^2} \tag{35}$$

$$= \frac{\sqrt{\pi}\,\Delta F e^{\beta^2}}{2\alpha} (1 - \mathrm{erf}\,\beta) \tag{36}$$

The error function is defined by

$$\mathrm{erf}\,\beta = \frac{2}{\sqrt{\pi}} \int_0^\beta dx \, e^{-x^2} \tag{37}$$

The use of (36) in (28) gives the linear gain,

$$g = \frac{\sqrt{\pi}\,\mathcal{R}\,\Delta F}{2\alpha} e^{\beta^2} (1 - \mathrm{erf}\,\beta) \tag{38}$$

We note that for $\beta \ll 1$ (Doppler limit)

$$e^{\beta^2}(1 - \mathrm{erf}\,\beta) \simeq 1 \tag{39}$$

Let

$$g_D \equiv \frac{\sqrt{\pi}\,\mathcal{R}\,\Delta F}{2\alpha} \tag{40}$$

$$= \frac{2\sqrt{\pi \ln 2}}{\epsilon_0 c \hbar} \cdot \frac{N \nu \delta^2 \Delta F}{\Delta\omega_D} \tag{41}$$

The spontaneous lifetime τ_s of the upper level is given by

$$\frac{1}{\tau_s} = \frac{e^2|\langle a|x|b\rangle|^2\omega^3}{3\pi\epsilon_0\hbar c^3} \tag{42}$$

$$= \frac{\wp^2\omega^3}{3\pi\epsilon_0\hbar c^3} \tag{43}$$

(For example, see Heitler, 1954, p. 178). The use of (43) to eliminate $\wp^2$ in (41) yields

$$g_D = \frac{3}{2}\left(\frac{\ln 2}{\pi}\right)^{1/2}\frac{\lambda^2 N\Delta F}{\tau_s\,\Delta\omega_D} \tag{44}$$

which is the gain in the Doppler limit.

Hence, the gain in the case of a constant or steady-state population inversion is given by

$$g = g_D\, e^{\beta^2}(1-\mathrm{erf}\,\beta) \tag{45}$$

$$= \frac{3}{2}\left(\frac{\ln 2}{\pi}\right)^{1/2}\frac{\lambda^2 N\Delta F}{\tau_s\,\Delta\omega_D}\, e^{\beta^2}(1-\mathrm{erf}\,\beta) \tag{46}$$

Step-function Inversion

For the case of a step-function inversion,

$$\rho_{aa}(z,t') - \rho_{bb}(z,t') = \begin{cases} 0 & t' < z/c \\ \Delta F & t' \geq z/c \end{cases} \tag{47}$$

In terms of the unit step function defined by

$$u(\xi) \equiv \begin{cases} 0 & \xi < 0 \\ 1 & \xi \geq 0 \end{cases} \tag{48}$$

(47) becomes

$$\rho_{aa}(z,t') - \rho_{bb}(z,t') = \Delta F\, u(t' - z/c) \tag{49}$$

In this case, the integral (29) becomes

$$I = \Delta F \int_{-\infty}^{t} dt'\, e^{-\alpha^2 (t-t')^2 - \Gamma (t-t')}\, u(t' - z/c) \tag{50}$$

$$= \Delta F \int_{z/c}^{t} dt'\, e^{-\alpha^2 (t-t')^2 - \Gamma (t-t')} \tag{51}$$

As in the previous section, we complete the square in the exponent and let $\tau = t - t'$ to obtain

$$I = \Delta F e^{\beta^2} \int_0^{\mu} d\tau\, e^{-(\alpha\tau + \beta)^2} \tag{52}$$

where μ is the retarded time,

$$\mu = t - z/c \tag{53}$$

With the change of variable, $x \equiv \alpha\tau + \beta$, (52) becomes

$$I = \frac{\Delta F e^{\beta^2}}{\alpha} \int_{\beta}^{\alpha\mu + \beta} dx\, e^{-x^2} \tag{54}$$

$$= \frac{\sqrt{\pi}\, \Delta F}{2\alpha} e^{\beta^2} \left[\operatorname{erf}(\alpha\mu + \beta) - \operatorname{erf} \beta \right] \tag{55}$$

The use of (55) in the expression (28) for the linear gain gives

$$g = \frac{\sqrt{\pi}\, R\, \Delta F}{2\alpha} e^{\beta^2} \left[\operatorname{erf}(\alpha\mu + \beta) - \operatorname{erf}\beta \right] \tag{56}$$

$$= g_0\, e^{\beta^2} \left[\operatorname{erf}(\alpha\mu + \beta) - \operatorname{erf}\beta \right] \tag{57}$$

where g_0 is given by (44). We note from (57) that the gain depends upon the retarded time μ. The gain builds up as μ increases and approaches the steady-state gain (45) in the limit of large μ.

Gain Rise Time

We next investigate how long it takes the gain to reach 95% of its limiting value. We want to find μ for

$$\operatorname{erf}(\alpha\mu + \beta) - \operatorname{erf}\beta = .95\,(1 - \operatorname{erf}\beta) \tag{58}$$

We first consider the Doppler limit in which

$$\beta = \frac{\Gamma}{2\alpha} \ll 1 \tag{59}$$

Then to a good approximation erfβ may be neglected in (58), so that

$$\operatorname{erf}(\alpha\mu + \beta) = .95$$

from which

$$\alpha\mu + \beta = 1.4 \tag{60}$$

Since we assumed $\beta \ll 1$, (60) means that

$$\alpha\mu \simeq 1.4$$

or

$$\mu \simeq \frac{1.4}{\alpha} \qquad (\beta \ll 1) \tag{61}$$

We see that in the Doppler limit, the rise time of the gain is of the order α^{-1}.

Next we consider the other extreme where $\beta >> 1$, which corresponds to $\Gamma >> 2\alpha$. Eq. (58) can be written

$$\operatorname{erf}(\alpha\mu + \beta) = .95 + .05 \operatorname{erf} \beta \tag{62}$$

For large β the error function can be approximated by

$$\operatorname{erf} \beta = 1 - \frac{e^{-\beta^2}}{\sqrt{\pi}\,\beta}\left(1 - \frac{1}{2\beta^2} + \ldots\right) \tag{63}$$

Eq. (62) can now be written

$$1 - \frac{e^{-(\alpha\mu+\beta)^2}}{\sqrt{\pi}\,(\alpha\mu+\beta)} = .95 + .05\left(1 - \frac{e^{\beta^2}}{\sqrt{\pi}\,\beta}\right) \tag{64}$$

or

$$e^{(\alpha\mu+\beta)^2}(\alpha\mu+\beta) = 20\beta e^{\beta^2} \tag{65}$$

The logarithm of (65) is

$$(\alpha\mu+\beta)^2 + \ln(\alpha\mu+\beta) = \ln 20 + \ln\beta + \beta^2 \tag{66}$$

We assume $\alpha\mu$ is small compared to β, then

$$(\alpha\mu+\beta)^2 \simeq \beta^2 + 2\alpha\mu\beta \tag{67}$$

Also,

$$\begin{aligned} \ln(\alpha\mu+\beta) &= \ln\left[\beta\left(\frac{\alpha\mu}{\beta}+1\right)\right] \\ &= \ln\beta + \ln\left(\frac{\alpha\mu}{\beta}+1\right) \\ &\simeq \ln\beta + \frac{\alpha\mu}{\beta} \end{aligned} \tag{68}$$

The use of (67) and (68) in (66) gives

$$\beta^2 + 2\alpha\mu\beta + \ln\beta + \frac{\alpha\mu}{\beta} = \ln 20 + \ln\beta + \beta^2$$

or

$$2\alpha\mu\beta + \frac{\alpha\mu}{\beta} = \ln 20$$
$$\alpha\mu = \ln 20 \left(2\beta + \frac{1}{\beta}\right)^{-1}$$
$$\simeq \frac{\ln 20}{2\beta} \tag{69}$$

Now $\beta = \frac{\Gamma}{2\alpha}$, so

$$\mu \simeq \frac{\ln 20}{\Gamma}$$
$$\simeq \frac{3}{\Gamma} \qquad (\beta >> 1) \tag{70}$$

In this case, we see that the gain rise time is $\sim \Gamma^{-1}$

In summary, for the Doppler limit in which $\beta << 1$ $(\alpha >> \Gamma)$, the rise time is of the order α^{-1} ; while in the opposite extreme $(\Gamma >> \alpha)$, the rise time is of the order Γ^{-1}.

We now consider some typical values of α and Γ and calculate the rise time of the gain. From the definition of α, $\alpha = \Delta\omega_D / 4\sqrt{\ln 2}$. We assume $\Delta\omega_D$ to be on the order of a few times 10^{10} so

$$\alpha \sim 10^{10}\ \text{sec}^{-1}$$

We assume τ_s to be on the order of 10^{-9} sec, and

$$\Gamma \sim \frac{1}{\tau_s} \sim 10^{9}\ \text{sec}^{-1}$$

then
$$\beta = \frac{\Gamma}{2\alpha} \sim \frac{1}{20} \ll 1$$

which corresponds to the Doppler limit. For the Doppler limit the gain rise time is on the order of α^{-1}, which in this case is 10^{-10} sec.

Delta-function Pumping

Consider the case where the population of the upper and lower levels are zero up until $t = z/c$, at which time the two levels are pumped differentially such that a population inversion is established instantaneously but not maintained. The pumping rates into levels a and b are then described by

$$\begin{aligned} \lambda_a &= F_a \, \delta(t - z/c) \\ \lambda_b &= F_b \, \delta(t - z/c) \\ F_a &> F_b \end{aligned} \tag{71}$$

where F_a and F_b are the fraction of atoms pumped into the respective levels. As a first approximation, we can neglect the action of the electric field in the population equations, (11) and (12). Eq. (11) then becomes

$$\frac{\partial \rho_{aa}}{\partial t} = F_a \, \delta(t - z/c) - \gamma_a \rho_{aa} \tag{72}$$

or

$$\frac{\partial \rho_{aa}}{\partial t} + \gamma_a \rho_{aa} = F_a \, \delta(t - z/c) \tag{73}$$

Eq. (73) can be integrated by using the integrating factor $e^{\gamma_a t}$:

$$\frac{\partial}{\partial t}\left(\rho_{aa} e^{\gamma_a t}\right) = F_a e^{\gamma_a t} \delta(t - z/c)$$

$$\therefore \rho_{aa}(z,t) = F_a \int_{-\infty}^{t} dt' e^{-\gamma_a (t-t')} \delta(t' - z/c)$$

$$= F_a e^{-\gamma_a (t - z/c)} u(t - z/c) \tag{74}$$

where the unit step function $u(t - z/c)$ insures that $\rho_{aa} = 0$ for $t < z/c$. Similarly,

$$\rho_{bb}(z,t) = F_b e^{-\gamma_b (t - z/c)} u(t - z/c) \tag{75}$$

We must use (74) and (75) in the integral (29). For convenience we do the integration in (29) in two steps,

$$I = I_a - I_b$$

where I_a represents the ρ_{aa} integration, and I_b represents the ρ_{bb} integration. Consider first the ρ_{aa} integration.

$$I_a \equiv \int_{-\infty}^{t} dt' e^{-\alpha^2 (t-t')^2 - \Gamma (t-t')} \rho_{aa}(z,t') \tag{76}$$

$$= F_a \int_{-\infty}^{t} dt' e^{-\alpha^2 (t-t')^2 - \Gamma (t-t') - \gamma_a (t' - z/c)} \times u(t' - z/c) \tag{77}$$

$$= F_a e^{-\gamma_a \mu} e^{\delta_a^2} \int_{0}^{\mu} d\tau\, e^{-(\alpha\tau - \delta_a)^2} \tag{78}$$

where

$$\delta_a \equiv \frac{\gamma_a - \Gamma}{2\alpha} \tag{79}$$

and μ and τ are defined as before. With the change of variable, $x \equiv \alpha\tau - \delta_a$ (78) becomes

$$I_a = \frac{1}{\alpha} F_a e^{-\gamma_a \mu} e^{\delta_a^2} \int_{-\delta_a}^{\alpha\mu - \delta_a} dx\, e^{-x^2}$$

$$= \frac{\sqrt{\pi}}{2\alpha} F_a e^{-\gamma_a \mu} e^{\delta_a^2} \left[\operatorname{erf}(\alpha\mu - \delta_a) - \operatorname{erf} \delta_a \right] \qquad (80)$$

The integral I_b is the same as (80) but with the subscript a replaced everywhere by b.

According to (28), the gain is then

$$g = \mathcal{R}\,(I_a - I_b)$$

$$= \frac{3}{2}\left(\frac{\ln 2}{\pi}\right)^{1/2} \frac{\lambda^2 N}{\tau_s \Delta\omega_D} \left[D_a(\mu) - D_b(\mu) \right] \qquad (81)$$

where
$$D_i(\mu) \equiv F_i\, e^{-\gamma_i \mu + \delta_i^2} \left[\operatorname{erf}(\alpha\mu - \delta_i) - \operatorname{erf} \delta_i \right] \qquad (i = a, b) \qquad (82)$$

Consider the case where γ_{ph} may be neglected in Γ. Then

$$\Gamma = \frac{\gamma_a + \gamma_b}{4\alpha} \qquad (83)$$

$$\therefore \; \delta_a = \frac{\gamma_a - \gamma_b}{4\alpha} \equiv \delta \qquad (84)$$

and
$$\delta_b = -\delta \qquad (85)$$

Now the gain expression (81) becomes

$$g = \frac{3}{2}\left(\frac{\ln 2}{\pi}\right)^{1/2} \frac{\lambda^2 N}{\tau_s \Delta\omega_D} e^{\delta^2} \left\{ F_a e^{-\gamma_a \mu}\left[\mathrm{erf}\,(\alpha\mu - \delta) - \mathrm{erf}\,\delta\right] - F_b e^{-\gamma_b \mu}\left[\mathrm{erf}\,(\alpha\mu + \delta) - \mathrm{erf}\,\delta\right] \right\} \tag{86}$$

Finally, if we go one step further and assume $\gamma_a = \gamma_b \equiv \gamma$, then $\delta = 0$, and (86) reduces to

$$g = \frac{3}{2}\left(\frac{\ln 2}{\pi}\right)^{1/2} \frac{\lambda^2 N \Delta F}{\tau_s \Delta\omega_D} e^{-\gamma\mu}\,\mathrm{erf}\,(\alpha\mu) \tag{87}$$

$$= g_D\, e^{-\gamma\mu}\,\mathrm{erf}\,(\alpha\mu) \tag{88}$$

In this simple case it is easy to see how the gain varies with retarded time μ. The gain will build up from zero, reach a maximum, and then fall off to zero as the exponential becomes dominant. The maximum value of g will depend upon the relative sizes of α and γ, but will be less than the steady-state Doppler-limit gain.

A summary of the gains for the three cases examined in the preceding discussion is presented in Table 2-1.

In conclusion we note that the effects of the swept excitation of a short-lived upper state are considerably more complicated than the above analysis describes. In particular, the assumption of a slowly varying electric field is not entirely consistent with a swept excitation in which the gain initially grows rapidly. Nevertheless, the present calculations serve as a useful background for the more detailed calculations of Hopf, Meystre, Scully, and Seely (1975); Bonifacio, Hopf, Meystre, and Scully (1975); and Hopf and Meystre (1975). These papers address the important aspects of laser lethargy (delayed response of the laser to an instantaneous pump), superradiance, and pulse propagation for an excitation swept at the speed of light. The more detailed theory predicts a linear gain which is less than that given by the simple theory; but, for large propagation distances, superradiance tends to compensate for this reduction (Hopf, Meystre, Scully and Seely, 1975).

TABLE 2-1

Linear Gain Expressions for Three Types Of Pumping

A. Constant Population Difference

$$g = g_D e^{\beta^2}(1 - \mathrm{erf}\,\beta)$$

where

$$g_D = \frac{3}{2}\left(\frac{\ln 2}{\pi}\right)^{1/2} \frac{\lambda^2 N \Delta F}{\tau_s \Delta\omega_D}$$

B. Step-Function Pumping

$$g(\mu) = g_D e^{\beta^2}\left[\mathrm{erf}(\alpha\mu + \beta) + \mathrm{erf}\,\beta\right]$$

C. Delta-Function Pumping

$$g(\mu) = g_D e^{-\gamma\mu}\,\mathrm{erf}(\alpha\mu) \qquad \begin{cases} \gamma = \gamma_a = \gamma_b \\ \gamma_{ph} = 0 \end{cases}$$

CHAPTER 3

EXCITATION BY NEAR-RESONANT CHARGE TRANSFER

In this chapter we consider six particular charge-transfer reactions as candidates for producing population inversions with radiative transitions in the soft x-ray and far ultraviolet regions. We being with a discussion of the charge-transfer process and some experimental data available in the literature. Next we factorize the steady-state gain formula in a way that is convenient for comparing the various reactions. After calculating the necessary parameters, including population inversion and Doppler spread, we calculate the linear gain per ion current density for each reaction.

The maximum population inversion which builds up as the ions move into the target is calculated as a function of the target atom density. We find that for target densities higher than 10^{17}-10^{18}, a relatively large increase in target density is required to produce relatively small increase in the population inversion, hence there is little advantage in going to higher target densities.

The Doppler spread which arises from scattering during charge transfer is calculated assuming a cut-off Coulomb interaction.

Near-resonant Charge Transfer

The ionization potentials of alkali atoms are often very close to those of rare gases in the first excited state, the difference being on the order of a tenth of an electron volt. For a reaction which involves the transfer of an electron from an alkali atom to a rare gas ion, the change in potential of the transferred electron will be small for transfer into certain excited states, whereas transfer into a ground state involves a much larger energy defect. The transfer of an electron in a reaction for which the energy defect is small (typically a few tenths of an electron volt) is called a near-resonant charge-transfer process. In contrast, a resonant charge-transfer process refers to a reaction of the type $A+A^+ \longrightarrow A^+ + A$. The typical near-resonant cross section is small at low velocities and increases exponentially until it reaches a broad maximum before decreasing. The resonant cross section, on the other hand, is large at small velocities and decreases with increasing velocity.

Peterson and Lorents (1969) have measured the total charge-transfer cross sections for the reactions of He^+ and

Ar^+ ions with K, Rb and Cs vapors for ion beam energies between 10 and 1500 eV. The magnitude of the cross sections were much larger than expected for ground state transitions leading them to conclude that essentially all the measured reactions led to the formation of excited states. At the maximum ion inergy of 1.5 keV, the measured cross sections were in the range of 0.5 x 10^{-14} to 2 x $10^{-14} cm^2$.

In particular, the cross section for He^+ + Cs at that energy was about 1.7 x $10^{-14} cm^2$. Total cross sections for He^+ + Cs have been measured at higher energies by Schlachter et al. (1968) who worked in the 1.5 - 25 keV range and by Montmagnon et al. (1973) in the 5 - 25 keV range. Although there is a slight discrepancy between the low energy and the high energy data, the cross section appears to have a maximum of about 1.5 x $10^{-14} cm^2$ at 1.5 keV.

Salop, Lorents, and Peterson (1971) studied the spectral radiation in the near ultraviolet and visible region resulting from charge-transfer excitation in the reactions of He^+ and Ne^+ with the alkali atoms K and Rb. Their results showed that the cross section for a final state consisting of an excited alkali ion is a relatively small fraction (0.1%) of the total charge-transfer cross section. The majority of the total cross section is attributed to the process in which the neutralized helium is left excited. Their interpretation of the results is that loosely bound orbitals favor near-resonant transitions at large distances and with large cross sections, while tightly bound orbitals interact only in close collisions with smaller cross sections and with no preference for near-resonant processes. It is more likely that the rare gas ion will pick up an electron into an excited state than for the alkali atom to be ionized into an excited state, since excitation of the alkali atom involves electrons in deeper orbitals.

Olson and Smith (1973) have performed a theoretical analysis of resonant charge transfer for He^+ colliding with K, Rb and Cs atoms. By applying a modified Demkov theory, they have obtained reasonable agreement with experimental data. The theory indicates that near-resonant charge transfer at large distances can be explained principally by the polarization of the alkali atom or by interaction with the quadropole moment of the neutral. The theory predicts that capture into $He(2^3P)$ will dominate. At energies near and above one keV, the distribution of the captures into $He(2^3P)$ and $He(2^1P)$ becomes nearly statistical; i.e., capture into the metastable triplet state is three times as likely as capture into the singlet state. The transition from 2 P to 1 S gives rise to 584 Å radiation. A surprising result is that even though capture into He(2'S) for He^+ + Cs has the smallest energy defect, the theory predicts a smaller cross section than for capture into the 2^3S, 2'P and 2^3P

helium states. The theoretical total cross section curve lies somewhat below the data of Peterson and Lorents. Olson and Smith note that rotational coupling has been neglected in their calculations, so the actual cross sections should be higher than the calculated ones. In addition, Perel and Daley (1971) have suggested that the cross sections of Peterson and Lorents may be too large due to the influence of secondary electron emission in their apparatus.

On the basis of the available theoretical and experimental investigations of near-resonant charge exchange, it appears that this process could be used to establish the population inversions necessary for laser radiation. A variety of charge transfer reactions have been listed by Perel and Daley (1971). From this list we have selected for further study reactions which produce transitions in the far ultra-violet.

We also include the near-resonant charge-transfer reaction of $Ne^+ + K$ (suggested by Seely 1974) and the (pseudo) near-resonant charge transfer

$$He^{++} + H \longrightarrow He^{+}(2p) + H^{+}$$

proposed by Scully et al. (1973). Because of the Coulomb interaction energy (a few eV) of the final ions in the latter reaction, it is not a true near-resonant charge transfer even though the H(1s) and $He^+(2p)$ levels themselves are of nearly equal energy.

TABLE 3-1. Selected Near-resonant Charge-transfer Reactions

Reactants	Excited Product	Transition to Ground State (Å)
He^{++} + H	He(2p)	304
He^{+} + Cs	$He(2^1P)$	584
Ne^{+} + K	$Ne[p^5(^2P)3s]$	736
Ar^{+} + Cs	$Ar[p^5(^2P)3s]$	1048
H^{+} + Cs	H(2p)	1216
Hg + Cs	$Hg[(6p\ ^1P_1{}^o)]$	1849

In the discussion which follows, we shall be concerned with the near-resonant charge-transfer reactions listed in Table 3-1.

Factorization of Gain Formula

In this section we divide the expression for linear gain into factors which are convenient for comparing various charge-transfer reactions. In the case of continuous pumping, the gain per unit length from Eq. (46) of Chapter 2 is

$$g = \frac{3}{2}\left(\frac{\ln 2}{\pi}\right)^{1/2} \frac{\lambda^2}{\tau_s} \frac{N \Delta F}{\Delta\omega_D} e^{\beta^2}(1-\operatorname{erf}\beta) \tag{1}$$

In the Doppler limit the factor $e^{\beta^2}(1-\operatorname{erf}\beta)$ approaches unity.

For the sake of simplicity we shall use the above steady-state gain expression for calculating gains in the remainder of this dissertation instead of using the more rigorous delta-function pumping theory. This approximation has some justification in that, as we shall show later, the inverse of the Doppler width is smaller than the spontaneous lifetime of the upper laser level for each of the reactions we consider. Consequently, the population inversion decays more slowly than the macroscopic polarization, and the conditions for steady state are approached albeit weakly.

For an ion beam focused to current density J, the ion density N which appears in (1) can be expressed as

$$N = \frac{J}{ne v} \tag{2}$$

where ne is the ion charge, and v is the velocity of ions in the beam.

The Doppler spread $\Delta\omega_D$ may arise from more than one source. Scattering by the charge-transfer process is one source. Another is the ion energy spread inherent in the beam. In order to compare the effects of different processes it is convenient to express the Doppler frequency spread in terms of the corresponding energy spread ΔE_D:

$$\Delta\omega = \frac{\omega}{c}\Delta v = \frac{2\pi}{\lambda}\Delta v$$

Also

$$\Delta E_D = m v \Delta v$$

$$\therefore \quad \Delta\omega_D = \frac{2\pi}{\lambda}\frac{\Delta E_D}{m v} \tag{3}$$

We now use (2) and (3) in (1) to obtain

$$g = \frac{3}{4\pi}\left(\frac{\ln 2}{\pi}\right)^{1/2}\frac{m_p}{e} \cdot \frac{A\lambda^3}{n\tau_s} \cdot \frac{J\Delta F}{\Delta E_D} e^{\beta^2}(1-\mathrm{erf}\,\beta) \tag{4}$$

where we have written the ion mass in terms of the proton mass m_p and the atomic mass A. Equation (4) is conveniently separated by the dots into three factors. The first factor is a constant whose value is 7.31 x 10^5 eV·sec^2·cm^{-2}·Coulomb^{-1}. The second factor consists of generally well-known parameters specific to the particular species being

TABLE 3-2. Data Used to Calculate ξ

	He^{++},H	He^{+},Cs	Ne^{+},K	Ar^{+},Cs	H^{+}, Cs	Hg^{+},Cs
A9amu)	4	4	20	40	1	201
λ(Å)	304	584	736	1048	1216	1849
τ_s(sec)[a]	10^{-10}	$5x10^{-10}$	$1.5x10^{-9}$	$2X10^{-9}$	$2.1x10^{-9}$	$1.2x10^{-9}$
ξ (eV-cm-A^{-1})	.41	1.0	3.9	17.	.66	774

[a]Spontaneous lifetimes have been taken from Wiese, Smith, and Glennon (1966) except for Hg which was calculated from data given by Allen (1963).

excited. The third factor contains the principal uncertainties for evaluating the gain and will be considered in detail in the following sections of this chapter.

We define the parameter ξ as the product of the first two factors in (4),

$$\xi \equiv \frac{3}{4\pi}\left(\frac{\ln 2}{\pi}\right)^{1/2} \frac{m_p}{e} \frac{A\lambda^3}{h\,\varepsilon_s} \tag{5}$$

The values of ξ presented in Table 3-2 for the reactions of interest serve as sort of crude figures of merit for comparing the potential gains. For a given current density, population difference, and energy spread, ξ will be a measure of the relative gains. (Note the relatively large value for the Hg^+ + Cs reaction.) A more complete estimate of the gains requires that we evaluate the parameters in the third factor of Equation (4) which we do in the following sections.

Population Inversion

In this section we calculate the fractional population difference ΔF for each reaction of interest. We consider a charge-transfer reaction described by

$$A^+ + B \longrightarrow A^* + B^+$$

where the projectile ion is neutralized by picking up an electron into an excited (denoted by the asterisk) atomic state.

In our notation we use $Q_{\alpha\beta}$ and $\Lambda_{\alpha\beta}$ to denote the cross section and the probability per unit length, respectively, for transitions from state α to state β.

For example,

Q_{+o} = atomic cross section for neutralization of an ion by a target atom.

Λ_{+o} = probability per unit distance for neutralization.

$$= Q_{+o} N_t \tag{6}$$

where N_t = atomic density of target

We assume that the ions are in a beam which strikes stationary target atoms. If the target atom density is much greater than the ion density then, as the ions travel a distance x into the target, the fraction F_+ of ions which remain unneutralized is described by

$$\frac{dF_+}{dx} = -\Lambda_{+o} F_+ \tag{7}$$

We take $F_+ = 1$ at $x = o$, so Eq. (7) yields

$$F_+ = e^{-\Lambda_{+o} x} \tag{8}$$

One of the possible excited levels of the neutralized ion is the upper laser level which we denoted by a. The upper level can decay spontaneously with mean life τ to a lower level denoted by b. We assume that the upper level is populated by electron pick-up (Λ_{+a}) and depopulated by spontaneous decay (Λ^{sp}_{ab}) and collisions (Λ^{coll}_{ab}). The fraction Fa of atoms in the upper level then satisfies

$$\frac{dF_a}{dx} = \Lambda_{+a} F_+ - (\Lambda^{sp}_{ab} + \Lambda^{coll}_{ab}) F_a$$

$$= \Lambda_{+a} e^{-\Lambda_{+o} x} - \Lambda_{ab} F_a \tag{9}$$

where $$\Lambda_{ab} = \Lambda^{sp}_{ab} + \Lambda^{coll}_{ab} \tag{10}$$

$$= \frac{1}{\tau v} + Q^{coll}_{ab} \cdot N_t \tag{11}$$

and v is the ion velocity. The solution to Eq. (9) under the condition that Fa = 0 at x = 0 is

$$F_a = \frac{\Lambda_{+a}}{\Lambda_{+o} - \Lambda_{ab}} \left(e^{-\Lambda_{ab} x} - e^{-\Lambda_{+o} x}\right) \tag{12}$$

We assume that the lower level b becomes populated solely by decay of the upper level, hence we neglect the small formation of level b during charge transfer. The fraction F_b of atoms in the lower level then satisfies

$$\frac{dF_b}{dx} = \Lambda_{ab} F_a \tag{13}$$

By putting (12) into (13) the solution for F_b can be found, and the fractional population difference ΔF is calculated:

$$\Delta F = F_a - F_b$$

$$\Delta F = \frac{Q_{+a}}{Q_{+o}} \frac{1}{1-L} \left[2 e^{-\Lambda_{ab} x} - (1+L) e^{-\Lambda_{+o} x} + L - 1 \right] \tag{14}$$

where the dimensionless parameter L is defined by

$$L \equiv \frac{\Lambda_{ab}}{\Lambda_{+o}} = \frac{1}{\tau \sigma Q_{+o} N_t} \tag{15}$$

From (14) we can calculate the depth x_m into the target at which ΔF has its maximum value ΔF_m. Differentiate (14) with respect to x and set the result equal to zero to obtain

$$0 = \frac{Q_{+a}}{Q_{+o}} \frac{1}{1+L} \left[-2 \Lambda_{ab} e^{-\Lambda_{ab} x_m} + (1+L) \Lambda_{+o} e^{-\Lambda_{+o} x_m} \right] \tag{16}$$

which gives

$$(1+L) e^{-\Lambda_{+o} x_m} = 2 L e^{-\Lambda_{ab} x_m} \tag{17}$$

Equation (17) can be solved for x_m which gives

$$x_m = \frac{1}{\Lambda_{+o}} \cdot \frac{\ln \left(\frac{L+1}{2L} \right)}{(1-L)} \tag{18}$$

To calculate ΔF_m we use (17) in (14) to get

$$\Delta F_m = \frac{Q_{+a}}{Q_{+o}} \frac{1}{1-L} \left[2 e^{-\Lambda_{ab} x_m} - 2 L e^{-\Lambda_{ab} x_m} + L - 1 \right]$$

$$= \frac{Q_{+a}}{Q_{+o}} \left[2e^{-\Lambda_{ab} x_m} - 1 \right] \tag{19}$$

By using (18) in (19) we can eliminate x_m to obtain

$$\Delta F_m = \frac{Q_{+a}}{Q_{+o}} \left[2\left(\frac{1+L}{2L}\right)^{-\frac{L}{1-L}} - 1 \right] \tag{20}$$

which gives the spatial maximum of ΔF.

ΔF_m is a function of the cross sections through the ratio Q_{+a}/Q_{+o} and through L, which depends upon Q_{+o} via (15). According to (20), ΔF_m approaches Q_{+a}/Q_{+o} for small values of L, while for large values of L, ΔF_m goes to zero; hence, the largest value that ΔF_m can assume is equal to Q_{+a}/Q_{+o}.

Eq. (20) can be rewritten to better show the behavior of the maximum population difference as a function of the density of target atoms. We define

$$\Delta f_m \equiv \Delta F_m \left(\frac{Q_{+a}}{Q_{+o}}\right)^{-1}$$

$$\ell \equiv \frac{1}{L} = \tau_s v Q_{+o} N_t$$

Note that ℓ is proportional to the target atom density, and Δf_m is the fractional population difference normalized to its maximum possible value Q_{+a}/Q_{+0}. With the above definitions, (20) can be written

$$\Delta f_m = 2\left(\frac{2}{\ell+1}\right)^{\frac{1}{\ell-1}} - 1 \tag{20a}$$

A plot of Δf_m vs ℓ is presented in Fig. 3-1. The plot shows that the fractional population difference reaches 50% of its maximum possible value when ℓ is about 5. Beyond that value of ℓ , large increases in the target density produce relatively small changes in the fractional population difference. At ℓ =100, Δf_m is about 92%.

The data used to calculate ΔF_m for each reaction are listed in Table 3-3. We have assumed that the effects of collisions are small compared to spontaneous decay. The tabulated target atom densities have been calculated by assuming L =.01 (ℓ=100), so these are the densities required in order to achieve a fractional population difference equal to 92% of its maximum possible value. The depth x_m into the target at which the population difference reaches a maximum (L =.01) is also presented for each reaction. The values of Q_{+0} listed in the table are experimental measurements taken from the literature. On the other hand, experimental values of Q_{+a}/Q_{+0} for the reactions of interest are

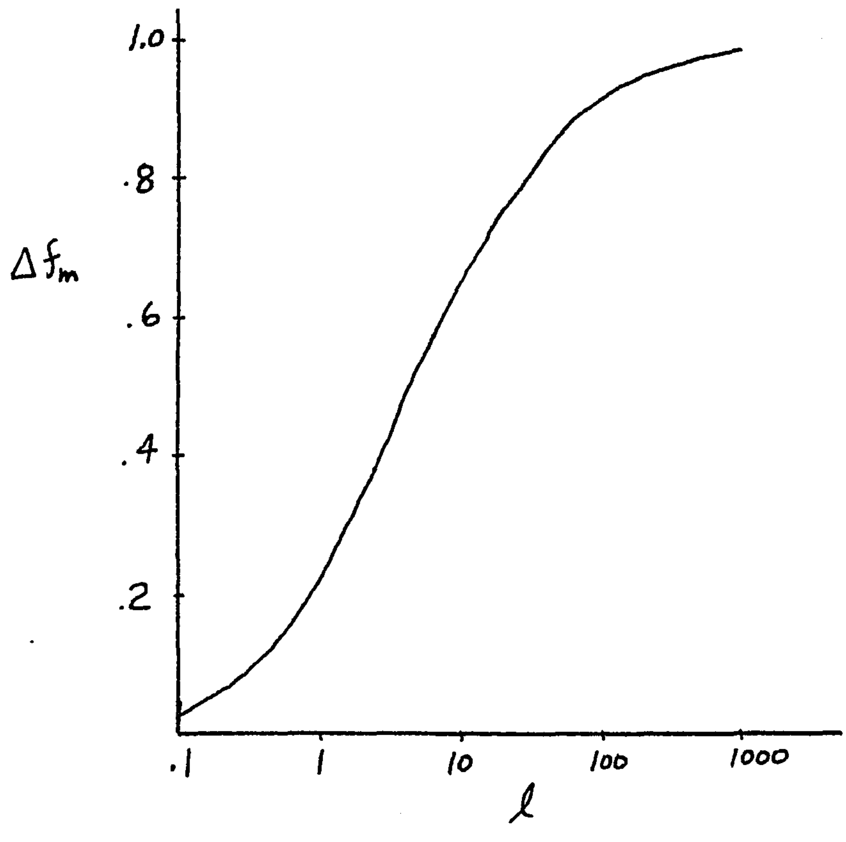

FIGURE 3-1. Normalized Fractional Population Inversion versus Target Density Parameter

TABLE 3-3. Fractional Population Inversions

		He^{++},H	He^{+},Cs	Ne^{+},K	Ar^{+},Cs	H^{+},Cs	Hg^{+},Cs
v (cm/sec)		$1.2x10^{8}$	$3x10^{7}$	$3x10^{7}$	$8x10^{6}$	$4.4x10^{7}$	$2x10^{7}$
E(keV)		25	1.9	9.3	1.3	1.0	42.
$Q_{+o}(10^{-14}cm^{2})$		.5[a]	1.5[b]	1[c]	.7[b]	1[d]	.6[e]
Q_{+a}/Q_{+o}		.2[a]	.19	.25	.25	.75	1
L=.01	$N_{\ell}x10^{-17}$)	17.	4.4	2.2	8.9	1.1	6.9
	x_m(cm)$x10^{4}$	4.7	5.9	18.	6.3	37.	9.5
	ΔF_m	.18	.17	.23	.23	.69	.93

[a]Louisell, Scully, and McKnight (1975).

[b]Peterson and Lorents (1969).

[c]Assumed.

[d]Schlachter et al.(1969).

[e]Perel and Daley (1971).

not available. In lieu of detailed quantum mechanical calculations, we estimate in Appendix A the ratio Q+a/Q+o for each reaction by assuming that only the near-resonant levels are populated by charge transfer.

The ion velocities used in calculating ΔF_m are those at which the charge-transfer cross sections are estimated to have maxima. The energy of 25 keV used for the He^{++}+H reaction corresponds to the value used by Louisell, Scully and McKnight (1975). The velocity for the He^{+}+Cs reaction was estimated from the data of Peterson and Lorents (1969) and Schlachter et al. (1968). Velocities for the other reactions were obtained by using Figure 1 of Perel and Daley (1971) which is an empirical plot of the velocity at cross section maximum as a function of a factor involving energy defect of the reaction and the ionization potential of the electron donor.

Example

Consider the He^{+}+Cs reaction. We assume the following values:

$$\begin{aligned} Q_{+o} &= 1.5 \times 10^{-14}\ \text{cm}^2 \\ Q_{+a}/Q_{+o} &= 3/16 \\ v &= 3 \times 10^{7}\ \text{cm/sec} \\ N_t &= 10^{17}\ \text{cm}^{-3} \end{aligned} \qquad (21)$$

from which we calculate L = .045, $x_m = 1.7 \times 10^{-3}$cm, and ΔF_m = .15. If we lower the Cs target density by a factor

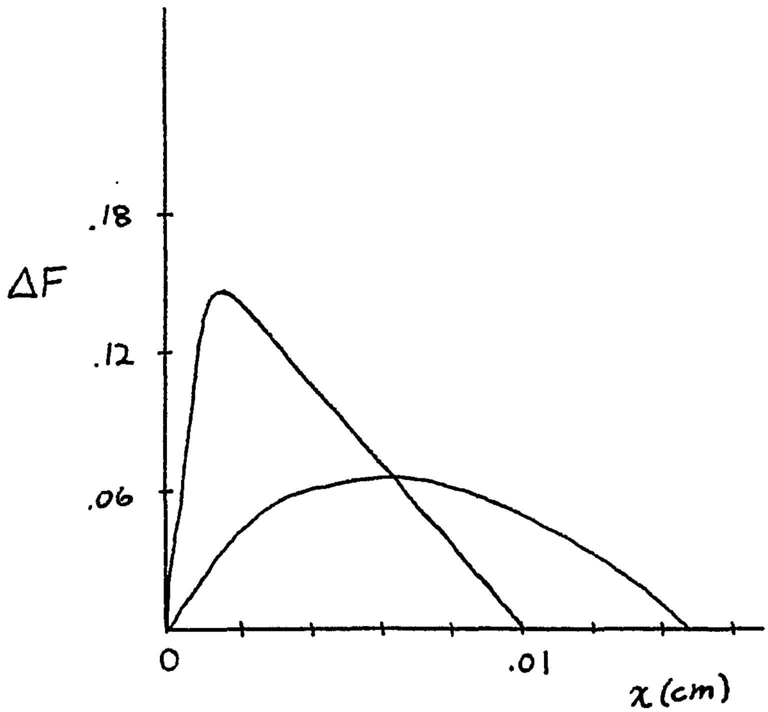

FIGURE 3-2. Fractional Population Difference versus Distance into Target for He^+ +Cs.

The two curves are for target densities of 10^{16} and 10^{17} atoms per cm^3. The He^+ velocity is taken to be $3x10^7$ cm/sec in the x-direction.

of ten to $10^{16}\,cm^{-3}$, then $L = 0.45$, $\Delta F_m = .06$, and $x_m = 7 \times 10^{-3}\,cm$. A plot of ΔF versus x for these two different target densities is presented in Figure 3-2. The figure shows a general feature of how ΔF vs x depends upon target density: as the target density decreases, the maximum value of ΔF also decreases and moves deeper into the target. The lower density also has a wider region over which the population inversion occurs.

Doppler Spread Arising from Charge-transfer Collisions

In this section we estimate the Doppler broadening which arises from scattering during charge transfer. For convenience we choose our coordinate system as shown in Figure 3-3. The target atom sits at the origin, and the Z-axis lies along the projectile ion's incoming velocity $\vec{v}_o$. The Z-Y plane is chosen to contain the fixed lasing direction denoted by the unit vector $\hat{n}$ which makes an angle γ with the Z-axis. The velocity of the projectile after scattering is denoted by $\vec{v}$. The velocity component v_n along the lasing direction is given by

$$\begin{aligned} v_n &= \vec{v}\cdot\hat{n} = v_y n_y + v_z n_z \\ &= v(\sin\theta \sin\phi \sin\gamma + \cos\theta \cos\gamma) \end{aligned} \qquad (22)$$

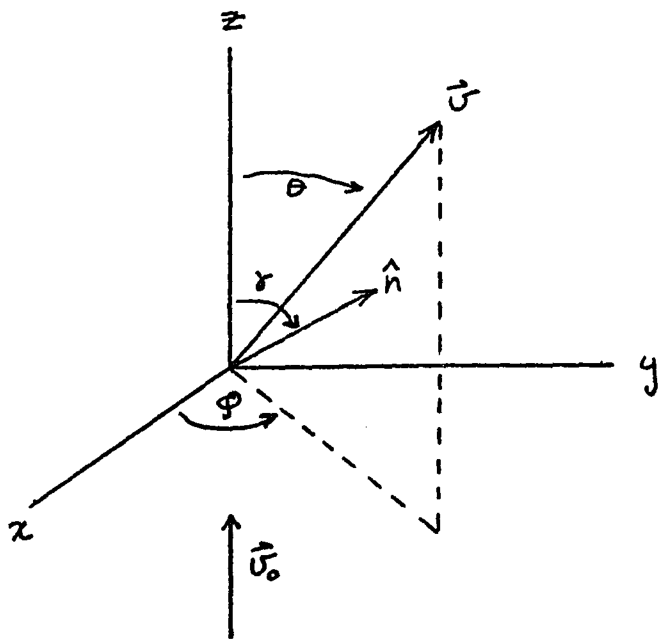

FIGURE 3-3. Coordinate System for Charge-transfer Scattering

The root-mean-square velocity spread in the lasing direction is defined by

$$\Delta v \equiv \left(\langle v_n^2 \rangle - \langle v_n \rangle^2 \right)^{1/2} \tag{23}$$

which we will use to estimate the Doppler spread. First we calculate $\langle v_n \rangle$. We take the average of Equation (22) and assume that scattering is isotropic in ϕ so that $\langle \sin\phi \rangle$ is zero. Then

$$\langle v_n \rangle^2 = v^2 \cos^2\gamma \langle \cos\theta \rangle^2 \tag{24}$$

Next we consider $\langle v_n^2 \rangle$. We square (22) and take the average to obtain

$$\langle v_n^2 \rangle = v^2 \left(\frac{1}{2} \langle \sin^2\theta \rangle \sin^2\gamma + \langle \cos^2\theta \rangle \cos^2\gamma \right) \tag{25}$$

where we have used $\langle \sin\phi \rangle = 0$ and $\langle \sin^2\phi \rangle = \frac{1}{2}$.

We put (24) and (25) into (23) to obtain

$$\Delta v = v \left[\frac{1}{2} \langle \sin^2\theta \rangle \sin^2\gamma + \left(\langle \cos^2\theta \rangle - \langle \cos^2\theta \rangle^2 \right) \times \cos^2\gamma \right] \tag{26}$$

If γ is not too small, and if the scattering angle θ is small, then to a first approximation

$$\Delta v \simeq \frac{v}{\sqrt{2}} \langle \theta^2 \rangle^{1/2} \sin\gamma \tag{27}$$

We recall that γ is the angle between the incoming ion trajectory and the direction of lasing.

The next step is to estimate $\langle\theta^2\rangle^{1/2}$. We make the simplifying assumption that scattering is due to a Coulomb interaction which cuts off at distances larger than b_m, the geometrical radius of the charge-transfer cross section Q. The formula for Coulomb scattering of charge Z_1e by a stationary charge Z_2e is given by

$$\tan\frac{\theta}{2} = \frac{Z_1 Z_2 e^2}{4\pi\epsilon_0}\cdot\frac{1}{2Eb} \tag{28}$$

where E is the projectile kinetic energy and b is the impact parameter. For small-angle scattering

$$\theta \simeq \frac{Z_1 Z_2 e^2}{4\pi\epsilon_0}\cdot\frac{1}{Eb} \tag{29}$$

The assumption of small angle scattering is meaningful in view of the conclusion of Olson and Smith (1973) that excitation of the neutralized atom is most likely for grazing collisions. The probability for scattering with an impact parameter between b and b+db is $\frac{2\,bdb}{b_m^2}$, if we assume equal likelihood for all impact parameters. Consequently,

$$\langle\theta^2\rangle = \left(\frac{Z_1 Z_2 e^2}{4\pi\epsilon_0}\right)^2 \frac{2}{b_m^2}\int_{b_0}^{b_m}\frac{db}{b} \tag{30}$$

$$= \left(\frac{Z_1 Z_2 e^2}{4\pi\epsilon_0 E}\right)^2 \frac{2 \ln (b_m/b_o)}{b_m^2} \tag{31}$$

The logarithmic integral in (30) requires that we choose a lower limit of integration b_o. For a grazing collision, b_o may be taken to be on the order of the Bohr radius; hence for a typical charge transfer which has a cross section of about $10^{-14} cm^2$,

$$\begin{aligned} \ln b_m/b_o &= \ln\left(\frac{1}{a_o}\sqrt{\frac{Q}{\pi}}\right) \\ &\simeq \ln 11 \\ &\simeq 2 \end{aligned}$$

This logarithmic term will be relatively insensitive to variations in the charge-transfer cross section. Therefore, to a good approximation,

$$\begin{aligned} \langle\theta^2\rangle^{1/2} &= \frac{Z_1 Z_2 e^2}{4\pi\epsilon_0 E} \cdot \frac{2}{b_m} \\ &= 2 Z_1 Z_2 \cdot \frac{a_o}{b_m} \cdot \frac{e^2/4\pi\epsilon_0 a_o}{E} \\ &= 2 Z_1 Z_2 \frac{a_o}{b_m} \cdot \frac{27\, eV}{E} \end{aligned} \tag{32}$$

Since E is typically a few KeV, we see that the small angle assumption is justified.

We now use (32) in (27) to obtain

$$\Delta v \simeq \sqrt{2}\, Z_1 Z_2 \frac{a_0}{b_m} \frac{27 eV}{E} v \sin\gamma \tag{33}$$

We recall that E is the incoming energy, whereas v is the velocity after scattering. We assume that the scattering is elastic so that $E = \frac{1}{2}mv^2$.

In the following discussion we shall assume that the projectile ion is singly charged, and that it penetrates the target atom such that it sees an effective charge of unity, then $Z_1 = Z_2 = 1$.

We can use (33) to calculate the Doppler spread and the corresponding ion energy spread ΔE due to charge-transfer scattering according to

$$\Delta E = 2\sqrt{\ln 4}\, m v \,\Delta v \tag{34}$$

and

$$\Delta \omega_D = 2\sqrt{\ln 4}\, \frac{2\pi}{\lambda} \Delta v \tag{35}$$

The factor $2\sqrt{\ln 4}$ is inserted so that ΔE and $\Delta\omega_D$ are full-width-at-half-maximum spreads, whereas Δv is assumed to be a Gaussian RMS spread.

If we use (33) in (34) we obtain

$$\Delta E = 8\sqrt{\pi \ln 2}\, \frac{a_0}{\sqrt{Q}} (27 eV) \sin\gamma$$

$$= 318 \frac{a_0}{\sqrt{Q}} \sin\gamma \quad (eV) \tag{36}$$

where $Q = \pi b_m^2$. We note that ΔE does not depend upon the projectile ion energy but depends weakly upon the cross section.

For $\gamma = 45^\circ$ and for a typical Q of $10^{-14} cm^2$, ΔE is about 11 eV. In practice, this value must be compared to the energy spread inherent in the ion beam to see which dominates. The energy spread of the beam will depend upon the type of ion source used and the energy of the delivered beam. We shall neglect the Doppler spread inherent in the beam and assume the Doppler spread arises only from charge-transfer collisions.

We put (33) into (35) to obtain the Doppler frequency spread

$$\Delta\omega_D = 8\pi\sqrt{\pi \ln 2}\, \frac{a_0}{\sqrt{Q}}\, \frac{v}{\lambda}\left(\frac{27 eV}{E}\right)\sin\gamma \tag{37}$$

We use $E = \frac{1}{2} mv^2$ to eliminate E from (37) to obtain

$$\Delta\omega_D = \left[16\pi\sqrt{\pi \ln 2}\, \frac{27 eV}{m_p c^2}\right] \frac{a_0 c^2}{A\lambda v\sqrt{Q}} \sin\gamma \tag{38}$$

where we have used $m = Am_p$. The unitless constant in brackets can be evaluated giving

$$\Delta\omega_D = \left(2.151 \times 10^{-6}\right) \frac{a_0 c^2}{A\lambda v\sqrt{Q}} \sin\gamma \tag{39}$$

Taking the centimeter as the unit of length, we can incorporate $a_o c^2$ into the constant so that

$$\Delta\omega_D = \left(1.02\times10^{7}\ \mathrm{cm}^{3}\cdot\mathrm{sec}^{-1}\right)\frac{\sin\gamma}{A\lambda v\sqrt{Q}} \tag{40}$$

By using (40) we can evaluate the factor $e^{\beta^2}(1-\mathrm{erf}\,\beta)$ which appears in the gain expression. The parameter β is defined by

$$\beta = \frac{\gamma_a+\gamma_b}{\Delta\omega_D}\sqrt{\ln 2} \tag{41}$$

We assume that the lower level does not decay, then $\gamma_b = 0$ and (41) can be written

$$\beta = \frac{\sqrt{\ln 2}}{\tau_s\,\Delta\omega_D}\,. \tag{42}$$

Using the above results and the assumption that the beam intercepts the target at 45 degrees, we have calculated the values of ΔE and $e^{\beta^2}(1-\mathrm{erf}\,\beta)$ to be used in calculating the gain for the charge-transfer reactions under consideration. These data are presented in Table 3-4.

TABLE 3-4. Parameters Involving Doppler and Energy Spreads Arising from Charge-transfer Collisions[a]

	He^{++},H	He^{+},Cs	Ne^{+},K	Ar^{+},Cs	H^{+},Cs	Hg^{+},Cs
$\sqrt{Q}$ (10^{-7}cm)	.71	1.22	1.0	.84	1.0	.77
ΔE (eV)	17	10	12	14	12	16
$\Delta\omega_D$ (10^{10}sec^{-1})	7.0	8.4	1.6	2.6	13.4	.125
β	.099	.0165	.0288	.0133	.00246	.462
$e^{\beta^2}(1-\mathrm{erf}\,\beta)$	.89	.98	.97	.98	1.0	.53

[a]The longitudinal energy spread in the ion beam is assumed to be negligible. In practice, for a duoplasmatron-type ion source, the spread is typically a few eV.

Calculated Gains

Finally, we tabulate the results of the preceding sections and calculate a gain per cm per unit current density for each of the charge-transfer reactions. These data are presented in Table 3-5. The ratio g/J is calculated according to

$$\frac{g}{J} = \frac{\xi \, \Delta E_m}{\Delta E} \, e^{\beta^2} (1 - \mathrm{erf}\, \beta) \tag{43}$$

which measures the relative gains of the various reactions for a given current density. We note the exceptionally high gain for Hg^+ + Cs compared to the other reactions. In general, the charge transfers yielding shorter-wavelength transitions have the lower linear gain per current density

The above analysis shows how the gain scales linearly with the ion current density. The problem of obtaining gain is, consequently, directly related to the problem of focusing a suitable ion current density on the target. In the following chapters we examine the factors which limit ion beam focusing.

TABLE 3-5. Factors Used in Calculating Gain

	He^{++},H	He^{+},Cs	Ne^{+},K	Ar^{+},Cs	H^{+},Cs	Hg^{+},Cs
ξ (eV-cm-A^{-1})	.41	1.0	3.9	17.	.66	774
ΔF_m	.18	.17	.23	.23	.69	.93
ΔE(eV)	17	10	12	14	12	16
	.89	.98	.97	.98	1.0	.53
g/J (cm-A^{-1})	.0049	.017	.072	.28	.039	23.

CHAPTER 4

EFFECTS OF SPACE CHARGE AND THERMAL VELOCITIES ON BEAM FOCUSING

There are two important effects which limit the size to which a ion beam can be focused. These are the effects of space charge and transverse thermal velocities. These effects are both present in any ion beam, but their relative importance can vary.

In this chapter we present a general discussion of space charge and thermal velocities. (The following two chapters will examine their effects in two particular ion beam focusing schemes.) We begin with the simple model of a cylindrical ion beam and show how the effects of space charge and thermal velocities can be compared in terms of the equivalent optical focal length of the "lens" system. Next, we review the use of Liouville's theorem in obtaining Langmuir's limiting current density. We present a calculation of the longitudinal velocity spread based upon Liouville's theorem. Finally, we review the concepts of beam emittance and brightness.

Space Charge in a Cylindrical Beam

Consider a cylindrical ion beam whose ions are moving along the z-axis with a constant velocity v_z. The ions will experience an outward radial force due to the electric field of the beam itself. By using Gauss' law and assuming cylindrical symmetry, we can calculate the electric field at a radius r:

$$\epsilon_0 \oint \vec{E} \cdot d\vec{A} = Q(r) \tag{1}$$

where Q(r) is the charge enclosed by the surface integral. For a length l of the beam, Equation (1) can be written

$$\begin{aligned} 2\pi \epsilon_0 E r l &= l \int_0^r \rho \pi r^2 dr \\ &= \frac{l}{v_z} \int_0^r J \pi r^2 dr \\ &= \frac{l}{v_z} I(r) \end{aligned} \tag{2}$$

so

$$E = \frac{I(r)}{2\pi \epsilon_0 v_z r} \tag{3}$$

We assume laminar flow, so the current enclosed by each ion's path remains constant. Then I(r) in (3) is a constant for a particular ion, and (3) can be used to obtain the equation of motion for the ion. Consider an ion at the edge of the beam. If I is the total current in the beam, at the edge of the beam

$$E = \frac{I}{2\pi\epsilon_0 v_z} \cdot \frac{1}{r} \tag{4}$$

$$= \frac{K}{r} \tag{5}$$

where

$$K \equiv \frac{I}{2\pi\epsilon_0 v_z} \tag{6}$$

From (5), the electrostatic potential ϕ may be obtained.

$$\frac{\partial \phi}{\partial r} = -E$$
$$= -K/r$$

$$\phi = -K \ln r + \text{const.} \tag{7}$$

By applying conservation of energy to the ion's path, we obtain

$$\frac{1}{2} m \dot{r}^2 - qK \ln r = \frac{1}{2} m \dot{r}_0^2 - qK \ln r_0 \tag{8}$$

where the subscript zero refers to the values taken at some reference time. Using η to denote q/m, (8) can be written

$$\dot{r}^2 - 2\eta K \ln r = \dot{r}_0^2 - 2\eta K \ln r_0 \tag{9}$$

Equation 9 can be integrated to obtain the equation of motion for the ion, but at this point we need not do that. We can examine the focusing effect of a "lens" as follows. We assume that r_o and $\dot{r}_o$ are the values for the outer radius of the beam just when it emerges from the lens. The effect of the lens causes all ions in the beam to be moving radially inward. The beam radius will shrink until it reaches some minimum value r_m, and then it will expand. At the minimum radius $\dot{r} = 0$, so (9) gives

$$\ln \frac{r_o}{r_m} = \frac{\dot{r}_o^2}{2\eta K} \tag{10}$$

or

$$\frac{r_m}{r_o} = e^{-\dot{r}_o^2/2\eta K} \tag{11}$$

It is informative to express (11) in terms of the equivalent optical focal length f of the lens. The effect of an ideal lens is to give each ion an inward radial velocity which is proportional to the ion's distance from the axis. That way, in the absense of other perturbations all ions cross the axis at the focal point of the lens. This equivalent optical focal length may be obtained by noting that after passing through the lens, the time it takes an ion to reach the axis is equal to the time it takes to reach the focal point; i.e.,

$$\frac{r_o}{\dot{r}_o} = \frac{f}{v_z} \tag{12}$$

Hence

$$\dot{r}_o = \frac{v_z r_o}{f} \tag{13}$$

We put (13) into (11) to obtain

$$\frac{r_m}{r_o} = \exp\left[\frac{-v_z^2}{2\eta K} \cdot \left(\frac{r_o}{f}\right)^2\right] \tag{14}$$

or

$$R_m = \exp\left[\frac{-v_z^2}{2\eta K} \cdot \frac{1}{F^2}\right] \tag{15}$$

where we define the unitless radius and focal length by

$$R_m \equiv r_m/r_o$$

$$F \equiv f/r_o \tag{16}$$

Equation (15) shows the important result that the focused size of the beam depends upon the effective optical focal length. The shorter the focal length, the tighter the beam is focused. Conversely, tight focusing cannot be obtained from long focal lengths.

Transverse Thermal Velocities

In this section we neglect the effect of space charge and consider only the effect of having a velocity spread transverse to the direction of beam travel. This spread arises in the ion source where there is an unavoidable thermal spread in ion velocities.

Consider a particular transverse cross section of the beam which exits an ideal lens at time t = 0. The position of the lens is z = 0, and the beam is moving in the positive z-direction. We shall use a statistical approach in calculating the effect of the transverse velocities. We consider the equation of motion for the x-component of an ion's position and velocity. Because of rotational symmetry about the z-axis, the equations in the x and y directions will be identical. The equation of motion for the x coordinate is

$$x = x_0 + \dot{x}_0 t \tag{17}$$

where x_0 and $\dot{x}_0$ are the position and velocity upon exiting the lens. We square (17) and take the average for the whole assembly of ions in the cross-section.

Then

$$\langle x\rangle^2 = \langle x_0\rangle^2 + 2\langle x_0\dot{x}_0\rangle t + \langle\dot{x}_0\rangle^2 t^2 \tag{18}$$

is the equation of motion for the mean-squared x-coordinate. We consider the beam to be focused when $\langle x^2\rangle$ reaches a minimum value $\langle x^2 \rangle_m$ at t_m, which we find by minimizing $\langle x^2 \rangle$ with respect to t.

$$\frac{d}{dt}\langle x^2 \rangle = 2\langle x_o \dot{x}_o \rangle + 2\langle \dot{x}_o^2 \rangle t_m = 0 \tag{19}$$

or

$$t_m = -\frac{\langle x_o \dot{x}_o \rangle}{\langle \dot{x}_o^2 \rangle} \tag{20}$$

We use this value of t_m in (18) to obtain

$$\langle x^2 \rangle_m = \langle x_o^2 \rangle - \frac{\langle x_o \dot{x}_o \rangle^2}{\langle \dot{x}_o^2 \rangle} \tag{21}$$

This equation gives the focused size of the beam in the x-direction in terms of average values of quantities upon exiting the lens. We want to know how the focused size depends upon the size and velocity spread upon entering the lens. Let x_1 and $\dot{x}_1$ be the x-coordinate and velocity of an ion at the time of entrance into the lens. In the thin lens approximation the position of an ion is not changed by the lens, so $x_1 = x_o$. The velocity, however, is changed by the lens so that

$$\dot{x}_o = \dot{x}_1 - Ax_1 \tag{22}$$

The proportionality constant A is related to the equivalent optical focal length by

$$A = \frac{\sigma_z}{f} \tag{23}$$

We square (22) and take the average over the beam cross-section as before:

$$\langle \dot{x}_0^2 \rangle = \langle \dot{x}_1^2 \rangle - 2A\langle x_1 \dot{x}_1 \rangle + A^2 \langle x_1^2 \rangle \tag{24}$$

From (22) we can also obtain

$$\langle x_0 \dot{x}_0 \rangle = \langle x_1 \dot{x}_1 \rangle - A \langle x_1^2 \rangle \tag{25}$$

by using the thin lens approximation. We put (24) and (25) into (21) and use $x_o = x_1$ to obtain

$$\langle x^2 \rangle_m = \langle x_1^2 \rangle - \frac{\left[\langle x_1 \dot{x}_1 \rangle - A \langle x_1^2 \rangle \right]^2}{\langle \dot{x}_1^2 \rangle - 2A\langle x_1 \dot{x}_1 \rangle + A^2 \langle x_1^2 \rangle} \tag{26}$$

We assume that prior to entering the lens x_1 and $\dot{x}_1$ are uncorrelated. Then

$$\langle x_1 \dot{x}_1 \rangle = \langle x_1 \rangle \langle \dot{x}_1 \rangle \tag{27}$$

$$= 0 \tag{28}$$

which follows since both $\langle x_1 \rangle$ and $\langle \dot{x}_1 \rangle$ are zero by symmetry. Now (26) becomes

$$\langle x^2 \rangle_m = \langle x_1^2 \rangle - \frac{A^2 \langle x_1^2 \rangle^2}{\langle \dot{x}_1^2 \rangle + A^2 \langle x_1^2 \rangle}$$

$$= \langle x_1^2 \rangle \left[1 - \frac{A^2 \langle x_1^2 \rangle}{\langle \dot{x}_1^2 \rangle + A^2 \langle x_1^2 \rangle} \right]$$

$$= \frac{\langle x_1^2 \rangle \langle \dot{x}_1^2 \rangle}{\langle \dot{x}_1^2 \rangle + A^2 \langle x_1^2 \rangle} \tag{29}$$

We now have an expression for the focused size of the beam in terms of: beam size $\langle x_1{}^2 \rangle$ when entering the lens, velocity spread $\langle \dot{x}_1{}^2 \rangle$ when entering the lens, and focal length of the lens. In the limit of tight focusing

$$\langle x^2 \rangle_m \ll \langle x_1^2 \rangle \tag{30}$$

which from (29) means that

$$A^2 \langle x_1^2 \rangle \gg \langle \dot{x}_1^2 \rangle \tag{31}$$

Then (29) becomes for tight focusing

$$\langle x^2 \rangle_m \simeq \frac{\langle \dot{x}_1^2 \rangle}{A^2} \tag{32}$$

We use the definition of A to write

$$\langle x^2 \rangle_m = \frac{\langle \dot{x}_1^2 \rangle}{v_z^2} f^2 \tag{33}$$

An identical equation applies to the y-component of motion, so it is easy to see that the radial component satisfies

$$\langle r^2 \rangle_m = \frac{\langle \dot{r}_1^2 \rangle}{v_z^2} f^2 \tag{34}$$

The root-mean-square radius of the focused beam is then

$$\langle r^2 \rangle_m^{1/2} = \frac{\langle \dot{r}_1^2 \rangle^{1/2}}{v_z} f \tag{35}$$

We see that the RMS focused spot size increases linearly with the equivalent optical focal length.

The position along the z-axis at which the RMS radius of the beam is the smallest is given by

$$\begin{aligned} z_m &= v_z t_m \\ &= \frac{v_z A \langle x_1^2 \rangle}{\langle \dot{x}_1^2 \rangle + A^2 \langle x_1^2 \rangle} \end{aligned} \tag{36}$$

In the limit of tight focusing

$$z_m \simeq \frac{v_z}{A} \simeq f \tag{37}$$

Otherwise, the focused RMS radius is not quite at the equivalent optical focal point.

If we assume that the ion velocity distribution is Maxwellian with temperature T, then

$$\frac{1}{2} m \langle \dot{r}_1^2 \rangle = kT \tag{38}$$

and by (35) the RMS focused radius is

$$\langle r^2 \rangle_m^{1/2} = \left(\frac{2kT}{m} \right)^{1/2} \frac{f}{v_z} \tag{39}$$

We now go back to (31) which gives the requirement for tight focusing as

$$A^2 \langle x_1^2 \rangle \gg \langle \dot{x}_1^2 \rangle$$

or in terms of the radial components and the definitions of **A**

$$\frac{v_z^2}{f^2} \langle r_1^2 \rangle \gg \langle \dot{r}_1^2 \rangle \tag{40}$$

which can be written

$$\frac{f}{\langle r_1^2 \rangle^{1/2}} \ll \frac{v_z}{\langle \dot{r}_1^2 \rangle}$$

$$\ll v_z \left(\frac{m}{2kT} \right)^{1/2} \tag{41}$$

For example, consider a 1 keV(2.2×10^7cm/sec) helium ion beam at a temperature of kT = 10eV. For these values the right side of (41) is equal to 10, i.e., the focal length must be considerably less than ten times the pre-lens radius of the beam in order for the tight-focus approximation to hold.

We define dimensionless values of the focused RMS radius and the focal length in units of the initial RMS radius of the beam:

$$R_m \equiv \frac{\langle r^2 \rangle_m^{1/2}}{\langle r_1^2 \rangle^{1/2}}$$

$$F \equiv \frac{f}{\langle r_1^2 \rangle^{1/2}}$$

Then (39) can be written

$$R_m = \left(\frac{2kT}{m} \right)^{1/2} \frac{F}{v_z} \tag{42}$$

which shows how the focused radius and focal length are related.

Comparison of Space Charge and Transverse Thermal Velocity Focusing Limitations

Considering the effects of space charge only, the focused radius of the beam was shown to be

$$R_m = \exp\left[-\frac{\sigma_z^2}{2\eta k}\cdot\frac{1}{F}\right] \tag{43}$$

while the effect of transverse thermal velocities limits the focused radius to a value given by

$$R_m = \left(\frac{2kT}{m}\right)^{1/2}\cdot\frac{F}{\sigma_z} \tag{44}$$

In order to compare these two effects we shall assume some representative values for the beam parameters and make a graph of R_m versus F. In Figure 4-1 we have plotted Equation (43) for 10mA and 100mA of beam current and Equation (44) for 1eV and 10eV in temperatures. The beam is assumed to be composed of 25 keV(1.1×10^8cm/sec)He^{++} ions. By examining the curves, we can see the focal length at which space charge dominates in determining the focused radius, and we can see where thermal velocities dominate. For example, for a beam which has a current of 100mA and a temperature of 10eV, the figure shows that for F less than 1.2, the focused radius will be limited mostly by beam temperature. For F

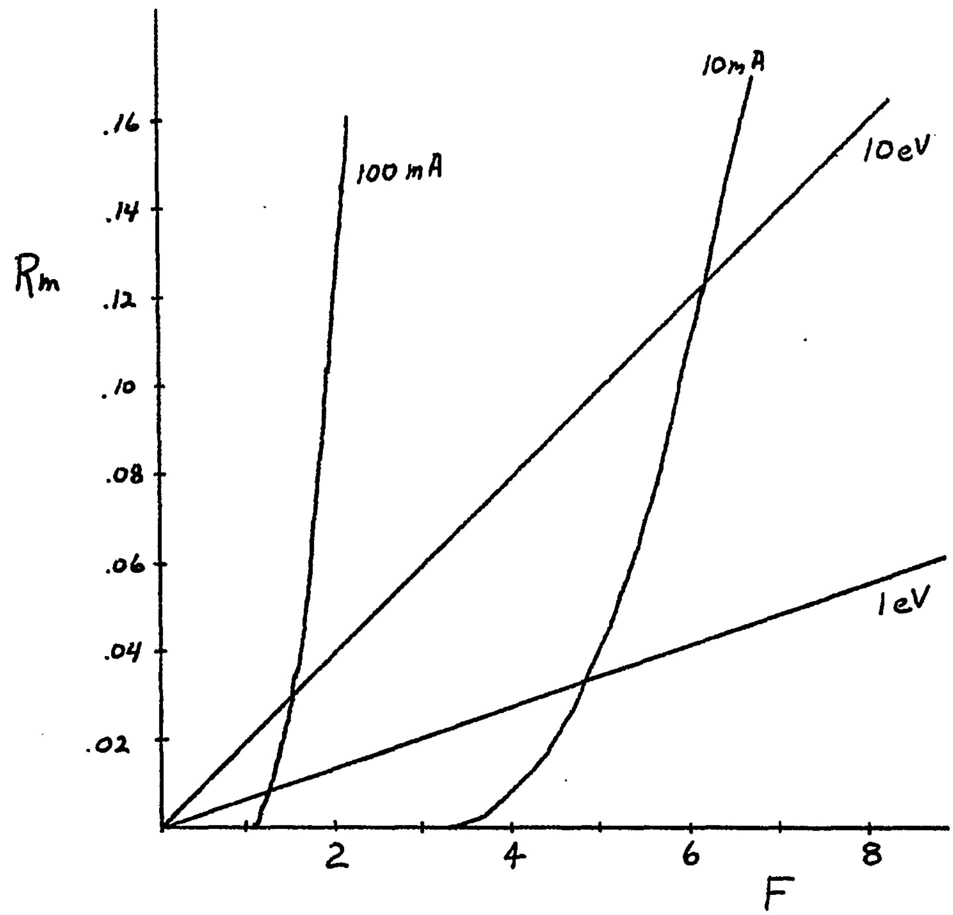

FIGURE 4-1. Comparison of Space Charge and Thermal Limitations for Focusing a 25keV He^{++} Beam.

Each curve shows how the focused radius increases with lens focal length. The 10mA and 100 mA curves were calculated considering only space charge. The 1eV and 10eV curves were calculated considering only beam temperature.

greater than 1.2, space charge will be more important in determining the focused size. The 100mA and 10eV curves cross at $F \cong 1.3$, but we see that the large slope of the 100mA curve at the point causes either space charge or beam temperature to be almost negligible at values of F not very far from 1.3. In order to determine the focused radius in the small region near $F = 1.3$, it is necessary to take space charge and beam temperature into account simultaneously, since both effects are comparable at that focal length. It is important to note that at short focal lengths focusing is limited mostly by beam temperature, while at long focal lengths focusing is space-charge limited.

Figure 4-2 shows a similar plot for a 10mA He^+ ion beam traveling at 3×10^7 cm/sec(1.9 keV). Figure 4-2 is plotted on the same scale as Figure 4-1 in order to show the dramatic effect of lower beam velocity on focusing. Much shorter focal lengths are required for the slower He^+ beam than for faster He^{++} beam in order to get comparable focusing.

By analyzing the effects of space charge and ion temperature separately we have been able to show that one or the other, depending upon the focal length, may predominate. The region where both are comparable is rather small, so that in practice it is quite likely that one or the other may be neglected to a first approximation when estimating the focused beam size. We have also shown that the size of

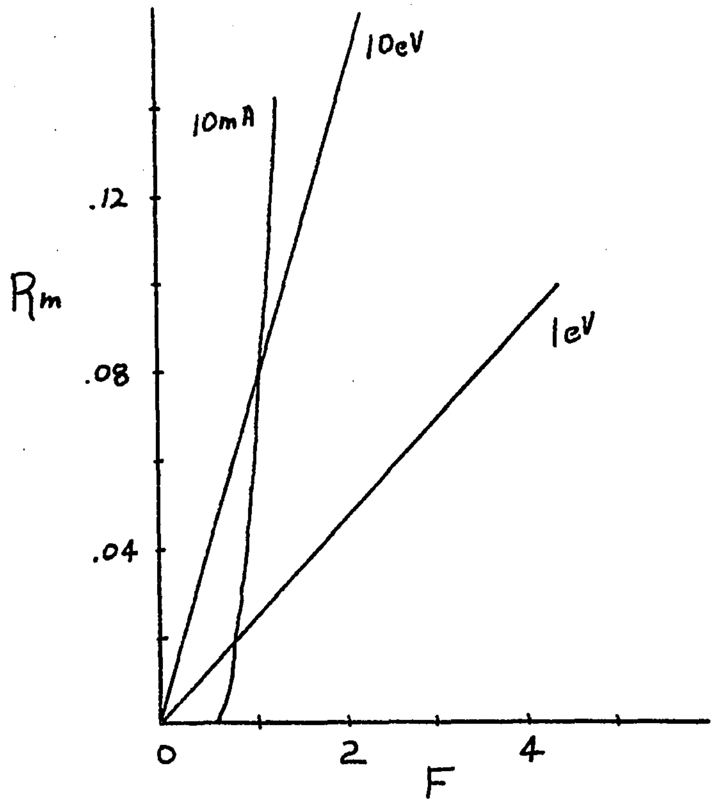

FIGURE 4-2. Comparison of Space Charge and Thermal Limitations for Focusing a 1.9 keV He^+ Beam.

The scale has been chosen to be the same as for Fig. 4-1 in order to show how the efforts of lower beam energy make focusing more difficult.

the focused beam depends upon the equivalent optical focal length of the ion focusing system. A tightly focused beam requires a short focal length.

Some Consequences of Liouville's Theorem

Transverse thermal velocities present in an ion beam provide a fundamental limitation on how well the beam can be focused (Wilson and Brewer 1973, p. 143). By describing the beam in terms of a volume in phase space, Liouville's theorem can be used to show that there is a maximum current density to which a beam can be focused. The phase-space description of the beam gives rise to the concept of emittance, which is essentially an area occupied by the beam in phase space. As a consequence of Liouville's theorem, the emittance is a constant of the motion for a drifting beam.

In the following sections we examine Liouville's theorem and show how it pertains to ion beam focusing.

Liouville's Theorem

The position and momentum of each particle in a beam can be described by a point in six-dimensional phase space. The number of particles remains constant, so the equation of continuity for the six-dimensional particle density ρ and the six-dimensional particle current density $\vec{j}$ is

$$\frac{\partial \rho}{\partial t} + \nabla \cdot \vec{j} = 0 \tag{45}$$

Equation (45) also applies to the assembly of points in a given two-dimensional plane of coordinate q and canonical momentum p. In this case p becomes the areal density of points and $\vec{j} = (j_q, j_p)$. Then

$$\nabla \cdot \vec{j} = \frac{\partial}{\partial q} j_q + \frac{\partial}{\partial p} j_p \tag{46}$$

$$= \frac{\partial}{\partial q}(\rho \dot{q}) + \frac{\partial}{\partial p}(\rho \dot{p}) \tag{47}$$

From (45) and (47)

$$\frac{\partial \rho}{\partial t} = -\rho\left(\frac{\partial \dot{q}}{\partial q} + \frac{\partial \dot{p}}{\partial p}\right) - \dot{q}\frac{\partial \rho}{\partial q} - \dot{p}\frac{\partial \rho}{\partial p} \tag{48}$$

If the particles do not interact then the motion of a particular particle is described by the Hamilton equations of motion,

$$\dot{q} = \frac{\partial H}{\partial p} \qquad \dot{p} = -\frac{\partial H}{\partial q} \tag{49}$$

from which

$$\frac{\partial \dot{q}}{\partial q} = \frac{\partial^2 H}{\partial q \partial p} \qquad \frac{\partial \dot{p}}{\partial p} = -\frac{\partial^2 H}{\partial p \partial q} \tag{50}$$

The use of (50) in (48) gives

$$\frac{\partial \rho}{\partial t} = -\dot{q}\frac{\partial \rho}{\partial q} - \dot{p}\frac{\partial \rho}{\partial p} \tag{51}$$

As we move along with a given particle, the time rate of charge of the areal density in the neighborhood of the particle is given by

$$\frac{d\rho}{dt} = \frac{\partial \rho}{\partial t} + \frac{\partial \rho}{\partial p}\dot{p} + \frac{\partial \rho}{\partial q}\dot{q} \tag{52}$$

The use of (51) in (52) then gives

$$\frac{d\rho}{dt} = 0 \tag{53}$$

which says that the areal density in the neighborhood of the particle as it moves along remains constant in time. This leads to the conclusion that the total area occupied by the particles in the q-p plane remains constant. Since this argument can be applied in each of the 3 q-p planes, it follows that the particle density in the neighborhood of a particular particle remains constant all along its trajectory in the six-dimensional phase space.

Langmuir's Limiting Current Density

The presentation here follows that of Pierce (1954, Chapter 8). Let $f(\vec{r}, \vec{v})$ be the particle density in the six-dimensional $(\vec{r}, \vec{v})$ phase space. If the particles are not subjected to a velocity-dependent potential, the cartesian coordinates and momenta are canonical. Consequently, as a result of Liouville's theorem, $f(\vec{r}, \vec{v})$ remains constant in the neighborhood of a particle as it moves through phase space.

Consider an infinite plane which emits ions which have a Maxwellian velocity distribution. The emitting surface is taken to be at zero potential. If v_o is the velocity of emission, at the surface the distribution function is given by

$$f(\vec{r}, \vec{v}) = K e^{-mv_o^2/2kT} \tag{54}$$

where K is a proportionality constant which will be evaluated later. By conservation of energy

$$\frac{1}{2} m v_o^2 = \frac{1}{2} m v^2 + q\varphi \tag{55}$$

where v is the velocity of the ion where it is at a potential φ with respect to the emitting surface.

By use of (55), Equation (54) becomes

$$f(\vec{r},\vec{v}) = K e^{-\alpha v^2 - \beta \varphi} \tag{56}$$

where

$$\alpha \equiv \frac{m}{2kT} \tag{57}$$

$$\beta \equiv \frac{q}{kT} \tag{58}$$

The number of ions per unit cell of phase space is

$$dn = f(\vec{r},\vec{v})\, d^3r\, d^3v \tag{59}$$

from which the number of ions per unit volume in coordinate space with velocities between $\vec{v}$ and $\vec{v} + d\vec{v}$ is seen to be given by

$$d\rho = f(\vec{r},\vec{v})\, d^3v \tag{60}$$

Consider a cylindrical ion beam traveling along the z-axis. The current density in the z-direction is given by

$$J = \int v_z f(\vec{r},\vec{v})\, d^3v \tag{61}$$

which by (56) can be written

$$J = K \int v_z e^{-\alpha v^2 - \beta \Phi} \tag{62}$$

To evaluate K we consider the current density J_o at the emitter ($\Phi = 0$) which according to (62) is given by

$$\begin{aligned} J_o &= K \int v_z e^{-\alpha v_z^2} d^3v \\ &= K \int_0^\infty v_z e^{-\alpha v_z^2} dv_z \int_{-\infty}^{\infty} e^{-\alpha v_x^2} dv_x \int_{-\infty}^{\infty} e^{-\alpha v_y^2} dv_y \\ &= K \cdot \frac{1}{2\alpha} \cdot \sqrt{\frac{\pi}{\alpha}} \cdot \sqrt{\frac{\pi}{\alpha}} \\ &= \frac{K\pi}{2\alpha^2} \end{aligned} \tag{63}$$

K may be expressed in terms of the current density at the emitter,

$$K = \frac{2\alpha^2}{\pi} J_o \tag{64}$$

Now assume that the beam has passed through a lens so that the trajectory of an outer ion makes an angle ϑ with the z-axis. We calculate J at the point of convergence. Switch to spherical coordinates in velocity space (v, φ, θ) so that $v_z = v\cos\theta$. The focused current density J_f is given by

$$J_f = J_0 \frac{2\alpha^2}{\pi} e^{-\beta\phi} \int_{\sqrt{\frac{-\beta\phi}{\alpha}}}^{\infty} v^3 e^{-\alpha v^2} dv \int_0^{\vartheta} \cos\theta \sin\theta \, d\theta \times \int_0^{2\pi} d\varphi \tag{65}$$

The θ integration gives $\frac{1}{2}\sin^2\vartheta$. The lower limit on the v integration comes from conservation of energy:

$$\alpha v^2 = \alpha v_0^2 - \beta\phi \tag{66}$$

The lower limit on the v integration corresponds to the minimum value of v_0, which is zero. Hence the lower limit is $\sqrt{\frac{-\beta\phi}{\alpha}}$. The value under the radical is positive since ϕ will be negative if the ion charge (and hence β) is positive.

Now consider the v integration. With the substitution $u = \alpha v^2$ we have

$$\begin{aligned} \int v^3 e^{-\alpha v^2} dv &= \int \left(\frac{u}{\alpha}\right)^{3/2} e^{-u} \frac{du}{2\alpha (u/\alpha)^{1/2}} \\ &= \frac{1}{2\alpha^2} \int u e^{-u} du \\ &= \frac{1}{2\alpha^2}\left(-u e^{-u} + \int e^{-u} du\right) \end{aligned} \tag{67}$$

then
$$\int_{(-\beta\varphi/\alpha)^{1/2}}^{\infty} dv\, v^3 e^{-\alpha v^2} = \frac{1}{2\alpha^2}\left[-u e^{-u} - e^{-u}\right]_{-\beta\varphi}^{\infty}$$

$$= \frac{e^{\beta\varphi}}{2\alpha^2}\,(1-\beta\varphi) \qquad (\beta\varphi<0) \tag{68}$$

where we note that $\beta\varphi$ is a negative quantity. Using the above results, (65) becomes

$$J_f = J_o\,(1-\beta\varphi)\sin^2\vartheta \tag{69}$$

which gives the upper limit for the current density at the focus of an ideal ion lens. This bounding expression is a theoretical limit based upon perfect focusing and an infinite plane emitting surface.

For a hollow cylindrical beam whose outer and inner radii are converging with angles ϑ_2 and ϑ_1, respectively, it is easy to see that

$$J_f = J_o\,(1-\beta\varphi)(\sin^2\vartheta_2 - \sin^2\vartheta_1) \tag{70}$$

Example: Solid Cylindrical Beam. As an example we assume that

$$-q\phi = 10 \text{ keV}$$
$$kT = 10 \text{ eV}$$
$$\vartheta = 45^\circ \tag{71}$$

so

$$-\beta\phi = -\frac{q\phi}{kT} = 10^3$$

then

$$J_f/J_0 = (1+10^3)\cdot\frac{1}{2}$$
$$\approx 500 \tag{72}$$

In this particular example the upper limit for the focused density is 500 times the current density at the source.

Example: Hollow Cylindrical Beam. Consider a hollow beam with ions converging on the axis between the angles ϑ_1, for the inner radius and ϑ_2 for the outer radius. If we assume a thin-walled beam, then we can let

$$\vartheta_2 = \vartheta + \frac{\delta\vartheta}{2}$$
$$\vartheta_1 = \vartheta - \frac{\delta\vartheta}{2} \tag{73}$$

with $\delta\vartheta$ being small. Then

$$\sin^2\vartheta_2 - \sin^2\vartheta_1 \simeq 2\sin\vartheta\cos\vartheta\,\delta\vartheta \tag{74}$$

We next express (74) in terms of the wall thickness δr.

In terms of the following figure

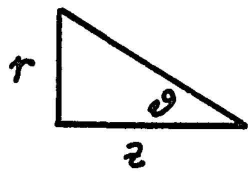

we see that

$$\frac{r}{z} = \tan\vartheta = \frac{\sin\vartheta}{\cos\vartheta} \tag{75}$$

for a fixed z,

$$\frac{\delta r}{z} = \frac{\cos^2\vartheta + \sin^2\vartheta}{\cos^2\vartheta} \cdot \delta\vartheta$$

$$= \frac{\delta\vartheta}{\cos^2\vartheta} \tag{76}$$

We solve (75) for z and put the result into (76) to obtain

$$\frac{\delta r}{r} = \frac{\delta\vartheta}{\cos^2\vartheta} \cdot \frac{1}{\tan\vartheta}$$

$$= \frac{\delta\vartheta}{\sin\vartheta\cos\vartheta} \tag{77}$$

We combine (74) and (77) to obtain

$$\sin^2\vartheta_2 - \sin^2\vartheta_1 \simeq 2\sin^2\vartheta\cos^2\vartheta\,\frac{\delta r}{r}$$

$$\simeq \frac{1}{2}\sin^2 2\theta \cdot \frac{\delta r}{r} \tag{78}$$

We use (78) in (70) to obtain

$$J_\delta/J_0 \cong \frac{1}{2}\left(1-\beta\phi\right)\frac{\delta r}{r}\sin^2 2\vartheta \tag{79}$$

To evaluate (79) we shall assume:

$$\frac{\delta r}{r} = 0.1 \qquad -q\phi = 10\ \text{keV}$$

$$\vartheta = 45^\circ \qquad kT = 10\ \text{eV}$$

Then from (79) we have

$$\begin{aligned} J_\delta/J_0 &= \frac{1}{2}\left(1+10^3\right)(.1) \\ &\cong 50 \end{aligned} \tag{80}$$

which is one-tenth of the value obtained for the solid beam.

Spread in Longitudinal Velocities

By use of conservation of energy and Liouville's theorem, we can calculate the root-mean-square spread in the component of the ion velocity along the axis of the beam. The RMS velocity spread for a beam traveling along the z-axis is given by

$$\Delta v_z = \left[\langle v_z^2\rangle - \langle v_z\rangle^2\right]^{1/2} \tag{81}$$

The average values on the right side of (81) may be calculated by using the Maxwellian distribution function $f(\vec{r}, \vec{v})$ from (56). By Liouville's theorem this function is constant in the neighborhood of a particle as it moves in phase space. For the present discussion we can neglect the normalization factor and take

$$f(\vec{r},\vec{v}) = e^{-\alpha v^2 - \beta\Phi} \tag{82}$$

where α and β are defined by (57) and (58). We assume that the ions are emitted by the x-y plane and are accelerated in the z-direction by an electric field. We shall calculate average values of v_z and v_z^2 at a location where the potential is Φ with respect to the emitting surface.

First we calculate the average value of v_z.

$$\langle v_z \rangle = \int v_z f(\vec{r},\vec{v})\, d^3v \Big/ \int f(\vec{r},\vec{v})\, d^3v$$

$$= \frac{e^{-\beta\Phi}\int v_z e^{-\alpha v_z^2} dv_z \int e^{-\alpha v_y^2} dv_y \int e^{-\alpha v_x^2} dv_x}{e^{-\beta\Phi} \int e^{-\alpha v_z^2} dv_z \cdot \int e^{-\alpha v_y^2} dv_y \cdot \int e^{-\alpha v_x^2} dv_x} \tag{83}$$

$$= \frac{\int_{\sqrt{-\frac{\beta\Phi}{\alpha}}}^{\infty} v_z e^{-\alpha v_z^2} dv_z}{\int_{\sqrt{-\frac{\beta\Phi}{\alpha}}}^{\infty} e^{-\alpha v_z^2} dv_z} \tag{84}$$

The lower limit on v_z arises from the conservation of energy. As discussed previously, we note that $\beta\Phi$ is inherently negative. As a simplification, we define a dimensionless potential ψ,

$$\psi \equiv -\beta\Phi = \frac{-q\Phi}{kT} \tag{85}$$

which is a positive quantity. If we let $u = \alpha v_z^2$, then the denominator of (84) may be written as

$$\int_{\sqrt{\psi/\alpha}}^{\infty} e^{-\alpha v_z^2} dv_z = \frac{1}{2\sqrt{\alpha}} \int_{\psi}^{\infty} u^{-1/2} e^{-u} du \tag{86}$$

The integral on the right side of (86) can be expressed as a series by successively integrating by parts:

$$\begin{aligned} \int_{\psi}^{\infty} u^{-1/2} e^{-u} du &= -u^{-1/2} e^{-u} \Big|_{\psi}^{\infty} - \frac{1}{2} \int_{\psi}^{\infty} u^{-3/2} e^{-u} du \\ &= \psi^{-1/2} e^{-\psi} - \frac{1}{2} \left[\psi^{-3/2} e^{-\psi} - \frac{3}{2} \int_{\psi}^{\infty} u^{-5/2} e^{-u} du \right] \\ &= \psi^{-1/2} e^{-\psi} - \frac{1}{2} \psi^{-3/2} e^{-\psi} + \frac{3}{4} \Big[\psi^{-5/2} e^{-\psi} \\ &\qquad - \frac{5}{2} \int_{\psi}^{\infty} u^{-7/2} e^{-u} du \Big] \\ &= \psi^{-1/2} e^{-\psi} \left(1 - \frac{1}{2} \psi^{-1} + \frac{3}{4} \psi^{-2} + \dots \right) \end{aligned} \tag{87}$$

For values of ψ much greater than unity, the series in (87) converges rapidly.

The numerator in (84) becomes

$$\int_{\sqrt{\psi/\alpha}}^{\infty} v_z e^{-\alpha v_z^2} dv_z = \frac{1}{2\alpha} \int_{\psi}^{\infty} e^{-u} du$$

$$= \frac{e^{-\psi}}{2\alpha} \tag{88}$$

We use the results of (87) and (88) to write

$$\langle v_z \rangle = \left(\frac{\psi}{\alpha}\right)^{1/2} \left(1 - \frac{1}{2}\psi^{-1} + \frac{3}{4}\psi^{-2} - \ldots\right) \tag{89}$$

To first order then

$$v_z \simeq \left(\frac{\psi}{\alpha}\right)^{1/2}$$

$$\simeq \left(\frac{-2q\phi}{m}\right)^{1/2} \tag{90}$$

Next we calculate the average value of v_z^2,

$$\langle v_z^2 \rangle = \frac{\int_{\sqrt{\psi/\alpha}}^{\infty} v_z^2 e^{-\alpha v_z^2} dv_z}{\int_{\sqrt{\psi/\alpha}}^{\infty} e^{-\alpha v_z^2} dv_z} \tag{91}$$

With the substitution $u = \alpha v_z^2$, the numerator of (91) becomes

$$\frac{1}{2\alpha^{3/2}}\int_{\psi}^{\infty} u^{1/2} e^{-u}\,du = \frac{1}{2\alpha^{3/2}}\left[\psi^{1/2}e^{-\psi} + \frac{1}{2}\int_{\psi}^{\infty} u^{-1/2}e^{-u}\,du\right] \tag{92}$$

We use (86) and (92) to rewrite (91) as

$$\langle v_z^2\rangle = \frac{\psi^{1/2}e^{-\psi} + \frac{1}{2}\int_{\psi}^{\infty} u^{-1/2}e^{-u}\,du}{\alpha\int_{\psi}^{\infty} u^{-1/2}e^{-u}\,du} \tag{93}$$

By use of (87), (93) can be written

$$\langle v_z^2\rangle = \frac{\psi}{\alpha}\left(1 - \frac{1}{2}\psi^{-1} + \frac{3}{4}\psi^{-2} - \ldots\right)^{-1} + \frac{1}{2\alpha} \tag{94}$$

We can now calculate the lowest order term in the mean-square deviation by using (89) and (94).

$$\begin{aligned}(\Delta v_z)^2 &= \langle v_z^2\rangle - \langle v_z\rangle^2 \\ &= \frac{\psi}{\alpha}\left(1 - \frac{1}{2}\psi^{-1} + \frac{3}{4}\psi^{-2}\ldots\right)^{-1} + \frac{1}{2\alpha} \\ &\quad - \frac{\psi}{\alpha}\left(1 - \frac{1}{2}\psi^{-1} + \frac{3}{4}\psi^{-2}\ldots\right)^{-2}\end{aligned}$$

$$\simeq \frac{\psi}{\alpha}\left(1+\frac{1}{2}\psi^{-1}-\frac{3}{4}\psi^{-2}\right)+\frac{1}{2\alpha}$$

$$-\frac{\psi}{\alpha}\left(1+\psi^{-1}-\frac{3}{2}\psi^{-2}\right)$$

$$\simeq \frac{3}{4\alpha\psi} = \frac{3}{2}\frac{(kT)^2}{m(-q\Phi)} \tag{95}$$

From (95) the RMS velocity spread is

$$\Delta v_z \simeq \left[\frac{3}{2m(-q\Phi)}\right]^{1/2} kT \tag{96}$$

We see that the spread in velocity actually decreases as Φ gets larger. In fact, conservation of energy in the case where $\langle v^2 \rangle$ is large compared to the initial velocity $\langle {v_o}^2 \rangle$ reduces to

$$\frac{1}{2} m \langle v^2 \rangle \simeq -q\Phi$$

which together with (96) shows that the RMS velocity spread is nearly proportional to the inverse of the RMS velocity. The velocity spread becomes smaller as the beam is accelerated.

We can show by a calculation similar to the above that the RMS velocity spread $(\Delta v_z)_o$ at the emitter itself

$(\alpha = 0)$ is given by

$$(\Delta v_z)_0 = \left(\frac{\pi - 2}{\pi} \cdot \frac{kT}{m} \right)^{1/2} \tag{97}$$

Emittance

The quality of an ion beam may be characterized in terms of its "emittance". As we shall show, the beam emittance is related to an area occupied by the beam in phase space. Consider an ion beam traveling along the z-axis from which we take a thin slice transverse to the direction of motion. The x-motion of each particle in this slice can be represented by a point on a plot of canonical coordinates (x, p_x). According to Liouville's theorem the total area occupied by the particles in the (x, p_x) plane will remain constant even though the shape of the area will change. If there are no velocity dependent forces in the x-direction, then $p_x = mv_x$, and for non-relativistic particles the size of the area occupied by the particles in the (x, p_x) plane will also remain constant.

As an example, suppose the beam is represented initially by a rectangle as in Figure 4-3a. It is easy to see that after a period of time, the shape will change to that in Figure 4-3b, which shows how the beam spreads out in

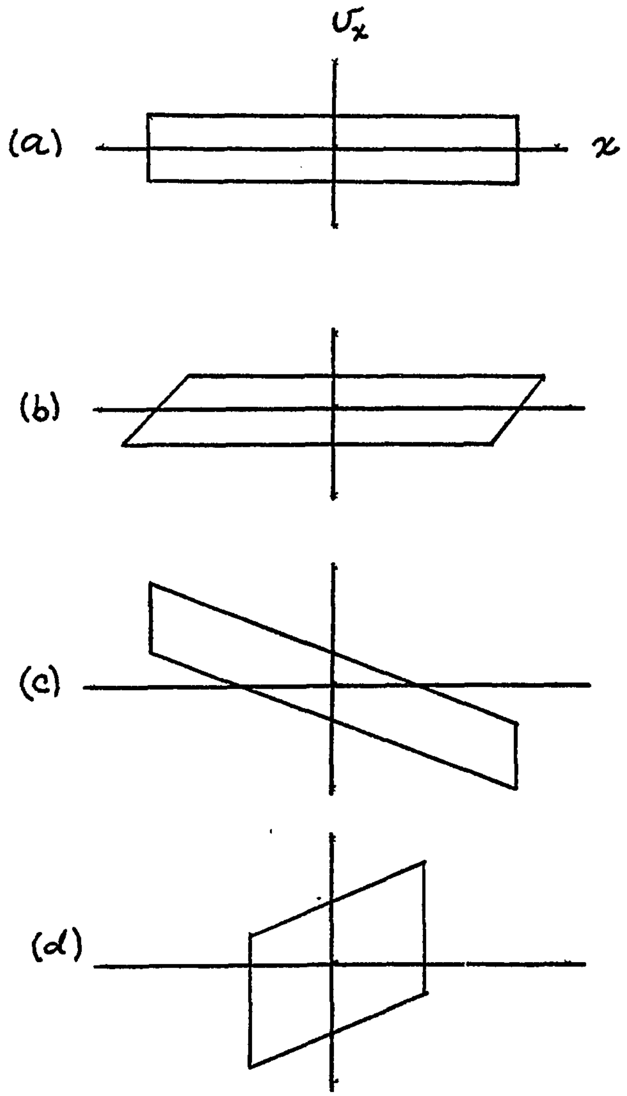

FIGURE 4-3. Emittance Diagrams

a) At t=0.
b) At some later time
c) After passing through a lens
d) When focused in the x-direction

the x-direction. The effect of a lens which focuses in the x-direction can be also shown on such a plot. The effect of an ideal thin lens is to change v_x by an amount proportional to x (without changing x). Hence, if Figure 4-3a represents the beam as it enters the lens, the beam as it emerges from the lens can be represented by Figure 4-3d shows that even the focused beam has a finite extent in the x-direction due to an initial velocity spread in that direction.

From each point of a transverse section of the ion beam there emanates a cone of ion trajectories. The slope of a trajectory in the x-z plane is given by

$$x' \equiv \frac{dx}{dz} = \frac{v_x}{v_z} \tag{98}$$

For the case where the beam velocity v_z is constant, the size of the area occupied by the ions in a (x,x') plot will remain constant as a result of Liouville's theorem. If we use $A(x,x')$ to denote the area occupied by a beam section in a(x,x')plot, then the emittance E of the beam is defined (Septier 1967, Vol. II, p. 150) by

$$E = \frac{A(x,x')}{\pi} \tag{99}$$

(If the beam is not cylindrical, an equivalent emittance can be defined for the y-direction). Hence, the emittance remains unchanged for a section of the beam drifting in the z-direction. The π appearing in the definition of the emittance is presumably used because the area $A(x,x')$ is often elliptical in shape, hence the emittance is then simply the product of the semi-major and semi-minor axes. The reason for defining the emittance in terms of an area in the (x,x') plane rather than in the (x,v_x) or (x,p_x) plane is that experimentally it is more easily measured. For example, a beam can be made to strike a metal plate which has small holes drilled along the beam diameter. Each hole acts like a point source for a conical beamlet. The mean slope and angular divergence of each beamlet can be measured as a function of distance from beam center.

A typical emittance diagram is shown in Figure 4-4. The usual units of x' are milliradians. The inner ellipse represents a high density in phase space and may contain $\sim$ 80% of the beam. The outer dotted line includes a larger percentage of the beam and shows the effect of aberrations in the ion optical system.

The area $A(x,x')$, and hence the emittance defined by (99), remains constant for a drifting beam or where the potential $\Phi(z)$ takes on the same values. In accelerated beams $A(x,x')$ varies, but the product $p_z A(x,x')$ is now

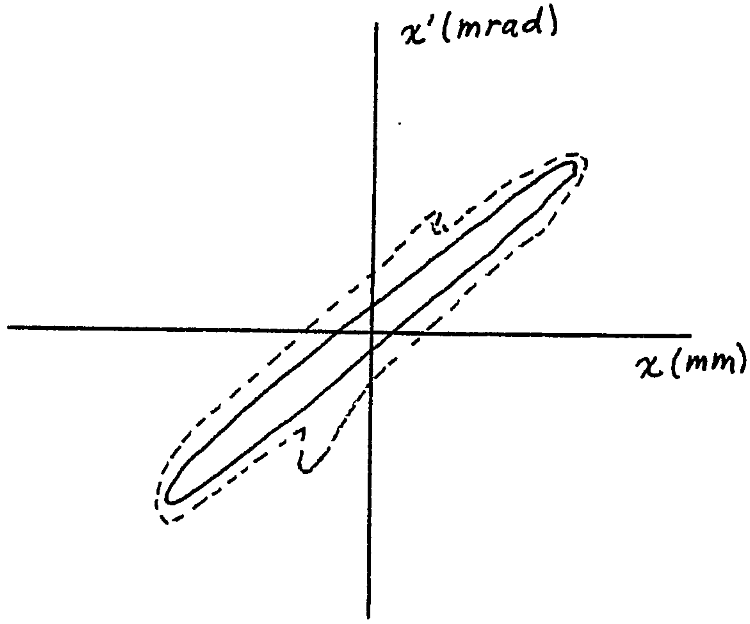

FIGURE 4-4. A Typical Emittance Diagram

invariant. This leads to the following definition of "normalized emittance".

$$E_n = \frac{p_z E}{mc} \tag{100}$$

$$= \beta\gamma E \tag{101}$$

$$= \frac{\beta\gamma}{\pi} A(x,x') \tag{102}$$

where β and γ are the usual relativistic factors.

This definition offers a way of comparing different ion sources and extraction systems. For a given ion current, the best source will have the smallest value of E_n. It is normalized emittance which is usually quoted in the literature.

It is possible to relate the normalized emittance to an equivalent transverse beam temperature as follows. Consider an emittance diagram which has a semimajor axis of length δx lying along the x-axis and a semiminor axis of length $\delta x'$ lying along the x'-axis. The normalized emittance from (102) is then

$$E_n = \beta\gamma\, \delta x\, \delta x' \tag{103}$$

Now

$$\delta x' = \frac{\delta v_x}{v_z} \tag{104}$$

and for a Maxwellian velocity distribution we can take

$$\delta v_x = \left(\frac{kT}{m}\right)^{1/2} \tag{105}$$

then

$$E_n = \frac{\gamma}{c}\,\delta x \left(\frac{kT}{m}\right)^{1/2}$$

or

$$kT = \frac{E_n^2}{(\delta x)^2} \cdot \frac{mc^2}{\gamma^2} \tag{106}$$

Equation (106) is useful, for example, for determining an equivalent transverse beam temperature for emittance data given in the literature. The normalized emittance is usually given along with an emittance diagram for a given beam energy. The semi-major axis can be estimated from the diagram. The value of γ is related to the beam kinetic energy by

$$\gamma^2 = 1 + \left(\frac{K.E.}{mc^2}\right)^2 \tag{107}$$

Brightness

In addition to emittance, the related concept of beam brightness is also used to describe the quality of an ion beam (Septier 1967, Vol. II, p. 152). Brightness is basically defined as the ion source current density per unit solid angle of beam divergence. For a point source which has a cone of divergence of half-angle α , the solid angle of divergence is approximately $\pi\alpha^2$ for small α . The brightness for a quasi-point source of area πr_0^2 is then given by

$$\beta = \frac{I}{\pi r_0^2 \cdot \pi \alpha^2} = \frac{I}{\pi^2 r_0^2 \alpha^2} \tag{108}$$

where I is the total current. For the case where the emittance diagram is an horizontal ellipse, we see that the denominator of (108) is proportional to the emittance squared. This leads to the definition of "normalized brightness"

$$\beta_n = \frac{2I}{\pi^2 E_n^2} \tag{109}$$

which is quoted in the literature for ion sources. The normalized brightness has the useful property of being invariant under acceleration or deacceleration of the ion beam.

In practice it has been found that the brightness decreases as the beam intensity is increased. This may be due to space charge effects, although the effect is not completely understood (van Steenbergen, 1965). The data presented by van Steenbergen (1965, Fig. 9) show that typically the normalized brightness for duoplasmatron sources varies from 10^9 to 10^8 mA-cm^{-2}-rad^{-2} for currents between 10 and 100 mA.

CHAPTER 5

DEFLECTION FOCUSING BY PLANE PARALLEL ELECTRODES

Because of the short life times ($\sim 10^{-10}$sec) of the excited electronic states created by the charge-transfer process, it is necessary to sweep the ion beam along the target at or near the velocity of light. In this way, the population inversion will travel along with the stimulated emission, and amplification can occur. McCorkle (1972) proposed a system in which an ion beam is sent lengthwise between the upper and lower plates of a parallel-plate transmission line. A voltage pulse of a few kilovolts applied to one end of the parallel plates will travel down the line with the velocity of light and will cause a traveling deflection of the ion beam toward the upper plate which houses the target material. The intersection of the beam with the target will thus travel with the velocity of light.

A modification of this scheme was proposed by Scully, Louisell, and McKnight (1973) in which the target is placed above the upper plate which contains a slot or grid to allow the deflected ions to pass through. This modification takes advantage of the focusing action which arises from the deflection. Ions at the bottom of the beam will attain a greater upward velocity than ions at the top of the beam and will catch up with them at some distance above the exit plate.

In this chapter we present an analysis of the focusing properties of the parallel plate deflection scheme by considering a) departures from ideal-lens focusing, 2) transverse thermal velocities, and c) space charge. We show that all three of these effects are important and must be taken into account, although their relative sizes will depend upon the particular system selected. Consider a plane geometry in which a sheet ion beam is initially traveling midway between two parallel plane electrodes as in Figure 5-1. We assume that the beam and the electrodes are infinite in the y-direction so that the problem is two-dimensional. The electrodes have a finite length along z, the direction of beam travel. At some time a voltage is applied across the electrodes at one of the ends. The voltage will travel down the electrodes with the velocity of light and cause an upward deflection of the ion beam. The upper electrode contains a grid which allows the ions to pass through. We examine the x-motion of the ions in a transverse section of the beam in terms of focusing, thermal velocities, and space charge. We assume that the beam is initially space-charge neutralized so that space-charge expansion is negligible prior to deflection. The deflection voltage will also strip away the neutralizing charges.

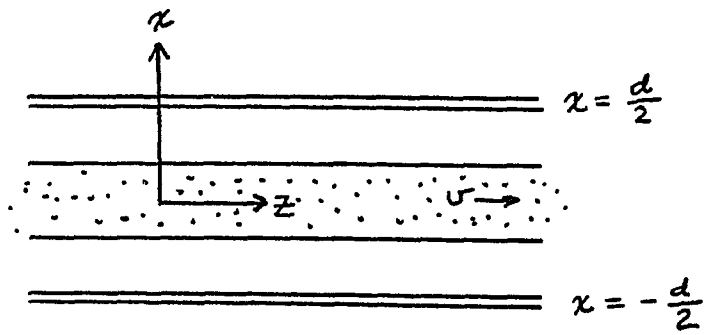

FIGURE 5-1. A Sheet Ion Beam Traveling between Planar Electrodes.

The ion beam will be deflected upward in the +x direction and through a grid in the upper electrode. If space charge is negligible, the beam comes to a focus at a distance above the top electrode equal to the plate separation d.

Focusing Condition

In this section we examine the focusing effect of the parallel plate deflection system neglecting the effects of space charge forces and ion thermal velocities. We consider the ions in a transverse section of the beam which meets the voltage V at a time taken to be t = 0. The equation of motion in the x-direction for an ion at a time t after meeting the voltage pulse is given by

$$x = \frac{\alpha}{2} t^2 + \dot{x}_0 t + x_0 \tag{1}$$

where

$$\alpha \equiv \frac{qV}{md} = \frac{\eta V}{d} \tag{2}$$

is the acceleration due to the electric field, and x_0 and $\dot{x}_0$ are the ion position and velocity at t = 0. For now we shall assume that $\dot{x}_0$ is zero. We choose our coordinate system such that the upper electrode is at $x = d/2$ and the bottom electrode is at $x = -d/2$. From (1) the time t_1 at which the ion reaches the upper electrode and exits the deflecting system is given by

$$t_1 = \left(\frac{d - 2x_0}{\alpha}\right)^{1/2} \tag{3}$$

The velocity $\dot{x}_1$ at exit will be given by

$$x_1 = \alpha t_1 \tag{4}$$

After exiting, the motion will be described by

$$x = \dot{x}_1 (t - t_1) + \frac{d}{2} \qquad (t > t_1) \tag{5}$$

from which

$$x(x_0, t) = \alpha t_1(x_0)\left[t - t_1(x_0)\right] + \frac{d}{2} \tag{6}$$

In (6) we have explicitly shown that x depends upon x_0 and t and that t_1 is a function of x_0.

Let δx be the difference in position at some time t between a particle which starts out at x_0 and one that starts out at the beam center $x = 0$:

$$\delta x(x_0, t) \equiv x(x_0, t) - x(0, t) \tag{7}$$

A Maclaurin series can be used to expand δx in terms of x_0:

$$\delta x(x_0, t) = \frac{dx}{dx_0}(0, t)\, x_0 + \frac{d^2 x}{dx_0^2}(0, t)\, x_0^2 + \ldots \tag{8}$$

The beam will be focused to first order in x_o when $\frac{dx}{dt_o}(o,t)$ is zero because $\delta x \cong 0$ for all x_o. All particles come together regardless of where they started.

We next find the condition for first order focusing. From (6) we find that

$$x'(x_o) = -\alpha t_1'(x_o)\left[2t_1(x_o) - t\right] \tag{9}$$

where the prime denotes differentiation with respect to x_o. First order focusing occurs when $x'(o) = 0$, which according to (9) means that the time t_f at which focusing occurs is

$$t_f = 2t_1(o) = 2\sqrt{\frac{d}{\alpha}} \tag{10}$$

When we let $x_o = 0$ and use (3) and (10) in (6), we find that the place where the beam comes to a focus is given by

$$x_f = \frac{3}{2}d \tag{11}$$

which is a distance d above the upper electrode.

Focusing Aberration

The deviation from perfect focusing may be estimated by considering the second term in the series in (8). The first term will be zero when $t = t_f$, so

$$\delta x(x_0, t_f) = \frac{d^2 x}{dx_0^2}(0, t_f)\, x_0^2 + \ldots \tag{12}$$

By differentiating (9) again with respect to x_0, we obtain

$$x''(0, t_f) = \alpha t_1''(0)\left[t_f - 2t_1(0)\right] - 2\alpha\left[t_1'(0)\right]^2 \tag{13}$$

The first term in brackets on the right of (13) is zero by the focusing condition (10), so

$$x''(0, t_f) = -2\alpha\left[t_1'(0)\right]^2 \tag{14}$$

From (3) we find that

$$t_1'(0) = (\alpha d)^{-1/2} \tag{15}$$

so (14) becomes

$$x''(0,t_f) = -\frac{2}{d} \tag{16}$$

The use of (16) in (12) gives

$$\delta x(x_0,t_f) \simeq -\frac{2}{d}x_0^2 \tag{17}$$

as the distance, at the time of focus, between an ion initially at a distance x_0 from the center of the beam and an ion at the center $(x_0 = 0)$ of the beam. Note that δx in (17) is a negative quantity and the particles starting at $\pm x_0$ will be at the same place at the instant of focus. Furthermore, (17) shows that at the instant of focus, the beam is folded over in the x-direction so that what was initially the center of the beam is now the leading edge as it sweeps upward in the x-direction. If we rewrite (17) as

$$\delta x(x_0,t_f) = -\frac{x_0}{d}\cdot 2x_0 \tag{18}$$

and let x_0 represent the boundary of the beam, we see that at the focus, the x-dimension of the beam has been reduced by a factor of x_0/d. This says that the larger the electrode spacing relative to the beam size, the smaller the focusing aberration will be. However, in practice we cannot focus the beam to an arbitrarily small size by increasing the electrode separation because of the effects of thermal velocities. We have shown previously by (11) that increasing d will also increase the effective focal length, and we know that the effect of thermal velocities on focusing gets worse with increasing focal length. Hence, for a given beam size and ion temperature, there will be a value of d which minimizes the sum of the effects of aberration and thermal velocities.

Transverse Thermal Velocities

To consider the effect of ion thermal velocities transverse to the original direction of beam motion, we go back to (1) and retain the $\dot{x}_o$ term. The time t_1 at which the ion reaches the upper electrode is obtained by solving

$$\frac{d}{2} = \frac{\alpha}{2} t_1^2 + \dot{x}_o t_1 + x_o \tag{19}$$

The solution to (19) is

$$t_1 (x_o, \dot{x}_o) = -\frac{\dot{x}_o}{\alpha} + \left[\left(\frac{\dot{x}_o}{\alpha}\right)^2 + \frac{d - 2x_o}{\alpha} \right]^{1/2} \tag{20}$$

The velocity upon reaching the upper electrode will be

$$\dot{x}_1 = \alpha t_1 + \dot{x}_0 \tag{21}$$

After passing through the upper electrode, the x-coordinate at time t will be given by

$$x = \dot{x}_1 (t - t_1) + \frac{d}{2} \tag{22}$$

$$= (\alpha t_1 + \dot{x}_0)(t - t_1) + \frac{d}{2} \tag{23}$$

We consider x to be a function of three parameters,

$$x = x(x_0, \dot{x}_0, t)$$

and perform a Maclaurian expansion in x_0 and $\dot{x}_0$.

$$x(x_0, \dot{x}_0, t) = x(0,0,t) + \frac{dx}{dx_0}(0,0,t) + \frac{dx}{d\dot{x}_0}(0,0,t)\dot{x}_0 + \ldots$$

Let

$$\delta x(x_0, \dot{x}_0, t) = x(x_0, \dot{x}_0, t) - x(0,0,t) \tag{24}$$

$$\simeq \frac{dx}{dx_0}(0,0,t) + \frac{dx}{d\dot{x}_0}(0,0,t)\dot{x}_0$$

(25)

The definition (24) means that δx measures, at time t, the distance between an ion initially at x_o with velocity $\dot{x}_o$ and an ion initially traveling along with $x_o = \dot{x}_o = 0$. We shall next calculate δx by evaluating the terms on the right side of (25).

First we evaluate dx/dx_o. This is conveniently done by using

$$\frac{dx}{dx_o} = \frac{dx}{dt_1} \cdot \frac{dt_1}{dx_o} \tag{26}$$

From (23) we obtain

$$\frac{dx}{dt_1} = \alpha\left(t - 2t_1\right) - \dot{x}_o \tag{27}$$

and from (20)

$$t_1(0,0) = \left(\frac{d}{\alpha}\right)^{1/2} \tag{28}$$

$$\therefore \quad \frac{dx}{dt_1}(0,0,t) = \alpha\left(t - 2\sqrt{\frac{d}{\alpha}}\right) \tag{29}$$

From (20)

$$\frac{dt_1}{dx_o} = -\frac{1}{\alpha}\left[\left(\frac{\dot{x}_o}{\alpha}\right)^2 + \frac{d-2x_o}{\alpha}\right]^{-1/2} \tag{30}$$

$$\therefore \quad \frac{dt_1}{dx_0}(0,0) = -(\alpha d)^{-1/2} \tag{31}$$

When we use (31) and (29) in (26) we get

$$\frac{dx}{dx_0}(0,0,t) = 2 - \sqrt{\frac{\alpha}{d}}\, t \tag{32}$$

Next we consider the second term in (25). We need to evaluate $\frac{dx}{d\dot{x}_o}(o,0,t)$. This is conveniently done by using (23) and the form

$$\frac{dx}{d\dot{x}_0} = \frac{\partial x}{\partial \dot{x}_0} + \frac{dx}{dt_1}\cdot\frac{dt_1}{d\dot{x}_0} \tag{33}$$

Now

$$\frac{\partial x}{\partial \dot{x}_0} = t - t_1 \tag{34}$$

so

$$\begin{aligned}\frac{\partial x}{\partial \dot{x}_0}(0,0,t) &= t - t_1(0,0) \\ &= t - \left(\frac{d}{\alpha}\right)^{1/2}\end{aligned} \tag{35}$$

by (28). From (20) we obtain

$$\frac{dt_1}{d\dot{x}_0} = -\frac{1}{\alpha} + \frac{\dot{x}_0}{\alpha}\left[\left(\frac{\dot{x}_0}{\alpha}\right)^2 + \frac{d-2x_0}{\alpha}\right]^{-1/2}$$

$$\therefore \quad \frac{dt_1}{d\dot{x}_0}(0,0) = -\frac{1}{\alpha} \tag{36}$$

Equation (33) can now be evaluated by using (35), (29) and (36):

$$\frac{dx}{d\dot{x}_0}(0,0,t) = t - \sqrt{\frac{d}{\alpha}} - \alpha\left(t - 2\sqrt{\frac{d}{\alpha}}\right)\frac{1}{\alpha}$$

$$= \left(\frac{d}{\alpha}\right)^{1/2} \tag{37}$$

Finally we use (37) and (32) in (25) to obtain

$$\delta x\left(x_0, \dot{x}_0, t\right) = \left(2 - \sqrt{\frac{\alpha}{d}}\,t\right)x_0 + \sqrt{\frac{d}{\alpha}}\,\dot{x}_0 \tag{38}$$

In the case where there are no transverse thermal velocities ($\dot{x}_0 = 0$), we recover the focusing condition (10),

$$t_f = 2\sqrt{\frac{d}{\alpha}}$$

The addition of the $\dot{x}_0$ term in (38) shows that there is no time when all the particles are perfectly focused.

We can, however, describe the focused beam in a statistical sense. We calculate the root-mean-square spread in the size of the beam.

$$(\delta x)_{RMS} = \langle (\delta x)^2 \rangle^{1/2}$$

Now

$$\langle \delta x^2 \rangle = \left(2 - \sqrt{\tfrac{\alpha}{d}}\, t\right)^2 \langle x_o^2 \rangle + \frac{d}{\alpha} \langle \dot{x}_o^2 \rangle$$
$$+ 2\sqrt{\frac{d}{\alpha}} \left(2 - \sqrt{\tfrac{\alpha}{d}}\, t\right) \langle x_o \dot{x}_o \rangle$$

(39)

If x_o and $\dot{x}_o$ are statistically independent, and if either $\langle x_o \rangle$ or $\langle \dot{x}_o \rangle$ are zero; then the last term on the right of (39) vanishes. Then it is obvious from (39) that $\langle \delta x^2 \rangle$ will be a minimum when $t = 2\sqrt{d/\alpha}$, which is the same time at which a beam having no transverse velocities is focused. At this time the beam can be considered to be focused to a size

$$(\delta x)_f = \sqrt{\frac{d}{\alpha}} \langle \dot{x}_o^2 \rangle^{1/2}$$

(40)

If the ions have a Maxwellian distribution with transverse temperature T, then $\langle \dot{x}_o^2 \rangle = \frac{kT}{m}$. So

$$(\delta x)_f = \left(\frac{d}{\alpha} \cdot \frac{kT}{m}\right)^{1/2}$$

(41)

gives the focused size in terms of the ion temperature. With the definition of d given by (2), (41) can be written

$$(\delta x)_f = \left(\frac{kT}{qV}\right)^{1/2} d \tag{42}$$

Since d is also the focal length, (42) shows the usual behavior for focusing which is limited by transverse thermal velocities, i.e., the focused size is proportional to the focal length.

As a numerical example, consider $qV = 10^3$eV and a transverse beam temperature of $kT = 10$eV. Then according to (42) the RMS spread in the focused beam will be equal to one-tenth of the electrode spacing d.

Focusing Against Space Charge

In this section we shall consider how the effects of space charge limit the focusing action of the parallel plate geometry of Figure 5-1. We neglect the effects of ion transverse thermal velocities. First we examine the diverging effect of space charge in a drifting semi-infinite sheet beam.

Divergence of a Drifting Sheet Beam

Consider an infinite sheet beam which lies in the horizontal y-z plane and which has a finite thickness in the vertical x-direction. The ions are traveling with velocity v in the z-direction. The y-z plane divides the beam into upper and lower halves. From Gauss' law the electric field at the upper surface of the beam is found to be

$$E = \frac{i}{2\epsilon_0 v} \tag{43}$$

where i = current per unit width in y-direction

(44)

The field at the boundary of the beam remains constant even as the beam expands. The equation of motion for the upper surface of the beam is

$$x = \frac{a}{2} t^2 + x_0 \tag{45}$$

where

$$a = \frac{\zeta i}{2\epsilon_0 v} \tag{46}$$

and we have assumed zero initial velocity in the x-direction. If we let $z = vt$, then (45) becomes

$$x = \frac{a}{2v^2} \cdot z^2 + x_0 \tag{47}$$

so a given cross section of the beam expands quadratically as it moves along the z-axis.

Focusing

We assume that initially we have a semi-infinite sheet beam in the geometry of Figure 5-1. We assume that initially $(t = o)$ the ions in the transverse section under consideration are moving parallel to the z-axis. The space-charge electric field inside the uniform beam at x_o is given by

$$E = \frac{i}{\epsilon_o v} \cdot \frac{x_o}{\Delta} = \frac{x_o}{\epsilon_o v} \cdot J$$

$$J \equiv i/\Delta \tag{48}$$

where Δ is the initial thickness of the beam in the x-direction and J is the initial current density of the beam. Thus $E(x_o)$ is the space charge field seen by an ion initially at the distance x_o. The magnitude of the space-charge field experienced by this ion does not change with beam expansion (assuming laminar flow). The acceleration of an ion starting at x_o will be a sum of the space charge acceleration and the acceleration due to the voltage across the electrodes:

$$\ddot{x}(x_o) = \alpha + \beta x_o \tag{49}$$

where $\alpha = \dfrac{\eta V}{d}$ from (2), and

$$\beta = \frac{\eta J}{\epsilon_0 v} \tag{50}$$

We assume $\dot{x}_o$ is zero so that (49) yields

$$x(x_0, t) = \frac{1}{2}(\alpha + \beta x_0)t^2 + x_0 \tag{51}$$

From (51) the time t_1 taken to reach the upper electrode is

$$t_1(x_0) = \left(\frac{d - 2x_0}{\alpha + \beta x_0}\right)^{1/2} \tag{52}$$

and the velocity at this time is

$$\dot{x}_1(x_0) = (\alpha + \beta x_0) \cdot t(x_0) \tag{53}$$

After passing through the upper electrode, the motion is described by

$$x(x_0, t) = \frac{1}{2}\beta x_0 (t - t_1)^2 + (\alpha + \beta x_0)(t - t_1)t_1 + \frac{d}{2} \tag{54}$$

Now we can expand $x(x_o,t)$ in a Maclaurin series in x_o:

$$x(x_o,t) = x(o,t) + \frac{dx}{dx_o}(o,t)\cdot x_o + \ldots \tag{55}$$

from which

$$\begin{aligned} \delta x(x_o,t) &\equiv x(x_o,t) - x(o,t) \\ &= \frac{dx}{dx_o}(o,t)\, x_o + \ldots \end{aligned} \tag{56}$$

Perfect focusing, $\delta x = 0$, to first order in x_o will occur when

$$\frac{dx}{dx_o}(o,t) = 0 \tag{57}$$

We shall show that for sufficiently weak space charge forces, condition (57) can be met, hence focusing down to zero size is possible in the first order approximation. The left side of (57) is conveniently evaluated by using

$$\frac{dx}{dx_o}(x_o,t) = \frac{\partial x}{\partial x_o} + \frac{dx}{dt_1}\cdot\frac{dt_1}{dx_o} \tag{58}$$

in conjunction with (54). We find that

$$\frac{\partial x}{\partial x_0}(x_0,t) = \frac{1}{2}\beta\left[t^2 - t_1^2(x_0)\right] \tag{59}$$

From (52),

$$t_1(0) = \sqrt{\frac{d}{\alpha}} \equiv \tau \tag{60}$$

Tau is a characteristic time for this problem and is equal to the time it takes for the center of the beam to reach the upper electrode. We use (60) in (59) to get

$$\frac{\partial x}{\partial x_0}(0,t) = \frac{1}{2}\beta\left(t^2 - \tau^2\right) \tag{61}$$

From (54)

$$\frac{dx}{dt_1}(x_0,t) = \alpha t - \left(2\alpha + \beta x_0\right)\cdot t_1(x_0) \tag{62}$$

which gives

$$\frac{dx}{dt_1}(0,t) = \alpha\left(t - 2\tau\right) \tag{63}$$

From (52) we obtain

$$\frac{dt_1}{dx_0}(x_0,t) = -\frac{1}{2}\left(\frac{\alpha+\beta x_0}{d-2x_0}\right)^{1/2}\cdot\frac{2\alpha+\beta d}{(\alpha+\beta x_0)^2} \tag{64}$$

which leads to

$$\frac{dt_1}{dx_0}(0,t) = -\frac{2+\beta\tau^2}{2\alpha\tau} \tag{65}$$

We now use (61), (63), and (65) in (58) to obtain

$$\frac{dx}{dx_0}(0,t) = \frac{\beta}{2}\left(t^2-\tau^2\right) - \frac{t-2\tau}{2\tau}\left(2+\beta\tau^2\right) \tag{66}$$

which we set equal to zero and solve for the time t_f at which focusing in the x-direction occurs. We obtain

$$\frac{t_f}{\tau} = \frac{1}{\gamma} + \frac{1}{2} \pm \frac{1}{\gamma}\left(1-3\gamma-\frac{3}{4}\gamma^2\right)^{1/2} \tag{67}$$

The dimensionless parameter γ is defined by

$$\gamma \equiv \beta\tau^2 = \frac{\eta d^2 J}{\epsilon_0 v V} \tag{68}$$

and is a measure of the space charge field relative to the deflection focusing field. For the case where $\gamma \rightarrow 0$ (vanishing space charge), (67) reduces to $t_f = 2\tau$ which agrees with (11) if we choose the (-) sign. Another physical requirement from (67) is that

$$1 - 3\gamma - \frac{3}{4}\gamma^2 \geq 0$$

or

$$\gamma \leq \frac{4}{3}\sqrt{3} - 2$$
$$\leq 0.3094$$

(69)

which specifies the condition necessary in order to obtain focusing down to zero size to first order.

Intuitively we expect that for value of γ larger than given by (69), the beam will not focus down to zero size in the x-direction but will reach some minimum size and then will expand again. In this case the beam will be focused according to (56) if

$$\frac{d}{dt} \cdot \frac{dx}{dx_0}(0,t) = 0$$

(70)

Equation (70) can be used to find the time at which the beam reaches its minimum size. We evaluate (70) by differentiating (66), setting the result equal to zero, and solving for the time of focus t_f . We find

$$t_f = \left(\frac{1}{\gamma} + \frac{1}{2}\right)\tau$$

(71)

We put (71) into (66) to obtain

$$\frac{dx}{dx_0}(0,t_f) = \frac{\frac{3}{4}\gamma^2 + 3\gamma - 1}{2\gamma} \tag{72}$$

which now can be put into (56) to obtain δx_f the spread at the time of focus:

$$\delta x_f = \frac{dx}{dx_0}(0,t_f)\cdot x_0$$

$$= \frac{1}{2\gamma}\left(\frac{3}{4}\gamma^2 + 3\gamma - 1\right) x_0 \tag{73}$$

We note that the numerator in (73) also appeared in (67), consequently we see that δx_f will be zero for $\gamma = .3094$ (see Eq. (69)). If x_o represents the initial size of the beam, then (73) gives the focused size. In order that the focused size be smaller than the initial size we require

$$\frac{3}{4}\gamma^2 + 3\gamma - 1 < 2\gamma$$

or

$$\gamma < 2/3 \tag{74}$$

From the above analysis we see that the focusing effect is divided into three regimes according to the size of the dimensionless parameter γ : 1) $0 \leq \gamma \leq 0.3094$. Focusing down to zero size is possible. At $\gamma = 0$, focus occurs at a distance above the top electrode equal to the electrode spacing d. The focus moves away with increasing γ until it reaches a distance of 2.73d from the top plate when $\gamma = .3094$. 2) $.3094 < \gamma < 2/3$. The focused size will be non-zero and smaller than the original size of the beam. As γ increases beyond .3094, the focus location moves back closer to the top electrode. When γ reaches 2/3, the focus is back at a distance d above the top electrode, and the focused size is equal to the original size. 3) $\gamma > 2/3$. The "focused" size of the beam is greater than the initial size and occurs less than a distance d above the top electrode.

Example. Consider the case of a He^{++} beam and a H target. Appropriate values for the parameters are:

$$v = 10^8 \text{ cm/sec}$$

$$V = 10^4 \text{ volts}$$

$$d = 1 \text{ cm}$$

We shall calculate the current density which corresponds to $\gamma = 2/3$, i.e., the maximum current density which will permit focusing. From (68) we obtain

$$J(\gamma = 2/3) = \frac{2}{3} \cdot \frac{\epsilon_0 \sigma V}{\eta d^2}$$

$$= 0.1 \ A/cm^2$$

for our particular example. This example shows that the parallel plate focusing scheme can focus only beams of relatively low current densities.

We shall show that the cylindrical focusing geometry analyzed in the following chapter is capable of focusing larger current densities than the parallel plate geometry.

CHAPTER 6

FOCUSING OF A HOLLOW CYLINDRICAL ION BEAM

In this chapter we analyze a cylindrical focusing system as an alternative to the parallel-plate system of the preceding chapter. We present calculations which assess the focusing limitations which arise from focusing aberration, transverse thermal velocities, and space charge. We show that the effects of aberration and thermal velocities in the cylindrical geometry are similar in magnitude to the same effects in the planar geometry, but the cylindrical geometry is much more effective against space charge. We estimate that order-of-magnitude larger focused current densities should be acheivable in the cylindrical geometry than in the planar geometry.

Condition for Ideal Focusing

We consider a hollow positive ion beam traveling between two coaxial conductors as shown in Figure 6-1. The inner conductor is a grid so as to allow the ion beam to pass through it and come to a focus on the axis. Focusing is started at some instant by applying a voltage V across the coaxial electrodes at one of the ends. The voltage pulse will travel with the velocity of light down the

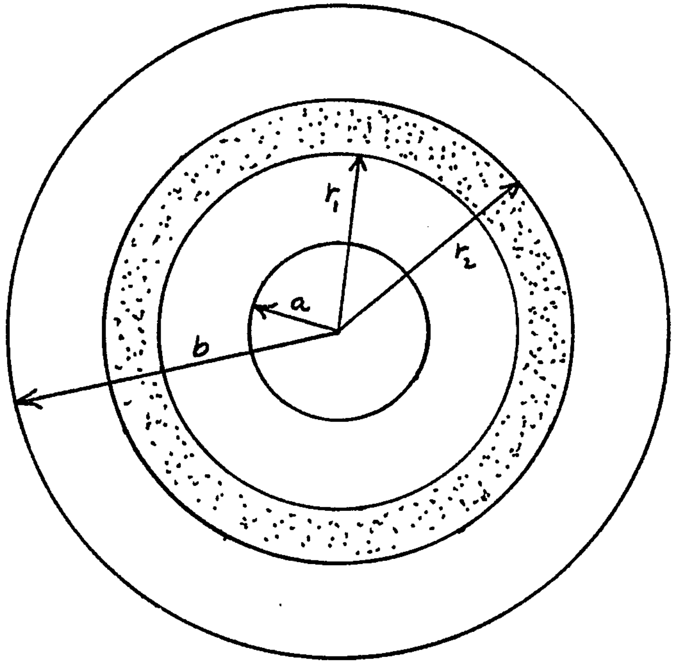

FIGURE 6-1. Hollow Ion Beam Traveling Between Coaxial Electrodes

electrodes and cause the ion beam to be deflected radially inward. The region of focus will travel along with the velocity of light. We shall examine the conditions necessary for the ion beam to come to a focus on the axis. We assume that the beam is initially space-charge neutralized so that space-charge expansion is negligible prior to deflection. The deflection voltage will also strip away the neutralizing charges. As a first approximation, we shall neglect the effects of space charge and transverse thermal velocities.

After the voltage is turned on, the potential between the inner and outer electrodes is given by

$$\phi(r) = K \ln \frac{r}{a} \tag{1}$$

where K is a scaled voltage defined by

$$K \equiv \frac{V}{\ln b/a} \tag{2}$$

where a and b are the radii of the inner and outer electrodes.

K is not too different than V if a and b are about the same size. Consider a particle which is at $r = r_o$ when the voltage pulse reaches it. By conservation of energy

$$\dot{r}^2 = \dot{r}_o^2 + 2\eta K \ln r_o/r \tag{3}$$

where η = q/m.

Assume for now that $\dot{r}_o^2 = 0$. Then

$$\dot{r}^2 = 2\eta K \ln \frac{r_o}{r} \tag{4}$$

$$\dot{r} = -\sqrt{2\eta K}\,(\ln r_o/r)^{1/2} \tag{4a}$$

We find the time it takes for the particle to reach r = a:

$$\int_0^{t_a} dt = -\int_{r_o}^{a} (2\eta K \ln r_o/r)^{-\frac{1}{2}}\, dr \tag{5}$$

with $y \equiv (\ln r_o/r)^{1/2}$

$$t_a = \frac{2 r_o}{\sqrt{2\eta K}} \int_0^{\sqrt{\ln r_o/a}} e^{-y^2}\, dy \tag{6}$$

Rewrite (6) as

$$t_a(r_o) = \left(\frac{2}{\eta K}\right)^{1/2} a\, e^{\ln r_o/a} \int_0^{(\ln r_o/a)^{1/2}} e^{-y^2}\, dy \tag{7}$$

If we let $$x \equiv \left(\ln {r_0}/{a}\right)^{1/2}$$

then

$$t_a(x) = \left(\frac{2}{\eta K}\right)^{1/2} a\, G(x) \tag{8}$$

where

$$G(x) \equiv e^{x^2} \int_0^x e^{-y^2}\, dy \tag{8a}$$

After the particle passes through the grid at r = a, it moves with constant velocity. The position is given by

$$r = \dot{r}_a (t - t_a) + a \qquad (r < a) \tag{9}$$

where $\dot{r}_a$ is the velocity achieved at r = a. From (4a)

$$\dot{r}_a = -\left(2 \eta K \ln {r_0}/{a}\right)^{1/2} \tag{10}$$

$$\therefore\ r = -\left(2 \eta K \ln {r_0}/{a}\right)^{1/2} \left[t - t_a(r_0)\right] + a \tag{11}$$

We now consider a transverse section of the beam at a particular time t after the voltage pulse arrives and investigate the size of the section. We want to look at how r varies as a function of r_o with t fixed.

$$r(r_o + \delta r_o, t) = r(r_o, t) + \frac{dr}{dr_o}(r_o, t)\,\delta r_o + \frac{1}{2}\frac{d^2 r}{dr_o^2}(r_o, t)\,\delta r_o^2 + \cdots \tag{12}$$

$$\therefore \quad \delta r = \frac{dr}{dr_o}(r_o, t)\,\delta r_o + \frac{d^2 r}{dr_o^2}(r_o, t)\frac{(\delta r_o)^2}{2} + \cdots \tag{13}$$

Equation (13) tells us how an initial spread δr_o varies with time as the beam moves inward.

Note that according to (11), r may be written as a function of the variable $x = (\ln r_o/a)^{\frac{1}{2}}$.

$$r(x) = -(2\eta K)^{1/2} x\,[t - t_a(x)] + a \tag{14}$$

Then

$$\frac{dr}{dr_o} = \frac{dr}{dx} \cdot \frac{dx}{dr_o} \tag{15}$$

Consider the first-order focus, i.e., $\frac{dr}{dr_o} = 0$. When this occurs, to first order in δr_o, δr will be zero:

$$\therefore \quad \frac{dr}{dr_o} = 0 \Rightarrow \frac{dr}{dx} = 0$$

also.

At focus,

$$\frac{dr}{dx} = -(2\eta K)^{1/2}[t_f - t_a(x)] + (2\eta K)^{1/2} x\, t_a'(x) \tag{16}$$

where the prime denotes differentiation with respect to the variable x. From (8),

$$t_a'(x) = \left(\frac{2}{\eta K}\right)^{1/2} a\, G'(x) \tag{17}$$

Now we require that the focus occur at $r = o$ at time t_f. Then (14) gives

$$-(2\eta K)^{1/2}[t_f - t_a(x)] = -\frac{a}{x} \tag{18}$$

Now put (18) and (17) into (16) to obtain

$$0 = -\frac{a}{x_1} + 2a x_1 G'(x_1) \tag{19}$$

or

$$2x_1 G'(x_1) = \frac{1}{x_1}$$

(20)

which is the condition for focusing on the axis. Here x_1 denotes the particular value of x which is the solution to (20). We want to solve (20) for x_1 to find the value of r_o/a which gives focusing on the axis.

First we consider the function $G(x)$. From (8a)

$$G(x) = e^{x^2}\int_0^x e^{-y^2}dy$$

(21)

$$\therefore \quad G'(x) = e^{x^2}e^{-x^2} + 2xe^{x^2}\int_0^x e^{-y^2}dy$$

(22)

$$= 1 + 2xG(x)$$

(23)

So we can express $G'(x)$ easily in terms of x and $G(x)$. To evaluate $G(x)$ we note that it is related to the error function:

$$\operatorname{erf} x = \frac{2}{\sqrt{\pi}}\int_0^x e^{-y^2}dy$$

(24)

So another way of expressing G(x) is

$$G(x) = \frac{\sqrt{\pi}}{2} e^{x^2} \operatorname{erf} x \tag{25}$$

which can be evaluated with the aid of the tabulated error function such as given in the handbook of Abramowitz and Stegun (1965, p. 310). A plot of G(x) is shown in Figure 6-2.

We now go back to the focusing condition (20) which can be written

$$2x_1\left[1 + 2x_1 G(x_1)\right] = \frac{1}{x_1}$$

or

$$G(x_1) = \frac{1}{2x_1}\left(\frac{1}{2x_1^2} - 1\right) \tag{34}$$

Equation (34) is solved graphically in Figure 6-3 by plotting G(x) versus g(x), the function on the right of (34), for various values of x. The solution to (34) is the value of x for which the curves intersect. The solution of (34) is found to be

$$x_1 = 0.54039 = \left(\ln r_0/a\right)^{1/2} \tag{35a}$$

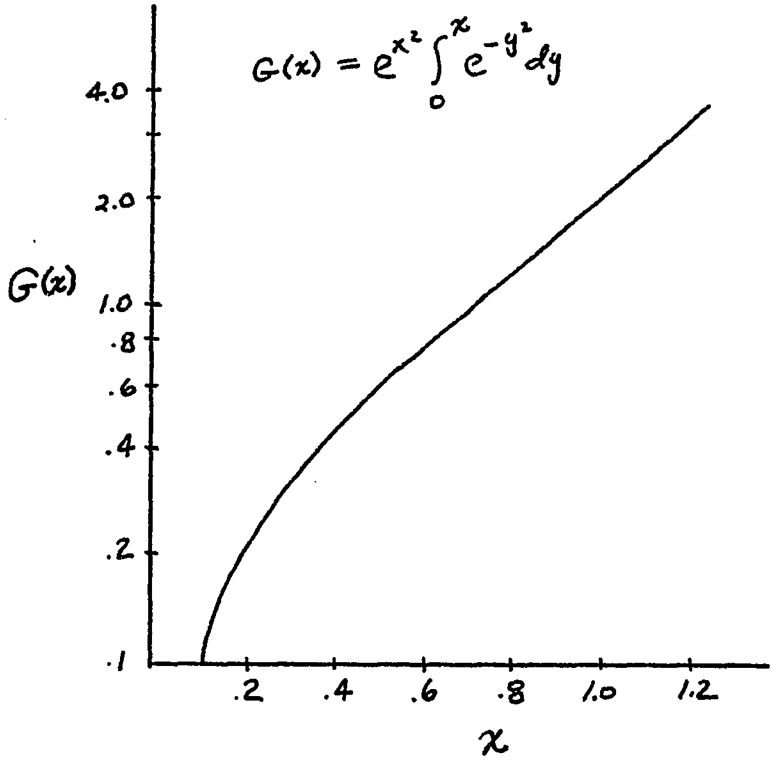

FIGURE 6-2. A Function Used to Calculate Focusing Against Space Charge

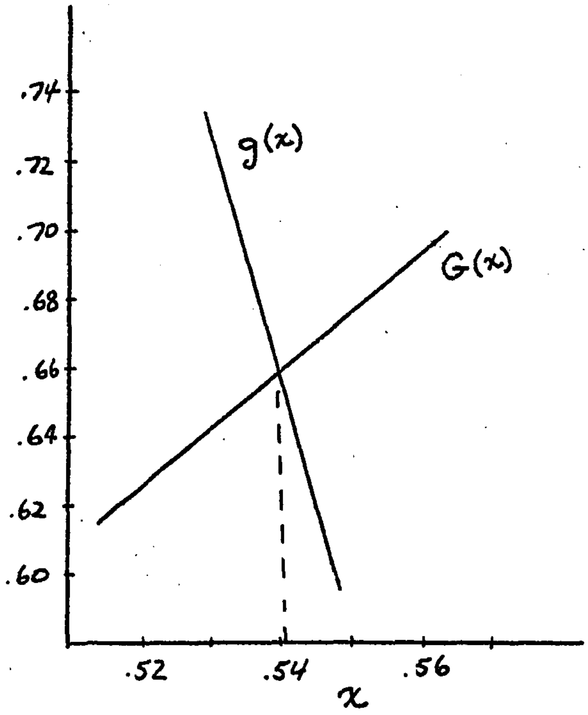

FIGURE 6-3. Graphical Solution to Focusing Condition.

(Eq. 34 of text).

or

$$\ln \frac{r_o}{a} = .29202 \tag{35b}$$

or

$$\frac{r_o}{a} = 1.339 \tag{35c}$$

which is the condition for focusing along the axis (r=o) of those ions which start off within a small increment δr_o at r_o.

Focusing Aberration

From the preceding analysis we saw that if we have a thin-walled hollow cylindrical beam with inner radius r_o, it is possible to get a first-order focusing at r=o by the proper choice of the ratio of r_o to the inner electrode radius a.

The next step is to calculate the size of the second-order effect which causes an aberration in the focusing. Recall from (13).

$$\delta r = \frac{dr}{dr_o}\delta r_o + \frac{d^2r}{dr_o^2}\cdot\frac{(\delta r_o)^2}{2} + \ldots \tag{36}$$

We now calculate the size of the second term on the right when we make the first term zero by choosing $r_o/a = 1.34$.

To calculate $\frac{d^2r}{dr_o^2}$ we use $\frac{d}{dr_o} = \frac{dx}{dr_o} \cdot \frac{d}{dx}$:

$$\frac{d^2r}{dr_o^2} = \frac{d}{dr_o}\left(\frac{dr}{dr_o}\right)$$

$$= \frac{dx}{dr_o} \cdot \frac{d}{dx}\left(\frac{dr}{dr_o}\right)$$

$$= \frac{dx}{dr_o} \cdot \frac{d}{dx}\left(\frac{dx}{dr_o} \cdot \frac{dr}{dx}\right)$$

$$= \frac{dx}{dr_o}\left(\frac{d^2x}{dx\,dr_o} \cdot \frac{dr}{dx} + \frac{dx}{dr_o} \cdot \frac{d^2r}{dx^2}\right)$$

$$= \left(\frac{dx}{dr_o}\right)^2 \frac{d^2r}{dx^2} \tag{37}$$

We have used the fact that $\frac{dr}{dx} \equiv o$ at the first-order focus. From Equation (16) we can write

$$\frac{d^2r}{dx^2} = (2\eta K)^{1/2} t_a'(x) + (2\eta K)^{1/2}\left[t_a'(x) + x t_a''(x)\right] \tag{38}$$

$$= 2(2\eta K)^{1/2} t_a'(x) + (2\eta K)^{1/2} x\, t_a''(x) \tag{39}$$

$$= 2(2\gamma k)^{1/2}\left(\frac{2}{\gamma k}\right)^{1/2} a\ G'(x)$$
$$+ (2\gamma k)^{1/2} x \left(\frac{2}{\gamma k}\right)^{1/2} a\ G''(x)$$

(40)

$$= 4a\ G'(x) + 2ax\ G''(x)$$

(41)

Now $\quad G'(x) = 1 + 2xG(x)$ (42a)

so $\quad G''(x) = 2\ x\ G'(\underline{x}) + 2G(x)$ (42b)

We want to evaluate (41) subject to the focusing condition (20) which can be written

$$G'(x_1) = \frac{1}{2x_1^2}$$

We can write (41) as

$$\left.\frac{d^2r}{dx^2}\right|_{x_1} = \frac{4a}{2x_1^2} + 2ax_1\left[2x_1 \cdot \frac{1}{2x_1^2} + 2G(x_1)\right]$$

$$= \frac{2a}{x_1^2} + 2a + 4ax_1\left[\frac{G'(x_1)-1}{2x_1}\right] \quad \text{via (42a)}$$

$$= \frac{3a}{x_1^2}$$

(43)

Also $$x = \left(\ln \frac{r_0}{a}\right)^{1/2}$$

then $$\frac{dx}{dr_0} = \frac{1}{2}\left(\ln \frac{r_0}{a}\right)^{-\frac{1}{2}} \cdot \frac{1}{r_0} \qquad (44)$$

and

$$\left(\frac{dx}{dr_0}\right)^2 = \frac{1}{4a^2} \cdot \frac{e^{-2x^2}}{x^2}$$

(45)

Finally, $$\left.\frac{d^2r}{dr_0^2}\right|_{x_1} = \left(\left.\frac{dx}{dr_0}\right|_{x_1}\right)^2 \cdot \left.\frac{d^2r}{dx^2}\right|_{x_1}$$

$$= \frac{3}{4a} \cdot \frac{e^{-2x_1^2}}{x_1^4} \qquad (46a)$$

Now $$x_1^2 = .292$$

$$\therefore \quad \left.\frac{d^2 r}{d r_0^2}\right|_{x_1} = \frac{4.92}{a} \tag{46b}$$

We now have the result that at the focus

$$\delta r_f \cong \frac{d^2 r}{d r_0^2} \cdot \frac{(\delta r_0)^2}{2}$$

$$\cong 2.46 \frac{(\delta r_0)^2}{a} \tag{47}$$

via (46b). Equation (47) gives the focused radius of the beam in terms of the initial thickness δr_0 of the shell. (Compare with Eq. 5-17 for the parallel plate case.)

Example

As an example consider the case where $\dfrac{\delta r_0}{r_0} = 0.1$

Equation (47) can be written

$$\begin{aligned} \frac{\delta r}{\delta r_0} &= 2.46 \frac{\delta r_0}{a} \\ &= 2.46 \frac{\delta r_0}{r_0} \cdot \frac{r_0}{a} \\ &= 2.46 (.1) 1.34 \end{aligned} \tag{48}$$

$$= 0.33 \tag{49}$$

If $r_o = 1cm$ and $\delta r_o = 0.1cm$, then the focused radius is 0.033 cm.

The above calculation has taken the focusing aberration into account but has neglected the important effect of transverse thermal velocities which we consider next.

Transverse Thermal Velocities

To take transverse thermal velocities into account we must go back to the equation of motion (3) and keep the term for the initial radial velocity $\dot{r}_o$, then

$$\dot{r}^2 = \dot{r}_o^2 + 2\eta K \ln \frac{r_o}{r} \tag{51}$$

We calculate the time that it takes for a particle starting at $r = r_o$ with an initial radial velocity $\dot{r}_o$ to reach the inner electrode at $r = a$.

First we consider the case of an ion moving inward ($\dot{r}_o < 0$) when the voltage pulse hits it.

$$\dot{r} = -\left[\dot{r}_o^2 + 2\eta K \ln \frac{r_o}{r} \right]^{1/2} \tag{52}$$

$$\int_0^{t_a} dt = -\int_{r_0}^{a} \left[\dot{r}_0^2 + 2\eta K \ln \frac{r_0}{r}\right]^{-1/2} dr$$

$$\therefore\ t_a = -(2\eta K)^{-1/2} \int_{r_0}^{a} \left[\ln \frac{r_0}{r} + \frac{\dot{r}_0^2}{2\eta K}\right]^{-1/2} dr$$

(53)

Let
$$y \equiv \left(\ln \frac{r_0}{r} + \frac{\dot{r}_0^2}{2\eta K}\right)^{1/2}$$

$$\therefore\ t_a = 2r_0 (2\eta K)^{-1/2} e^{\dot{r}_0^2/2\eta K} \int_{(\dot{r}_0^2/2\eta K)^{1/2}}^{(\ln \frac{r_0}{a} + \dot{r}_0^2/2\eta K)^{1/2}} dy\, e^{-y^2} \qquad (54)$$

Equation (54) can be written in terms of the function G,

$$t_a = 2a(2\eta K)^{-1/2}\, G\left(\left[\ln \frac{r_0}{a} + \dot{r}_0^2/2\eta K\right]^{1/2}\right)$$

$$- 2r_0 (2\eta K)^{-1/2}\, G\left(\left[\dot{r}_0^2/2\eta K\right]^{1/2}\right)$$

(55)

For the case where $\dot{r}_o > 0$ we must be a little more careful. In this case we assume the ion is initially moving outward. Because of the electric field, it reaches a maximum radius r_1 and then is pulled backed inward.

In this case

$$ta = t_1 + t_{1a} \tag{56}$$

where t_1 = (time it takes ion to go from $r = r_o$ to $r = r_1$) and t_1a = (time it takes to go from $r = r_1$ to $r = a$)

From (51) we write

$$\dot{r} = \left(\dot{r}_o^2 + 2\eta K \ln \frac{r_o}{r}\right)^{1/2} \tag{57}$$

$$= \left(\dot{r}_o^2 - 2\eta K \ln \frac{r}{r_o}\right)^{1/2} \tag{58}$$

for the first part of the motion when $r > r_o$. The analysis follows the same as before and we get

$$t_1 = \frac{-2r_o}{(2\eta K)^{1/2}} e^{\dot{r}_o^2/2\eta K} \int_{(\dot{r}_o^2/2\eta K)^{1/2}}^{0} e^{-y^2} dy \tag{59}$$

where we have used the fact that $\dot{r} = 0$ at r_1. Equation

(59) can be written

$$t_1 = 2r_0(2\eta K)^{-1/2}\, G\left([\dot{r}_0^2/2\eta K]^{1/2}\right) \tag{60}$$

Equation (55) can be used to get t_{1a} by letting

$$r_0 \rightarrow r_1$$
$$\dot{r}_0 \rightarrow \dot{r}_1 = 0$$

$$\therefore \quad t_{1a} = 2a(2\eta K)^{-1/2}\, G\left([\ln r_1/a]^{1/2}\right) \tag{61}$$

$$\begin{aligned} \therefore \qquad t_a &= t_1 + t_a \qquad (\dot{r}_0 > 0) \\ &= 2r_0(2\eta K)^{-1/2}\, G\left([\dot{r}_0^2/2\eta K]^{1/2}\right) \\ &\quad + 2a(2\eta K)^{-1/2}\, G\left([\ln r_1/a]^{1/2}\right) \end{aligned} \tag{62}$$

We can eliminate r_1 by using (57) and $\dot{r}_1 = 0$;

$$\begin{aligned} &\dot{r}_0^2 + 2\eta K \ln \frac{r_0}{r_1} = 0 \\ &\therefore \quad \ln r_1/a = \dot{r}_0^2/2\eta K + \ln \frac{r_0}{a} \end{aligned} \tag{63}$$

We put (63) into (62) to get

$$t_a = 2a(2\gamma K)^{-1/2}\, G\left(\left[\ln\frac{r_0}{a} + \frac{\dot r_0^2}{2\gamma K}\right]^{1/2}\right) + 2r_0(2\gamma K)^{-1/2}\, G\left(\left[\dot r_0^2/2\gamma K\right]^{1/2}\right) \tag{64}$$

If we compare (55) and (64) we see that

$$t_a = 2a(2\gamma K)^{-1/2}\, G\left(\left[\ln\frac{r_0}{a} + \frac{\dot r_0^2}{2\gamma K}\right]^{1/2}\right) \pm 2r_0(2\gamma K)^{-1/2}\, G\left(\left[\dot r_0^2/2\gamma K\right]^{1/2}\right) \tag{65}$$

$$\left\{\begin{array}{l}\text{take + for } \dot r_0 > 0 \\ \text{take - for } \dot r_0 < 0\end{array}\right\}$$

We would like to have a single expression for t_a which holds for both $\dot r_0 > 0$ and $\dot r_0 < 0$. To obtain this, we consider the size of the dimensionless parameter $\xi \equiv (\dot r_0^2/2\gamma K)^{1/2}$. Suppose that the ion beam has a Maxwellian velocity distribution.

Then

$$\frac{1}{2} m\langle v_r^2\rangle = kT \tag{66}$$

$$\therefore \langle v_r^2 \rangle = \frac{2kT}{m} \tag{67}$$

Consider He^{++} ions, and kT = 10eV, then

$$\langle v_r^2 \rangle = 4.8 \times 10^8 \ m^2/sec^2 \tag{68}$$

If we take K on the order of 10^4 volts, then

$$2\eta K = 4.8 \times 10^{11}$$

$\therefore$ If we take $\dot{r}_0^2 = \langle v_r^2 \rangle$, then

$$\frac{\dot{r}_0^2}{2\eta K} \simeq 10^{-3}$$

and

$$\zeta \simeq .03 \tag{69}$$

For such a small value of ζ we can show that $G(\zeta) \simeq \zeta$:

$$G(\zeta) = e^{\zeta^2} \int_0^{\zeta} e^{-y^2} dy \tag{70}$$

$$\simeq \zeta + \frac{2}{3}\zeta^3 \tag{71}$$

We see that for the value of ζ given by (69), $G(\zeta) \simeq \zeta$ is an excellent approximation. We use this fact to rewrite (65) as

$$t_a \simeq 2a(24K)^{-1/2} G\left(\left[\ln \frac{r_0}{a} + \dot{r}_0^2/24K\right]^{1/2}\right) + \frac{r_0 \dot{r}_0}{4K} \tag{72}$$

which holds for both $\dot{r}_0 > 0$ and $\dot{r}_0 < 0$.

After the ions have passed through the grid at $r = a$, the motion is given by

$$r = \dot{r}_a (t - t_a) + a \tag{73}$$

If we show the functional dependence explicitly,

$$r(r_0, \dot{r}_0, t) = \dot{r}_a(r_0, \dot{r}_0)\left[t - t_a(r_0, \dot{r}_0)\right] + a \tag{74}$$

Hence we can write

$$\delta r \simeq \frac{dr}{dr_0}(r_0, 0, t)\,\delta r_0 + \frac{dr}{d\dot{r}_0}(r_0, 0, t)\,\delta \dot{r}_0 \tag{75}$$

The first term on the right of (75) has been analyzed previously, and we found it could be made to vanish by choosing $r_o/a = 1.34$. The second term is new and gives rise to a smearing out of the beam due to radial emittance.

We now evaluate $dr/d\dot{r}_o$. From (73)

$$\frac{dr}{d\dot{r}_o} = -\dot{r}_a \cdot \frac{dt_a}{d\dot{r}_o} + \frac{d\dot{r}_a}{d\dot{r}_o} \cdot (t - t_a) \tag{76}$$

First consider $dt_a/d\dot{r}_o$. From (72)

$$\frac{dt_a}{d\dot{r}_o} = 2a(2\eta K)^{-1/2} \frac{dG}{d\varsigma} \frac{d\varsigma}{d\dot{r}_o} + \frac{r_o}{\eta K} \tag{77}$$

where ς is the argument of G in (72):

$$\varsigma \equiv \left(\ln \frac{r_o}{a} + \frac{\dot{r}_o^2}{2\eta K} \right)^{1/2} \tag{78}$$

$$\therefore \frac{d\varsigma}{d\dot{r}_o} = \left(\ln \frac{r_o}{a} + \frac{\dot{r}_o^2}{2\eta K} \right)^{-1/2} \frac{\dot{r}_o}{2\eta K} \tag{79}$$

and

$$\left. \frac{d\varsigma}{d\dot{r}_o} \right|_{\dot{r}_o = 0} = 0 \tag{80}$$

$$\therefore \quad \left.\frac{dt_a}{d\dot{r}_o}\right|_{\dot{r}_o=0} = \frac{r_o}{\eta K}$$

(81)

Now consider $d\dot{r}_a/d\dot{r}_o$. From (51)

$$\dot{r}_a = -\left[\dot{r}_o^2 + 2\eta K \ln r_o/a\right]^{1/2}$$

$$\therefore \quad \frac{d\dot{r}_a}{d\dot{r}_o} = -\left[\dot{r}_o^2 + 2\eta K \ln \frac{r_o}{a}\right]^{-1/2} \dot{r}_o \qquad (82)$$

and

$$\left.\frac{d\dot{r}_a}{d\dot{r}_o}\right|_{\dot{r}_o=0} = 0$$

(83)

Using (83), (82) and (81) in (76) we have

$$\left.\frac{dr}{d\dot{r}_o}\right|_{\dot{r}_o=0} = \frac{r_o}{\eta K}\left(2\eta K \ln \frac{r_o}{a}\right)^{1/2}$$

(84)

$$= \left(\frac{2}{\eta K} \ln \frac{r_o}{a}\right)^{1/2} r_o$$

(85)

Put (85) into (75) to get

$$\delta r_f = \left(\frac{2}{\eta K} \ln \frac{r_o}{a}\right)^{1/2} r_o \,\delta\dot{r}_o$$

(86)

Equation (86) relates the radial spread δr_f at focus to the initial radial spread $\delta \dot{r}_o$ in velocities.

If we assume that the initial spread in radial velocities is Maxwellian, then we can express the spread in radius as a function of the transverse temperature of the beam. We can express (86) in terms of root-mean-square values:

$$(\delta r_f)_{RMS} = \langle(\delta r_f)^2\rangle^{1/2} = r_o\left[\frac{2\ln\frac{r_o}{a}}{\eta K}\right]^{1/2}\langle(\delta \dot{r}_o)^2\rangle^{1/2} \tag{87}$$

We can also use (67) to write

$$\langle(\delta \dot{r}_o)^2\rangle = \frac{2kT}{m} \tag{88}$$

The use of (88) in (87) gives

$$(\delta r_f)_{RMS} = 2\left(\ln\frac{r_o}{a}\cdot\frac{kT}{qK}\right)^{1/2} r_o \tag{89}$$

$$= 1.08\left(\frac{kT}{qK}\right)^{1/2} r_o \tag{90}$$

(Compare with Eq. 5-42 for the parallel plate case.)

To obtain (90) from (89) we have used condition (35a) for optimum focusing. Equation (90) shows the familiar result that when thermal velocities are important, the focused radius is proportional to the focal length. (In this case r_o is the effective focal length.) Tight focusing requires a small initial beam radius.

Examples

As numerical examples we consider focusing of He^{++} and He^{+} beams. We assume that both beams are characterized by a transverse temperature of one eV. The (He^{++}, H) charge-transfer reaction requires that the He^{++} energy be about 25 keV, therefore we take $qK = 2.5 \times 10^4$ eV. From (87) we obtain (δr_f)RMS = .0068 r_o. For r_o = 1cm the focused RMS radius is .068 mm. The He^{+}, Cs charge transfer is optimal for a He^{+} energy of 1.9 keV, therefore we take $qK = 1.9 \times 10^3$ eV. If we use r_o = 1cm, then the focused RMS radius is 0.25 mm.

Space Charge Effects

In this section we consider the effect of space charge on a cylindrical focusing geometry. We shall show how space charge limits the size to which a hollow ion beam can be focused axially.

Expansion Due to Space Charge

Consider a length l of an ion beam whose outer radius is r and which carries current I. The beam moves along the z-axis with velocity v.

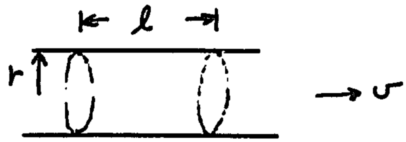

From symmetry and Gauss' law we can find the radial electric field at the outer radius of the beam:

$$\epsilon_0 \oint \vec{E}.d\vec{A} = Q \text{ (enclosed)}$$
$$2\pi\epsilon_0 r \ell E = \int_0^r \rho \ell dA$$
$$= \frac{\ell}{v} \int_0^r J dA$$
$$= \frac{\ell I}{v}$$

Then

$$E = \frac{I}{2\pi\epsilon_0 v} \cdot \frac{1}{r} = -\frac{\partial \phi}{\partial r} \tag{91}$$

from which the potential is calculated to be

$$\phi = -A\ln r + \text{const.}$$

where

$$A \equiv \frac{I}{2\pi\epsilon_0 v} \quad \text{(volts)} \tag{92}$$

From conservation of energy,

$$\frac{1}{2} m \dot{r}^2 - qA \ln r = \frac{1}{2} m \dot{r}_0^2 - qA \ln r_0 \tag{93}$$

where r_o and $\dot{r}_o$ are the initial values. If we assume that $r_o = 0$, then (93) can be written

$$\dot{r} = \left(2\eta A \ln \frac{r}{r_0}\right)^{1/2} \tag{94}$$

or

$$\int_0^t dt = \int_{r_0}^{r} \left[2\eta A \ln \frac{r}{r_0}\right]^{-1/2} dr \tag{95}$$

If we let

$$y \equiv \left(\ln \frac{r}{r_0}\right)^{1/2} \tag{96}$$

then (95) becomes

$$t = \left(\frac{2}{\eta A}\right)^{1/2} r_0 \int_0^{\left(\ln \frac{r}{r_0}\right)^{1/2}} e^{y^2} dy \tag{97}$$

With the definition

$$F(x) \equiv e^{-x^2} \int_0^x e^{y^2} dy \tag{98}$$

equation (97) becomes

$$t = \left(\frac{2}{\eta A}\right)^{1/2} r\, F\left([\ln \frac{r}{r_0}]^{1/2}\right) \tag{99}$$

Dawson's integral is tabulated by Abramowitz and Stegun (1965, p. 319). A plot of F(x) taken from Pierce (1954) is shown in Figure 6-4. In terms of the z-coordinate (z = vt), (99) can be written

$$z = \left(\frac{2}{\eta A}\right)^{1/2} v\, r\, F\left([\ln \frac{r}{r_0}]^{1/2}\right) \tag{100}$$

With the definition of A, (100) can be written

$$k\left(\frac{z}{r_0}\right) = \left(\frac{r}{r_0}\right) \cdot F\left([\ln \frac{r}{r_0}]^{1/2}\right) \tag{101}$$

with

$$k \equiv \left[\frac{\eta I}{4\pi \epsilon_0 v^3}\right]^{1/2} \tag{102}$$

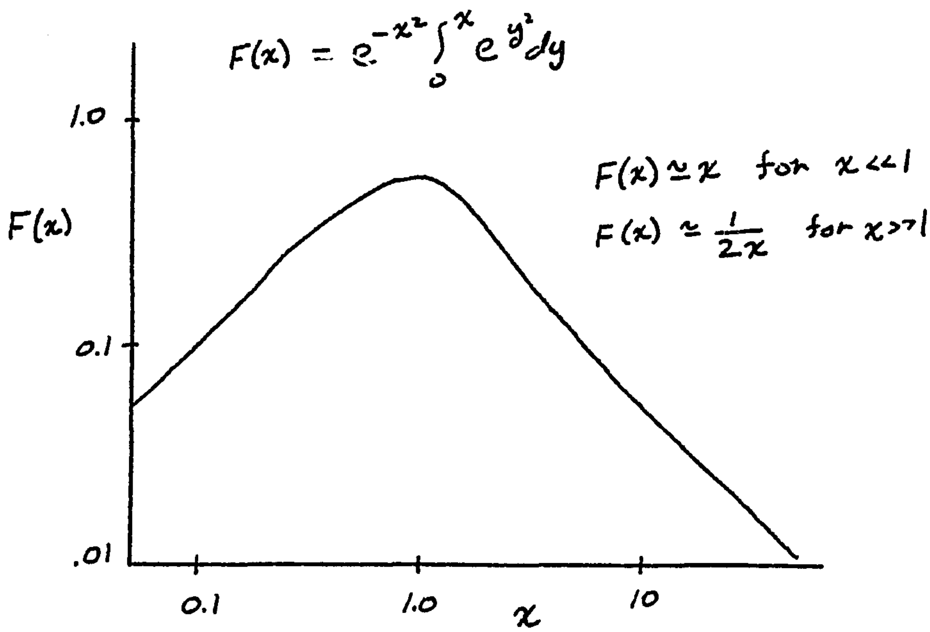

FIGURE 6-4. Dawson's Integral.

A function useful in evaluating the diverging effect of space charge (after Pierce, 1954).

A plot of r/r_o versus $k(z/r_o)$ according to (101) is called the "universal beam-spread curve" and is shown in Fig. 6-5 (Kirstein, Kino, and Waters, 1967, p. 139). The diverging effect of space charge may be assessed with the aid of F(x) or equivalently with the universal beam-spread curve.

Example. As an example we shall compare the effects of space charge in two different beams which carry the same current of 10mA. We shall calculate the distance each beam must travel for it to double in radius under space charge forces. First we consider a 10mA He^{++} beam traveling at 1.2×10^6 m/sec(25 keV). The value of k from (102) is .05. The right side of (101) is evaluated for $r/r_o = 2$ with the help of Figure 6-5.

$$\frac{r}{r_o} F\left(\left[\ln \frac{r}{r_o}\right]^{1/2}\right) = 2\, F\left(\left[\ln 2\right]^{1/2}\right)$$
$$= 1.08$$

The distance the beam travels before doubling in radius is then found from (101).

$$\frac{z}{r_o} = \frac{1.08}{.067} = 16$$

As a second example we consider a 10mA He^{+} beam traveling at 3×10^5 m/sec(1.9keV). For this beam the value of k is calculated to be 0.90. The radius doubling distance is then

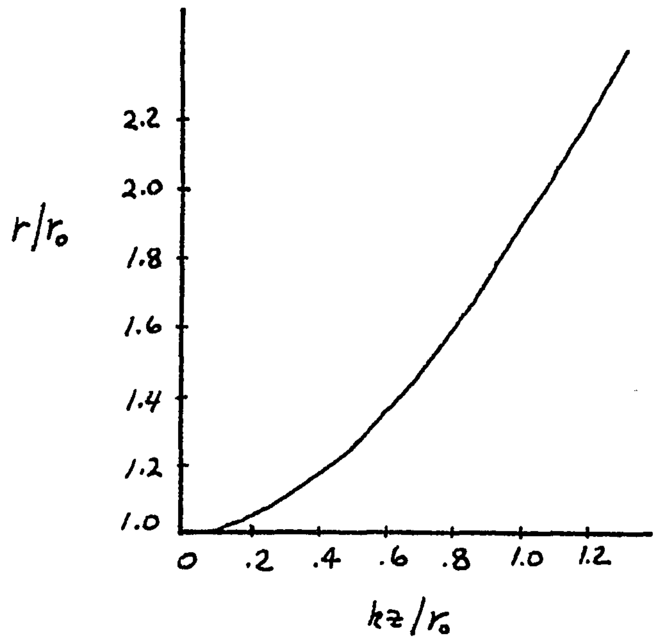

FIGURE 6-5. Universal Beam Spread Curve for Round Beams.

(after Kirstein et al. 1967).

then

$$\frac{z}{r_o} = \frac{1.08}{.90} = 1.2$$

which shows the large divergence for the lower velocity beam. The rapid expansion of the ion beam in this case indicates that space charge neutralization of the beam will be necessary.

The velocities chosen in this example for He^{++} and He^{+} correspond to maxima in the (He^{++}, H) and (He^{+}, Cs) charge transfer reactions.

Focusing Against Space Charge

We now consider the effect of space charge in focusing the hollow ion beam of Figure 6-1. We shall calculate the inward motion of a transverse section of the beam after the focusing voltage pulse intercepts it. We neglect radial thermal velocities.

While an ion is between the coaxial electrodes it experiences the electric fields due to the electrodes and the space charge of the beam:

$$E = -\left[\frac{V}{\ln \frac{b}{a}} - \frac{I(r_o)}{2\pi \epsilon_o v_z} \right] \cdot \frac{1}{r} \tag{103}$$

where r_o is the radial coordinate of the ion at the time $(t=o)$ when the focusing voltage reaches it, r is the radial coordinate at some later time t, and $I(r_o)$ is the current enclosed by $r = r_o$. We assume laminar flow so that $I(r_o)$ remains constant as the beam is focused inward.

From (103) the electric potential is found to be

$$\phi = \left[\frac{V}{\ln \frac{b}{a}} - \frac{I(r_o)}{2\pi \epsilon_o v_z} \right] \ln r + \text{const.}$$

As before we let

$$K \equiv \frac{V}{\ln b/a} \tag{104}$$

and

$$A(r_o) \equiv \frac{I(r_o)}{2\pi \epsilon_o v_z} \tag{105}$$

Now let

$$B(r_o) \equiv K - A(r_o) \tag{106}$$

so that

$$\phi = B(r_o) \ln r + \text{const.} \tag{107}$$

Equation (107) gives the potential of a particle in terms of r, its position, and r_o. its initial position.

Use (107) and energy conservation to get

$$\frac{1}{2} m \dot{r}^2 + q B(r_o) \ln r = \frac{1}{2} m \dot{r}_o^2 + q B(r_o) \ln r_o$$

We assume that $\dot{r}_o = o$, then

$$\dot{r} = -\left(2 \eta B \ln \frac{r_o}{r}\right)^{1/2} \tag{108}$$

We take the minus because we consider a particle which is moving inward. The velocity when the particle reaches the grid at $r = a$ is

$$\dot{r}_a = -\left(2 \eta B \ln \frac{r_o}{a}\right)^{1/2} \tag{109}$$

We integrate (108) to get the equation of motion

$$t = (2 \eta B)^{-1/2} \int_{r_o}^{r} \left[\ln \frac{r_o}{r}\right]^{-1/2} dr \qquad (r > a)$$

Let

$$y = \left(\ln \frac{r_o}{r}\right)^{1/2}$$

then

$$t = \frac{2r}{(2\eta B)^{1/2}} e^{\ln r_0/r} \int_0^{(\ln r_0/r)^{1/2}} e^{-y^2} dy$$

$$= \frac{2r}{(2\eta B)^{1/2}} G\left([\ln r_0/r]^{1/2} \right) \tag{110}$$

where the function G(x) is the same as defined in (8a) and plotted in Figure 6-2. In particular, the time it takes an ion starting at r_o to reach the grid at $r = a$ is given by

$$t_a = \frac{2a}{(2\eta B)^{1/2}} G\left([\ln r_0/a]^{1/2} \right) \tag{111}$$

We next consider the motion of an ion after it has passed through the grid, and the only field it sees is due to space charge. From (93), the motion is given by

$$\dot{r}^2 - 2\eta A(r_0) \ln r = \dot{r}_a^2 - 2\eta A(r_0) \ln a \tag{112}$$

for $r < a$. Where $A\ (r_o)$ is given by (105). We solve (112) to get the equation of motion,

$$\frac{dr}{dt} = -\left(\dot{r}_a^2 - 2\eta A \ln a/r \right)^{1/2} \tag{112a}$$

The integral of (112a) gives

$$t - t_a = (2\eta A)^{-1/2} \int_a^r \left(\frac{\dot{r}_a^2}{2\eta A} - \ln \frac{a}{r} \right)^{-\frac{1}{2}} dr \tag{113}$$

which can be written as

$$\begin{aligned} t - t_a = & -\frac{2r}{(2\eta A)^{1/2}} \cdot F\left(\left[\frac{\dot{r}_a^2}{2\eta A} - \ln \frac{a}{r} \right]^{1/2} \right) \\ & + \frac{2a}{(2\eta A)^{1/2}} \cdot F\left(\left[\frac{\dot{r}_a^2}{2\eta A} \right]^{1/2} \right) \end{aligned} \tag{114}$$

Where F is the function defined previously in (98). Now rewrite (114) using the expressions for t_a and $\dot{r}_a$:

$$\begin{aligned} t = & \frac{2a}{(2\eta B)^{1/2}} \cdot G\left(\left[\ln \frac{r_0}{a} \right]^{1/2} \right) + \frac{2a}{(2\eta A)^{1/2}} \cdot F\left(\left[\frac{B}{A} \ln \frac{r_0}{a} \right]^{1/2} \right) \\ & - \frac{2r}{(2\eta A)^{1/2}} \cdot F\left(\left[\frac{B}{A} \ln \frac{r_0}{a} - \ln \frac{a}{r} \right]^{1/2} \right) \end{aligned} \tag{115}$$

Equation (115) is the equation of motion for an ion after it has passed through the grid at $r = a$. The time t is measured from the time the ion first sees the voltage pulse.

The complexity of (115) does not allow an analytical solution for r as a function of t and r_o. Bear in mind that A and B are also functions of r_o.

To estimate the effects of space charge on the focusing we shall take the following approach. First we use (115) to find the time at which the inner surface of the beam just reaches $r = o$. Then we find where the outer surface of the beam is at this same time and consider this to be the focused size of the beam. If we compare this result with the focused size in the absence of space charge, we can get a feel for the importance of space charge.

Let

r_{o1} = initial radius of inner surface of beam

r_{o2} = initial radius of outer surface of beam

For convenience we define

$$x_1 \equiv \left(\ln \frac{r_{o1}}{a}\right)^{1/2} \qquad (116a)$$

$$x_2 \equiv \left(\ln \frac{r_{o2}}{a}\right)^{\frac{1}{2}} \qquad (116b)$$

We now find the time t_1 when the inner edge of the beam just reaches $r = o$.

First we note that at the inner edge of the beam there is no space-charge effect since the current enclosed by

$r = r_1$ is zero: $I(r_{10}) = 0$. This implies that $A(r_{10}) = 0$. If we try to put $A = 0$ in (115) we get an indeterminate quantity, so we must take the limit as $A \rightarrow 0$. We use the fact that

$$F(x) \simeq \frac{1}{2x} \qquad \text{for large } x.$$

Thus for small A,

$$t \simeq \frac{2a}{(2\gamma B)^{1/2}} G\left(\left[\ln \frac{r_0}{a}\right]^{\frac{1}{2}}\right) + \frac{a}{(2\gamma A)^{1/2}} \left(\frac{A}{B}\right)^{1/2} \left(\ln \frac{r_0}{a}\right)^{-\frac{1}{2}}$$

$$- \frac{r}{(2\gamma A)^{1/2}} \left(\frac{A}{B}\right)^{\frac{1}{2}} \left(\ln \frac{r_0}{a} - \frac{A}{B} \ln \frac{a}{r}\right)^{-\frac{1}{2}}$$

so that for $A \rightarrow 0$,

$$t = \frac{2a}{(2\gamma B)^{1/2}} G\left(\left[\ln \frac{r_{01}}{a}\right]^{\frac{1}{2}}\right) + \frac{a}{(2\gamma B)^{1/2}} \left(\ln \frac{r_{01}}{a}\right)^{-\frac{1}{2}}$$

$$- \frac{r_1}{(2\gamma B)^{1/2}} \left(\ln \frac{r_{01}}{a}\right)^{-\frac{1}{2}} \tag{117}$$

which is exact for the motion of the inner edge of the beam. We now evaluate (117) for $r_1 = 0$:

$$t_1 = \frac{2a}{(2\gamma B)^{1/2}} G(x_1) + \frac{a}{(2\gamma B)^{1/2}} \cdot \frac{1}{x_1} \tag{118}$$

This is the time at which the inner edge reaches $r = 0$. To find the position of the outer edge at this time, we set the right side of (118) equal to the right side of (115) evaluated at $r = r_2$, $r_o = r_{o2}$:

$$\frac{2a}{(2\eta B_1)^{1/2}} G(x_1) + \frac{a}{(2\eta B_1)^{1/2}} \cdot \frac{1}{x_1} = \frac{2a}{(2\eta B_2)^{1/2}} G(x_2) + \frac{2a}{(2\eta A_2)^{1/2}} F\left(\left(\frac{B_2}{A_2}\right)^{1/2} x_2\right) - \frac{2r_2}{(2\eta A_2)^{1/2}} F\left(\left[\frac{B_2}{A_2} x_2^2 - \ln\frac{a}{r_2}\right]^{1/2}\right) \tag{119}$$

The subscripts on A and B are reminders that they are to be evaluated at r_{o1} or r_{o2}. We want to solve (119) for r_2 which appears twice in the last term. We shall do this numerically for some particular parameters.

We rewrite (119) as

$$\frac{r_2}{a} F\left(\left[\frac{B_2}{A_2} x_2^2 - \ln\frac{a}{r_2}\right]^{1/2}\right) = \left(\frac{A_2}{B_2}\right)^{1/2} G(x_2) - \left(\frac{A_2}{B_1}\right)^{\frac{1}{2}} G(x_1) + F\left(\left(\frac{B_2}{A_2}\right)^{\frac{1}{2}} x_2\right) - \frac{1}{2}\left(\frac{A_2}{B_1}\right)^{\frac{1}{2}} \frac{1}{x_1} \tag{120}$$

From Equations (105) and (106)

$$A_1 = 0 \qquad A_2 = \frac{I}{2\pi\epsilon_0 \sigma_t}$$
$$B_1 = K - A_1 = K = \frac{V}{\ln b/a}$$
$$B_2 = K - A_2 \tag{121}$$

We define a dimensionless parameter γ which is a measure of the ratio of the focusing voltage to the space charge voltage:

$$\gamma \equiv \frac{B_1}{A_2} = \frac{V / \ln b/a}{I / 2\pi\epsilon_0 v_z} \tag{122}$$

Then

$$\frac{B_2}{A_2} = \frac{K - A_2}{A_2} = \frac{K}{A_2} - 1 = \gamma - 1 \tag{123}$$

Equation (120) can now be written as

$$\begin{aligned} \frac{r_2}{a} F\left(\left[(\gamma-1)x_2^2 - \ln \frac{a}{r_2}\right]^{1/2}\right) &= \frac{G(x_2)}{(\gamma-1)^{1/2}} + F\left([\gamma-1]^{1/2} x_2\right) \\ &\quad - \gamma^{-1/2}\left[G(x_1) + \frac{1}{2x_1}\right] \end{aligned} \tag{124}$$

We want to solve (124) for r_2 for various values of γ and x_2. In the following analysis we shall always assume that x_1 is the value from (35a) which corresponds to optimum focusing in the absence of space charge:

$$x_1 = \left(\ln \frac{r_{10}}{a} \right)^{1/2} = 0.54039 \qquad (35a)$$

From (34) the condition for optimum focusing can be expressed

$$G(x_1) + \frac{1}{2x_1} = \frac{1}{4x_1^3} = 1.5842 \qquad (125)$$

which can be used in the right side of (124).

We can rewrite (124) as

$$u\, F\left([y^2 + \ln u]^{1/2}\right) = R(\gamma, x_2) \qquad (126)$$

where

$$u \equiv r_2/a \qquad (127a)$$

$$y \equiv (\gamma-1)^{1/2} x_2 \qquad (127b)$$

$$R(\gamma, x_2) \equiv \frac{G(x_2)}{(\gamma-1)^{1/2}} + F\left([\gamma-1]^{1/2} x_2\right) - \gamma^{-1/2} \cdot 1.5842 \qquad (127c)$$

For given values of γ and x_2, (126) can be solved numerically for u as follows. First, evaluate R and y^2. Next, evaluate the left side of (126) for several trial values of u until a value of u is found which satisfies (126) to the required accuracy. The function F, Dawson's integral, can be evaluated to good accuracy (a few parts in 10^5) by linear interpolation in the table of Abramowitz and Stegun (1965, p. 319).

Next, we make an assumption which allows us to obtain an approximate analytical solution to (126). Consider the argument of F in (126) for the case when $y^2 \gg \ln u$:

$$
\begin{aligned}
(y^2 + \ln u)^{\frac{1}{2}} &= y\left(1 + \frac{\ln u}{y^2}\right)^{1/2} \\
&= y\left(1 + \frac{1}{2}\frac{\ln u}{y^2} + \ldots\right) \\
&\simeq y + \frac{\ln u}{2y}
\end{aligned}
$$

so
$$F\left([y^2 + \ln u]^{\frac{1}{2}}\right) \simeq F\left(y + \frac{\ln u}{2y}\right)$$

We can use a Taylor series expansion to obtain

$$F\left(y + \frac{\ln u}{2y}\right) = F(y) + \frac{dF}{dy}(y)\,\frac{\ln u}{2y} + \ldots$$

From the definition of F, we can show that

$$\frac{dF(y)}{dy} = 1 - 2y\,F(y)$$

$$
\begin{aligned}
\therefore\ F\left(y + \frac{\ln u}{2y}\right) &\simeq F(y) + \left[1 - 2y\,F(y)\right]\frac{\ln u}{2y} \\
&\simeq F(y)\left[1 + \frac{1 - 2y\,F(y)}{F(y)} \cdot \frac{\ln u}{2y}\right]
\end{aligned}
$$

$$F\left(y+\frac{\ln u}{2y}\right) \simeq F(y)\left[1+\ln u^{\frac{1-2yF}{2yF}}\right]$$

At this point we use the approximation that

$$1+\ln u^{x} \simeq e^{\ln u^{x}} = u^{x}$$

We use this approximation in (126) to obtain

$$F(y)\, u^{\frac{1}{2yF}} \simeq R$$

$$\therefore \quad u \simeq \left[\frac{R}{F(y)}\right]^{2yF(y)} \tag{128}$$

The right side of (128) can be numerically evaluated to yield an approximate solution for $u \equiv r_2/a$ for various values of the parameters γ and x_2. (The solution can then be checked to see how well it fits the initial assumption that $y^2 \gg \ln u$.)

Eq. (128) was used to obtain the curves shown in Fig. 6-6 which show how the dimensionless focused radius, $u = r_2/a$, becomes smaller as the parameter γ increases. Two different cases were plotted: $r_{20}/r_{10} = 1.1$ and $r_{20}/r_{10} = 1.2$. A check against the more precise numerical solution of (126) showed that at $\gamma = 5$ the plotted values of r_2/a are about 10% too low. At larger values of γ

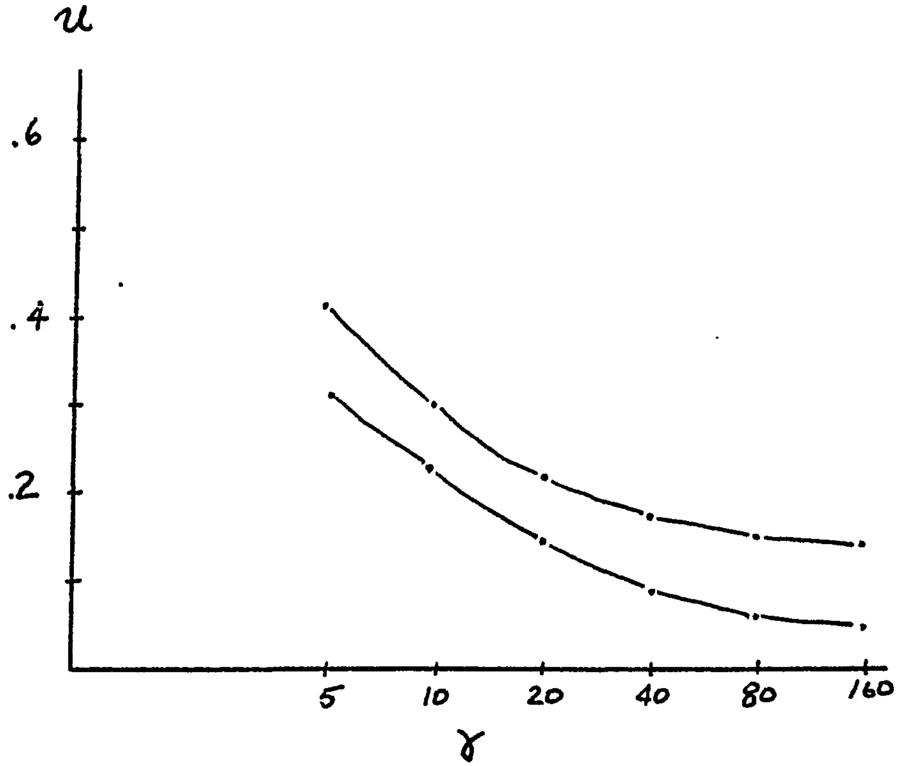

FIGURE 6-6. Unitless Beam Radius versus Focusing Parameter γ .

the difference will be even less. Consequently, these curves are a good approximation to Eq. (126) in describing the effect γ has on focusing.

Maximum Value of γ

In the previous discussion we have shown that focusing against space charge can be measured by means of the dimensionless parameter γ. As γ becomes larger, the focused radius becomes smaller. However, γ can not be made arbitrarily large and still satisfy the requirement that the ions have the particular energy required for the charge transfer reaction. We shall next show that for a particular ion energy there is a maximum value of γ consistent with this energy.

Consider the inner surface of the hollow beam. An ion at this surface will see no space charge field, so according to (10), the inward radial velocity attained due to the application of the focusing voltage V is given by

$$\dot{r}_1 = -\left(\frac{2\eta V}{\ln\frac{b}{a}}\right)^{1/2}\left(\ln\frac{r_{10}}{a}\right)^{1/2} \qquad (129)$$

The energy due to this radial motion is then

$$E_r = \frac{1}{2}m\dot{r}_1^2 = \frac{qV}{\ln\frac{b}{a}}\ln\frac{r_{10}}{a} \qquad (130)$$

The part of the ion energy due to longitudinal motion along the z-axis is given by

$$E_z = \frac{1}{2} m v_z^2 \tag{131}$$

We assume that there is no θ-component to the velocity, so the total ion energy is

$$E_t = E_r + E_z \tag{132}$$

The expressions for E_r and E_t can be used in the defining equation for γ, Eq. (122), to obtain

$$\gamma = \frac{2\pi\epsilon_0}{I}\left(\frac{2}{M}\right)^{\frac{1}{2}} \frac{E_r E_z^{1/2}}{q \ln \frac{r_{10}}{a}} \tag{133}$$

which combined with (132) can be written

$$\gamma \sim \left(E_t - E_z\right) E_z^{1/2} \tag{134}$$

From (134) we can find the value of E which maximizes γ :

$$\frac{d\gamma}{dE_z} = 0 = \frac{1}{2}\left(E_t - E_z\right)^{\frac{1}{2}} E_z^{-\frac{1}{2}} - E_z^{1/2} \tag{135}$$

Eq. (135) gives

$$E_z = \frac{1}{3} E_t \tag{136a}$$

$$\therefore \quad E_r = \frac{2}{3} E_t \tag{136b}$$

Eq. (136) shows how the total energy should be distributed in order to maximize γ and so obtain optimum focusing. We use (136) in (133) to obtain the following expression for γ_m, the maximum value of γ :

$$\gamma_m = \frac{b_0 \left[E_t\,(eV)\right]^{3/2}}{I \; M^{1/2} \, Q} \tag{137}$$

where

$$b_0 = \frac{4\pi\epsilon_0}{3} \left(\frac{2e}{3m_a}\right)^{\frac{1}{2}} \frac{1}{\ln r_0/a} \tag{138a}$$

$$= 1.017 \times 10^{-6} \;\; A - (eV)^{-3/2}$$

m_a = atomic mass unit = 1.66×10^{-27} kg

M = ion mass in a.m.u.

Q = q/e

In evaluating the constant b_0 we have used the focusing condition, Eq. (35b).

The value of γ_m given by (137) is the largest possible γ consistent with a charge transfer energy E_t. Consequently, when γ_m is used in Eq. (126), the corresponding focused radius will be the smallest possible for a particular current I.

The focused radius depends upon the beam current through γ_m. We note that there are two opposing effects which play a part in the focused current density. To obtain a large focused current density we should like to have as large a beam current as possible; but, according to (137) γ_m varies inversely with the current so that large values of I reduce γ_m and increase the focused radius. Intuitively we expect that there will be an optimum value of I which will maximize the current density at focus. We consider this next.

Maximum Focused Current Density

The focused current density is given by

$$J_f = \frac{I}{\pi r_2^2} = \frac{I}{\pi a^2 u^2} \tag{139}$$

where $u = r_2/a$. From (137)

$$I = \frac{b_o E_t^{3/2}}{\gamma_m M^{1/2} Q} \tag{140}$$

so

$$J_f = \frac{b_o E_t^{3/2}}{M^{1/2} Q \pi a^2} \cdot \frac{1}{\gamma_m u^2} \tag{141}$$

Now, u is also dependent upon γ via (126), so from (141) J_f will be a maximum with respect to γ when the quantity $\gamma^{1/2} \cdot u$ is a minimum.

The value of γ, which minimizes $\gamma_m^{1/2} \cdot u$ can be found graphically and used to calculate the corresponding beam current which maximizes the focused current density.

As an example consider a hollow beam with the ratio of outer to inner radii of $r_{20}/r_{10} = 1.1$. From the definition (116b).

$$
\begin{aligned}
x_2 &= \left(\ln \frac{r_{20}}{a}\right)^{1/2} \\
&= \left(\ln r_{20}/r_{10} + \ln r_{10}/a\right)^{1/2} \\
&= (.09531 + .29202)^{1/2} \\
&= .6224
\end{aligned}
$$

This value of x_2 is then used in (127) to compute the parameters necessary to evaluate the approximate expression (128) for various values of γ. The results are plotted in Fig. 6-7 as $\gamma^{1/2} \cdot u$ versus γ. The figure shows that $\gamma^{1/2} \cdot u$ has a minimum value of .55 near $\gamma = 50$, therefore at this value of γ

$$\frac{r_2}{a} = u \simeq \frac{.55}{\sqrt{50}} = .078 \tag{142}$$

This equation gives the focused radius for which the

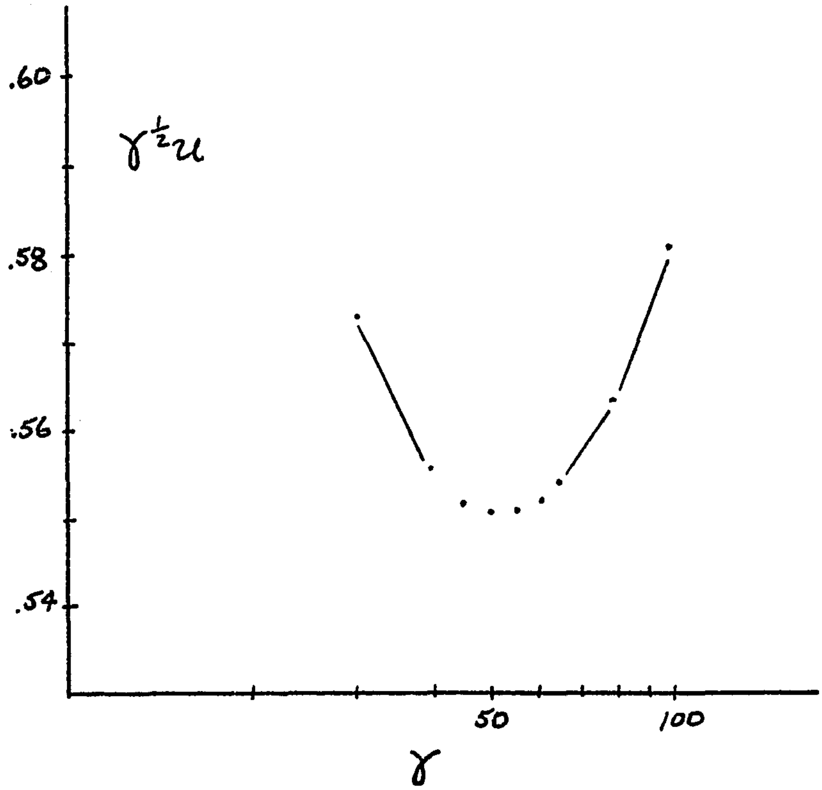

FIGURE 6-7. A Graph for Determining Minimum Value of $\gamma^{\frac{1}{2}}u$.

The ratio $r_{20}/r_{10} = 1.1$ was used.

current density is a maximum under the condition that $r_{20}/r_{10} = 1.1$. For example if a, the radius of the inner grid, is one centimeter, then the focused radius is .078 cm. The maximum current density can be calculated from (141). The current which gives this current density can be calculated from (140) in this particular case by using $\gamma_m = 50$.

In summary it is important to note that for a given ratio of r_{20}/r_{10} there is a particular value of γ, and hence I, which maximizes the focused current density. Although γ depends only upon the ratio r_{20}/r_{10}, the optimum current depends additionally upon the energy, charge, and mass of the ion.

Example. Consider the case of an He^{++} beam and a H target located along the ion beam axis. We assume the ratio of the outer-to-inner radii of the beam to be $r_{20}/r_{10} = 1.1$, so $\gamma_m \simeq 50$. From Eq. (141) we find that the focused current density in 4.2 A/cm^2. In the preceding chapter we calculated a focused current density of 0.1 A/cm^2 for a parallel-plate geometry of similar dimensions.

Harris Flow

We note in passing that Harris flow may be used to control the diverging effects of space charge in a hollow beam and may offer some advantage in forucins. A detailed analysis of focusing under Harris flow shall not be presented here, but Appendix B contains a brief description and a discussion of certain limitations.

CHAPTER 7

CALCULATED GAINS

In previous chapters we have considered two possible means of focusing a beam of ions: deflection by parallel plane electrodes, and inward compression of a hollow cylindrical beam. The analysis of Chapter 5 showed that the planar geometry was relatively ineffective for focusing against space charge, so we shall not consider this planar geometry for further analysis. The cylindrical geometry, however, provides better focusing against space charge, and we shall extend the calculations of Chapter 6 to estimate laser gains for the charge transfer reactions which were proposed in Chapter 3.

We shall assume in the following calculations that the ratio of outer to inner radii in the unfocused beam is $r_{2o}/r_{1o} = 1.1$. The notation used follows that of Chapter 6. We begin by comparing the relative sizes of the effects of focusing aberration, transverse thermal velocities, and space charge for the cylindrical focusing scheme.

Comparison of Focusing Limitations

Focusing Aberration

Eq. (6.47) gives the radius of the focused beam due to the focusing aberration inherent in the cylindrical geometry:

$$r_f = 2.46 \frac{(\delta r_o)^2}{a}$$

where δr_o is the initial radial thickness of the beam, and a is the radius of the inner cylindrical grid. Since $\delta r_o = r_{2o} - r_{1o}$, the above equation may be rewritten

$$\frac{r_f}{a} = 2.46 \left(\frac{r_{20}}{r_{10}} - 1\right)^2 \left(\frac{r_{10}}{a}\right)^2 \tag{1}$$

We take r_{2o}/r_{1o} =1.1 and use the condition (6.35c) for optimum focusing, $r_{1o}/a=1.339$, to obtain

$$\frac{r_f}{a} = .044 \tag{2}$$

for the case of aberration-limited focusing.

Thermal Limitation

From Eq. (6.89) the root-mean-squared focused radius in thermal-limited focusing is

$$\frac{\langle r_f \rangle_{RMS}}{a} = 2\frac{r_{10}}{a}\left(\ln \frac{r_{10}}{a}\right)^{\frac{1}{2}}\left(\frac{kT}{qK}\right)^{\frac{1}{2}}$$

$$= 1.447\left(\frac{kT}{qK}\right)^{\frac{1}{2}} \tag{3}$$

where we have used r_{10}/a =1.339. With the help of Eqs. (6.2), (6.130), and (6.136b), Eq. (3) can be written

$$\frac{\langle r_f \rangle_{RMS}}{a} = .9577\left(\frac{kT}{E_t}\right)^{\frac{1}{2}} \tag{4}$$

where E_t is the ion energy for optimum charge transfer, and T is the transverse temperature of the beam. If we multiply (4) by $\sqrt{2}$, we convert the root-mean-squared radius to the radius of an equivalent uniform beam:

$$\frac{r_f}{a} = 1.354\left(\frac{kT}{E_t}\right)^{1/2} \tag{5}$$

Eq. (5) gives the focused radius for the case of thermal-limited focusing. Consider the value of $E_t = 10^3$ eV which is the lowest value for those reactions listed in Table 3-3. Assume $kT = 1$ eV, then

$$r_f/a = 1.354\cdot(10^{-3})^{1/2}$$

$$= .043 \tag{6}$$

For the other reactions in Table 3-3, $\frac{r_f}{a}$ will have even smaller values.

Space Charge

From Eq. (6.142) the focused radius is given by

$$\frac{r_f}{a} = .078 \tag{7}$$

for space-charge-limited focusing of a beam with r_{20}/r_{10} =1.1. Recall that this value depended only upon the ratio r_{20}/r_{10} and represents maximization of the focused current density.

A comparison of Eqs. (2), (6), and (7) above shows that space charge is the most important limitation in focusing under the assumed conditions. Consequently, in the next section we present the results of gain calculations which consider only the effect of space charge upon focusing.

Calculated Gains for Space-charge-limited Focusing of a Hollow Beam

We have used the results of Chapter 6 to calculate gains for the charge-transfer reactions considered in Chapter 3, and the results are presented in Table 7-1. In the following discussion we explain how the values in the table were calculated.

TABLE 7-1. Linear Gains for Optimized Ion Currents

	He^{++},H	He^{+},Cs	Ne^{+},K	Ar^{+},Cs	H^{+},Cs	Hg^{+},Cs
I(mA)	20	.84	4.1	.15	.64	12.3
$J_f(A/cm^2)$	4.2	.18	.84	.032	.14	2.6
$g(cm^{-1})$	.021	.0031	.060	.0090	.0055	(60)[a]
d(cm)	26	26	183	16	468	21
e^{gd}	1.7	1.08	$6x10^4$	1.15	13.1	(a)

[a]Small signal theory is not valid.

From Eq. (6.140) the beam current which gives rise to the maximum possible focused current density is

$$I = \frac{b_o E_t^{3/2}}{\gamma_m M^{1/2} Q} \tag{8}$$

where b_o = 1.017×10^{-6} A.(eV)$^{-3/2}$

E_t = ion energy (eV) for optimum charge transfer

M = ion mass in a.m.u.

Q = (ion charge)/(electron charge)

$\gamma_m \simeq 50$, for $r_{20}/r_{10} = 1.1$

The focused current density is then given by

$$J_f = \frac{I}{\pi r_f^2} \tag{9}$$

From Eq. (7), $r_f = .078a$, so (9) becomes

$$J_f = \frac{I}{\pi a^2 (.078)^2} \tag{10}$$

We shall assume that the radius, a, of the inner grid is 0.5 cm. The beam current I and the focused current density J_f for each charge transfer reaction have been calculated according to (8) and (10). Note that the calculated currents are in the milliampere range. It is worth repeating here that these currents are optimum values calculated to yield the maximum possible focused ion current density for each particular ion beam. The linear gains (g) were calculated according to

$$g = \left(\frac{g}{J}\right) \cdot J_f \tag{11}$$

where the values of g/J were taken from Table 3-5. The lasing lengths (d) over which diffraction losses are negligible were calculated according to the usual expression

$$d = \frac{(\Delta r)^2}{\lambda}$$

which for our focusing scheme becomes

$$d \approx \frac{(v_r \tau_s)^2}{\lambda} \tag{12}$$

To calculate v_r, we have used the previously obtained relationship, $E_r = \frac{2}{3} E_t$. Finally, the factor e^{gd} is presented as the amplification factor for a lasing length equal to the diffraction length. (We note that the diffraction lengths are all approximately 20 cm or greater, so that in practice lasing lengths may be limited by ion beam and target constraints rather than by diffraction.) The large gain for the (Hg^+, Cs) reaction suggests that this reaction would be a good one for experimental trial of this lasing scheme. Obviously, the large gain in this case is not consistent with the linear theory used to obtain it.

Theoretical Limit to Focusing Under the Effect of Transverse Thermal Velocities

The gains calculated in the previous section were specific to the coaxial scheme for focusing a hollow ion beam and were based upon space-charge-limited focusing. According to the calculations in Chapter 4, the focusing of a solid cylindrical ion beam by an ideal lens is ultimately limited by the transverse temperature of the beam, since space charge can be overcome if the focal length is short enough. By using Langmuir's limiting current density we can calculate a theoretical value for the focused current density which is independent of the focusing system. From Eq. (4-69)

$$J_f = J_0 \left(1 - \frac{q\phi}{kT}\right) \sin^2\theta$$

$$\simeq J_0 \frac{E_t}{kT} \tag{13}$$

where

J_f = focused current density

J_o = current density at emitting surface

E_f = ion energy

T = transverse temperature of beam

And we have assumed $\sin^2\theta$ = 1 which is a good approximation for short focal length ($\theta \simeq \frac{\pi}{2}$). Equation (13) has been used to obtain the current densities in Table 7-2. We have assumed that $J_o = 1\ A\cdot cm^{-2}$ and $kT = 10\ eV$ which are consistent with a duoplasmatron ion source. The current densities and resulting gains presented in Table 7-2 are, consequently, the theoretical limits. Based upon the results in the table, we conclude that large gains are possible, in theory, for a solid beam and a focusing system which approaches that of an ideal lens.

Summary

In most cases considered the calculated gains are rather low for the hollow beam focusing scheme. The $Ne^+ + K$ and the $Hg^+ + Cs$ reactions are exceptions, and the high gains in these cases suggest that the focusing scheme could be tested with these reactions. On the other hand, theoretical gains calculated for the general case of emmittance-limited focusing are much higher, and realization

TABLE 7-2. Calculated Gains for Emittance-limited Focusing

	He^{++},H	He^{+},Cs	Ne^{+},K	Ar^{+},Cs	H^{+},Cs	Hg^{+},Cs
$J_f(A/cm^2)$	2500	190	930	130	100	4200
$g(cm^{-1})$	12.2	3.2	66	36	4	$9x10^4$

The values are based upon an ion source current density of one A/cm^2 and a transverse beam temperature of 10 eV.

of a practical laser depends upon being able to construct a suitable lens system to obtain sufficient current densities.

APPENDIX A

CROSS-SECTION RATIOS

During the process of near-resonant charge transfer there are, in general, several excited atomic levels into which the electron may be transferred. Only one of these levels corresponds to the upper laser level. We make the simplifying assumption that the near-resonant levels become populated statistically, i.e., each level in proportion to its number of sublevels. This assumption neglects quantum mechanical details, but there is some evidence for it in the experiments of Olson and Smith (1973). In their charge-transfer studies they found that at kinetic energies approaching 10^3eV the populations tend to be distributed statistically.

For each reaction we list the atomic levels of the captured electron which are in near-resonance with the initial neutral atom. We then calculate the fraction of the atomic states which contribute to the desired radiative transition. The notation used for atomic states is that of Moore (1949). The Grotrian diagrams of Candler (1964) were useful for determining near-resonant levels and probable transitions.

a) $He^{++} + H$:

The near-resonant levels in He II are listed below:

Configuration	Term	J
2s	^2S	$\frac{1}{2}$
2p	$^2P^o$	$\frac{1}{2}$ 3/2

The number of sublevels (states) in each level is given by $(2J + 1)$, therefore the total number of resonant states is $2 + 2 + 4 = 8$. It is the 2p configuration which decays to the ground state. The fraction of states in the 2p configuration is $6/8 = 3/4$.

Hence we estimate that

$$\frac{Q+a}{Q+o} = \frac{3}{4} .$$

b) $He^{+} + Cs$:

The near-resonant levels in HeI are:

Configuration	Term	J
1s 2s	^3S	1
1s 2s	^1S	0
1s 2p	$^3P^o$	2 1 0
1s 2p	$^1P^o$	1

The ^1P term gives the 584Å radiation. The number of ^1P states is 3. The total number of states is 3 + 1 + 5 + 3 + 1 + 3 = 16. Thus the fraction of states giving 584Å radiation is 3/16:

$$\frac{Q+a}{Q+o} = \frac{3}{16} .$$

c) $Ne^+ + K$:

The near-resonant levels of NeI are:

Configuration	Designation	J
$2p^5(^2P^o_{3/2})3s$	$3s\,[3/2]^o$	2 1
$2p^5(^2P^o_{1/2})3s$	$3s'\,[1/2]^o$	1 0

The total number of states is 5 + 3 + 1 + 3 = 12. The $3s^1[\frac{1}{2}]_1$ level consists of 3 states which give the 736Å radiation. Then

$$\frac{Q+a}{Q+o} = \frac{3}{12} .$$

d) $Ar^+ + Cs$:

The near-resonant levels of ArI are:

Configuration	Designation	J
$3p^5(^2P_{3/2}{}^o)4s$	$4s[3/2]^o$	2 1
$3p^5(^2P_{1/2}{}^o)4s$	$4s^1[1/2]^o$	0 1

The total number of states is 5 + 3 + 1 + 3 = 12. The three states of the $4s^1[\frac{1}{2}]^o{}_1$ level give the 1048Å radiation.

$$\therefore \quad \frac{Q+a}{Q+o} = \frac{3}{12} \ .$$

e) $H^+ + Cs$:

The near-resonant levels in H are:

Configuration	Term	J
2p	$^2P^o$	$\frac{1}{2}$
2s	^2S	$\frac{1}{2}$
2p	$^2P^o$	3/2

The total number of states is 2 + 2 + 4 = 8. The six $^2P^o$ states give the 1216Å radiation.

$$\frac{Q+a}{Q+o} = \frac{6}{8} \ .$$

f) $Hg^+ + Cs$:

Hg I has one near-resonant term, $6p\,^3P^o$. We assume this term to be the only one excited. Then

$$\frac{Q+a}{Q+o} = 1 .$$

APPENDIX B

HARRIS FLOW

The diverging effects of space charge in a cylindrically symmetric ion beam may be cancelled by putting the beam into Harris flow (Harris, 1952). In Harris flow a hollow cylindrical beam is set rotating by passing it through a radial magnetic field. The charge density is tailored to vary radially as r^{-4}. The beam is injected into a region which has a radial electric field produced by applying a voltage across a hollow outer cylindrical electrode and a central wire. As the beam travels axially between the electrodes, the combined effects of space charge and centrifugal forces are cancelled by the applied radial electric field.

The applied voltage necessary to sustain Harris flow is denoted by V. We define a scaled voltage K by

$$K \equiv \frac{V}{\ln (b/a)}$$

where a and b are the radii of the inner and outer electrodes, respectively. In terms of the parameters of the beam, the required value of K can be shown to be

$$K = \frac{I}{2\pi\epsilon_0 v_z \left(1 - \frac{r_{10}^2}{r_{20}^2}\right)} \tag{1}$$

where r_{10} and r_{20} are the beam's inner and outer radii. The required rotational velocity for an ion at a radius r can be shown to be

$$v_\theta = (\eta K)^{\frac{1}{2}} \frac{r_{10}}{r} \tag{2}$$

It can also be shown that if a beam is traveling in Harris flow and if an additional voltage is applied across the electrodes, then the ions will focus inward under the effect of the increased field. A detailed analysis (Seely, Louisell, and Bousek 1976) shows that the thickness of the beam decreases as the beam shrinks inward causing the ion density to increase. Eventually the inner surface of the beam reaches a minimum radius where the radial velocity slows to zero and reverses in direction. The inner surface of the beam moves outward passing through the inward-moving outer portion of the beam. At this point the ion flow ceases to be laminar, so Harris flow no longer applies. Smooth flow breaks down and the beam can be expected to diverge as a result of trajectory crossings. By placing the target atoms in the region where the compressed ion beam just reaches its minimum size, it may be possible to take advantage of the increased ion density arising from the focusing effect. The use of Harris flow has the advantage of counteracting space-charge divergence prior to the application of the focusing voltage as well as providing some focusing effect.

In calculating the applicability of Harris flow to the charge exchange scheme, we must take into account the fact that the ions in the focused beam have velocity components in both the θ and z directions. (We shall neglect the radial velocity which approaches zero at the focus.) It is the total velocity which must be matched to optimum energy for the charge-transfer reaction.

Owing to conservation of angular momentum, (2) also applies to an ion as it moves inward under the effect of the focusing voltage. Consider an ion at radius r.

By (1) and (2)

$$\left(\frac{r}{r_{10}}\right)^2 = \frac{\eta K}{v_\theta^2}$$

$$= \frac{(v_\theta^2 v_z)^{-1} \eta I}{2\pi \epsilon_0 \left(1 - \frac{r_{10}^2}{r_{20}^2}\right)} \qquad (3)$$

Equation (3) shows the relationship between the radial position of an ion and the θ-component of its velocity. Now, v_θ and v_z are related through the total velocity v so that

$$v^2 \simeq v_z^2 + v_\theta^2$$
$$\simeq v_z^2 (1-u) \tag{4}$$

where

$$u \equiv v_\theta^2 / v_z^2$$

Then

$$v_\theta^2 v_z = \frac{u v^3}{(1+u)^{3/2}} \tag{5}$$

The product $v_\theta^2 v_z$ will be maximized and r minimized at a given velocity when the parameter u equals 2, i.e., when the rotational energy is twice the longitudinal energy. Then

$$(v_\theta^2 v_z)_{max} = \frac{2}{3^{3/2}} v^3 \tag{6}$$

Using (6) in (3) we have

$$\left(\frac{r_m}{r_{10}}\right)^2 = \frac{3^{3/2} \eta I}{v^3 4\pi \epsilon_0 \left(1 - \frac{r_{10}^2}{r_{20}^2}\right)} \tag{7}$$

Equation (7) gives the minimum radius r_m an ion can move to and still have a total velocity of v or less. For example, consider an He^+ ion with a velocity of 3×10^7 cm/sec. If we assume an ion beam current of 10 mA and a ratio of $r_{20}/r_{10} = 1.2$, then by (7)

$$r_m = 1.2\ r_{10}$$

Note that this is actually <u>outside</u> of the beam. In this case, the ions in the (unfocused) beam will all initially have energies greater than the optimum energy of 1 keV. Applying a focusing voltage would further increase the ion velocities to the detriment of the charge exchange reaction.

In order for focusing of Harris flow to be usable, the velocity at which charge exchange occurs must be large enough so that r_m is less than r_{10}. For example, if v were 10^8 cm/sec, then we would have $r_m = 0.2 r_{10}$; i.e., the radius at which ion velocities would reach 10^8 cm/sec would be one-fifth of the initial inner radius. This would allow some focusing action to be used.

Next we consider the effect of transverse thermal velocities upon Harris flow.

The radial equation of motion for an ion in Harris flow can be shown to be

$$\ddot{r} = -\eta V_A \frac{r_{10}^2}{r_0^2} \cdot \frac{1}{r} + \eta V_A \frac{r_{10}^2}{r^3} \tag{8}$$

where V_A = voltage (radial) to sustain Harris flow

$$= \frac{I}{2\pi\epsilon_0 \sigma_z \left(1 - \frac{r_{10}^2}{r_{20}^2}\right)} \tag{9}$$

Equation (8) can be written,

$$\ddot{r} = -\eta V_A \frac{r_{10}^2}{r_0^2} \left(\frac{1}{r} - \frac{r_0^2}{r^3} \right) \tag{10}$$

Consider a small displacement from the equilibrium position r_o such that

$$r = r_0 (1 + \delta) \qquad (\delta \ll 1) \tag{11}$$

Then

$$\ddot{r} = -\eta V_A \frac{r_{10}^2}{r_0} \left[\frac{1}{1+\delta} - \frac{1}{(1+\delta)^3} \right]$$

$$\simeq -\eta V_A \frac{r_{10}^2}{r_0} \left(1 - \delta \ldots - 1 + 3\delta \ldots \right) \tag{12}$$

From (11)

$$\ddot{r} = r_0 \ddot{\delta}$$

$$\therefore \quad r_0 \ddot{\delta} \simeq -2\eta V_A \frac{r_{10}^2}{r_0^3} \delta$$

and

$$\ddot{\delta} \simeq -2\eta V_A \frac{r_{10}^2}{r_0^4} \delta \qquad (12a)$$

From (12a) we see that small displacements give rise to simple harmonic motion to a first approximation; i.e., the ion trajectory is a stable one.

The frequency of oscillation from (12a) is obviously,

$$\omega = (2\eta V_A)^{1/2} \frac{r_{10}}{r_0^2}$$

The solution to (12a) is

$$\delta = \frac{\dot{\delta}_0}{\omega} \sin\omega t + \delta_0 \cos\omega t$$

Furthermore,

$$r = r_o (1+\delta) \Rightarrow \delta_o = 0$$

and

$$\dot{\delta}_o = \frac{\dot{r}_o}{r_o} \tag{13}$$

Finally

$$\delta = \frac{\dot{r}_o}{r_o} \cdot \frac{1}{\omega} \sin \omega t \tag{14}$$

The amplitude of the oscillation in (14) is then

$$\delta_m = \frac{\dot{r}_o}{r_o} \cdot \frac{1}{\omega} \tag{15}$$

which depends linearly upon the initial particle velocity $\dot{r}_o$. The maximum radial displacement Δr_m is given by

$$\Delta r_m \equiv r_m - r_o = r_o \delta_m \qquad \text{via (11).}$$

$$\therefore \quad \Delta r_m = \frac{\dot{r}_o}{\omega} \tag{16}$$

Example. Assume a He^+ beam with the following parameters:

$$I = 10^{-2}\ A$$

$$v_z = 10^5\ m/sec$$

$$\left(\frac{r_{10}}{r_{20}}\right)^2 = \left(\frac{1}{1.1}\right)^2 = .826$$

$$r_{10} = 1\ cm$$

By (9)

$$V_A = 1.03 \times 10^4\ volts$$

Then

$$\omega = \frac{(2\eta V_A)^{1/2}}{r_{10}} \cdot \left(\frac{r_{10}}{r_o}\right)^2 \tag{17}$$

Note that ω depends upon the ion's initial position r_o. For now we assume a thin radial thickness so that $r_{10} \simeq r_o$. Then

$$\omega \simeq \frac{(2\eta V_A)^{1/2}}{r_{10}}$$

$$\simeq 7 \times 10^7\ sec^{-1} \quad (He^+)\ \text{ions}$$

$$f = \frac{\omega}{2\pi} \simeq 10^7\ Hz$$

The time it takes an He^+ ion to travel 10 cm in the z-direction is 10^{-6} sec. Therefore during this time it oscillates through ten periods.

Now consider the frequencies for ions starting at r_{10} and r_{20} which we denote by ω_1 and ω_2. From (17)

$$\frac{\omega_1}{\omega_2} = \left(\frac{r_{20}}{r_{10}}\right)^2$$

$$= 1.21 \qquad \text{in our example.}$$

Note that if $r_{20} = \sqrt{2}\, r_{10}$, the ions at r_{10} will oscillate twice as fast as the ions at r_{20}.

We now consider the amplitude Δr_m of the radial oscillations given by (16). We consider that at each point in the beam there is a Maxwellian spread in velocities. We recall that the equations of motion under Harris flow assume a laminar flow. This means that the radial oscillations must be small compared to the thickness of the beam. Otherwise, an ion's trajectory will not always enclose a constant beam current. The larger the radial oscillation, the more trajectory-crossing will occur.

We shall assume that

$$\dot{r}_0 = \left(\frac{2kT}{m}\right)^{1/2}$$

i.e., we consider the Maxwellian RMS radial velocity. Then (16) becomes

$$\Delta r_m = \left(\frac{kT}{q V_A}\right)^{1/2} \frac{r_0^2}{r_{10}} \tag{18}$$

We now assume

$$kT = 10\,eV$$
$$q V_A = 10^4\,eV$$
$$r_0 \simeq r_{10}$$
$$r_{10} = 1\,cm$$

Then

$$\Delta r_m = (10^{-3})^{1/2}$$
$$= .03\,cm \tag{19}$$

is the amplitude of oscillation.

Equation (19) gives the oscillation amplitude which corresponds to an RMS thermal velocity of 10eV. Some ions will have larger oscillations, some will have smaller. For the laminar flow approximation to hold, the oscillation must be much smaller than the beam thickness. If the beam thickness is 0.1 cm or so, an amplitude of .03 cm may be too large to be consistent with the laminar theory. From (18) we note that the amplitude Δr_m can be made smaller by increasing V_A. To see if this is possible we use (9) in (18) to get the explicit dependence upon r_{10} and r_{20}:

$$\Delta r_m = \left(\frac{2\pi\epsilon_0 \sigma_z kT}{8I}\right)^{1/2}\left(1 - \frac{r_{10}}{r_{20}}\right)^{\frac{1}{2}} \frac{r_0^2}{r_{10}^2}\, r_{10} \tag{20}$$

From (20) we see that Δr_m will be largest for $r_o = r_{o2}$. We calculate Δr_m for $r_o = r_{o2}$.

First define

$$\alpha \equiv \frac{r_{20}}{r_{10}} \tag{21}$$

$$C \equiv \left(\frac{2\pi\epsilon_0 \sigma_z kT}{8I}\right)^{\frac{1}{2}} \tag{22}$$

Then for $r_o = r_{20}$,

$$\Delta r_m = C\left(1 - \frac{1}{\alpha^2}\right)^{\frac{1}{2}} \alpha^2 r_{10} \tag{23}$$

or

$$\Delta r_m = C\left(\alpha^2 - 1\right)^{1/2} \alpha\, r_{10} \tag{24}$$

We want Δr_m to be small compared to the beam thickness

$$r_{20} - r_{10} = \alpha r_{10} - r_{10}$$

$$= r_{10}(\alpha - 1) \tag{25}$$

From (24) and (25) we can write

$$\frac{\Delta r_m}{r_{20} - r_{10}} = C\,(\alpha^2 - 1)^{1/2}\,\frac{\alpha}{\alpha - 1}$$

$$= C\,\alpha\left(\frac{\alpha + 1}{\alpha - 1}\right)^{1/2} \tag{26}$$

The right side of (26) must be much less than unity in order for the laminar flow approximation to be valid.

We now calculate C for

$$v_z = 10^5 \text{ m/sec}$$
$$kT = 10 \text{ eV}$$
$$q = e$$
$$I = 10^{-2} \text{ A}$$

$$C = \left(\frac{4\pi\epsilon_0}{2} \cdot \frac{v_z kT}{qI}\right)^{1/2} \tag{27}$$

$$= .075 \tag{28}$$

If we denote the function of α in (26) by

$$f(\alpha) \equiv \left(\frac{\alpha+1}{\alpha-1}\right)^{1/2} \alpha \tag{29}$$

Then for $\alpha = 1.1$

$$f(1.1) = 5.05$$

$$\therefore \quad \frac{\Delta r_m}{r_{20} - r_{10}} = .38 \tag{30}$$

which is not $\ll 1$.

We can make $\Delta r_m/(r_{20}-r_{10})$ smaller by increasing the current as (27) shows, but it takes a large increase in I due to the square root dependence.

Another possibility is to minimize $f(\alpha)$ with respect to α. From (29) we find that it does have a minimum at $\alpha = 1.62$. This minimum value is

$$f(1.62) = 3.33 \tag{31}$$

which is not very much smaller than $f(1.1) = 5.05$.

The point here is that the value of $\Delta r_m(r_{20}-r_{10})^{-1}$ can be made very small only by adjusting the parameter C given by (27). Adjusting α has but a small effect.

The results of the analysis show that the presense of a small radial component in the velocity of an ion in

Harris flow introduces radial oscillations in the ion's trajectory. The frequency of the oscillation depends upon the ion's position in the beam while the amplitude depends both upon position and initial radial velocity. Thus, for a Maxwellian distribution, ions at the same radial position will oscillate with the same frequency but with amplitudes depending upon their initial radial velocities. The assumption of laminar flow depends upon oscillations which are small compared to the radial thickness of the beam. This criterion must be examined for a given beam to assure its applicability.

APPENDIX C

ADDITIONAL BIBLIOGRAPHICAL SOURCES

ARPA/NRL X-Ray Laser Program - Semiannual Technical Report to Defense Advanced Research Projects Agency - July 1975 to 31 December 1975, NRL Memorandum Report 3241, Naval Research Laboratory, Washington, D. C., March (1975).

Bex, L., P. Bernard, and C. E. N. Saclay, "Ionization Phenomenona Inside a Duoplasmatron Expansion Cup," Electron and Ion Beam Science and Technology - Fourth International Conference, R. A. Bakish, ed. (Electrochemical Society, New York (1970).

Cantrell, C. D., and M. O. Scully, "Review of Soft X-Ray Lasers using Charge Exchange," in Progress in Lasers and Laser Fusion, A. Perlmutter and S. M. Widmayer, eds., Plenum Press, New York (1975).

Cook, E. J., "Axially Symmetric Electron Beams of Uniform Axial Velocity," J. Appl. Phys. 30, 860 (1959).

Cook, E. J., "Tangential Magnetic Field Immersion of a Hollow Beam Electron Gun," IRE Transactions on Electron Devices ED-8, 140 (1961).

Coupland, J. R., T. S. Green, D. P. Hammond, and A. C. Riviere, "A Study of the Ion Beam Intensity and Divergence Obtained from a Single Aperture Three Electrode Extraction System," Rev. Sci. Instrum. 44, 1258 (1973).

Crumly, C. B., "A UHF Traveling-wave Amplifier Tube Employing and Electrostatically Focused Hollow Beam," IRE Transactions on Electron Devices ED-3, 62 (1956).

Davis, R. C., O. B. Morgan, L. D. Stewart, and W. L. Stirling, "A Multiampere Duo PIG atron Ion Source," Rev. Sci. Instrum. 43, 278 (1972).

El-Kareh, A. B., and J.C.J. El-Kareh, Electron Beams, Lenses, and Optics, Academic Press, N. Y. (1970)

Emigh, C. R., "Statistical Beam Transport for High Intensity Ion Current," IEEE Proceedings of the 1972 Proton Linear Accelerator Conference, p. 182 (1972).

Gautherin, C. Tejeume, and A. Septier, "Characteristic Properties of Duoplasmatron-type Ion Sources and of Extracted Beams," Electron and Ion Beam Science and Technology - Third International Conference, R. A. Brakish, ed. Electrochemical Society, N. Y. (1968).

Humpheries, S., J. J. Lee, and R. N. Sudan, "Generation of Intense Pulsed Ion Beams," Appl. Phys. Lett. 25, 20 (1974).

Kyhl, R. L., and H. F. Webster, "Breakup of Hollow Cylindrical Electron Beams," IRE Transactions on Electron Devices ED-3 172 (1956).

Lichtenberg, A. J., Phase-Space Dynamics of Particles, Wiley and Sons, N. Y. (1969).

Linder, E. G., and K. G. Hernqvist, "Space Charge Effects in Electron Beams and Their Reduction by Positive Ion Trapping," J. Appl. Phys. 21, 1088 (1950).

Morgan, O. B., G. G. Kelly, and R. C. Davis, "Technology of Intense DC Ion Beams," Rev. Sci. Instrum. 38, 467 (1967).

Okamoto, Y., and H. Tamagawa, "Production of Large Area High Current Ion Beams," Rev. Sci. Instrum. 43, 1193 (1972).

Steffen, K. G., High Energy Beam Optics, Interscience, N.Y. (1965).

LIST OF REFERENCES

Abramowitz, M., and I. A. Stegun, ed., Handbook of Mathematical Functions, Dover Publications, New York (1965)

Allen, C. W., Astrophysical Quantities, Oxford U. Press, New York, 2nd ed. (1963).

Bonifacio, R., F. A. Hopf, P. Meystre, and M. O. Scully, Phys. Rev. A 12, 2568 (1975).

Brewer, G. R., Ion Propulsion Technology and Applications, Gordon and Breach, New York (1970).

Candler, A. C., Atomic Spectra and the Vector Model, Van Nostrand, Princeton, 2nd ed. (1964).

Harris, L. A., Proc. IRE 40, 700 (1952).

Heitler, W., The Quantum Theory of Radiation, Oxford Univ. Press, London, 3rd ed. (1954).

Hopf, F. A., and P. Meystre, Phys. Rev. A 12, 2534 (1975).

Hopf, F. A., P. Meystre, and D. W. McLaughlin, Phys. Rev. 13A, 777 (1976).

Hopf, F. A., P. Meystre, M. O. Scully, and J. F. Seely, Phys. Rev. Lett. 35, 511 (1975).

Kirstein, P., G. Kino, and W. Waters, Space Charge Flow McGraw-Hill, New York (1967).

Louisell, W. H., M. O. Scully, and W. B. McKnight, Phys. Rev. A 11, 989 (1975).

McCorkle, R. A., Phys. Rev. Lett. 29, 982 (1972).

Montmagnon, J. L., H. DePalmas, J. P. Grouard, P. Lefebvre, and E. Mercier, Phys. Lett. 46A, 227 (1973).

Moore, C. E., Atomic Energy Levels, U.S. Government Printing Office, Washington, D.C. (1949).

Olson, R. E., and F. T. Smith, Phys. Rev. A 7, 1529 (1973).

Perel, J., and H. L. Daley, Phys. Rev. A 4, 162 (1971).

Peterson, J. R., and D. C. Lorents, Phys. Rev. 182, 152 (1969).

Pierce, J. R., Theory and Design of Electron Beams, D. Van Nostrand, New York, 2nd ed. (1954).

Salop, A., D. C. Lorents, and J. R. Peterson, J. Chem. Phys. 54, 1187 (1971).

Sargent, M., M. O. Scully, and W. E. Lamb, Jr., Laser Physics Addison-Wesley, Reading, PA (1974).

Schlacter, A. S., D. H. Lloyd, P. J. Bjorkholm, L. W. Anderson, and W. Haeberli, Phys. Rev. 174, 201 (1968).

Scully, M. O., W. H. Louisell, and W. B. McKnight, Opt. Commun. 9, 246 (1973).

Seely, J. F., Research Assoc., Univ. of So. Calif., private communication (1974).

Seely, J. F., Research Assoc., Univ. of So. Calif., "Hg (1849A) Laser," unpublished.

Seely, J. F., W. H. Louisell, and R. R. Bousek, "Coaxial Sweep Scheme for Ion-beam Lasers," IEEE J. Quantum Electron. QE-12, 515 (1976).

Septier, A., ed., Focusing of Charged Particles, Vol. II Academic Press, New York (1967).

Terrill, H. M., and L. Sweeny, J. Franklin Inst. 238, 220 (1944).

Van Steenbergen, A., IEEE Trans. Nucl. Sci., 746 (1965).

Wiese, W. L., M. W. Smith, and B. M. Glennon, Atomic Transition Probabilities, U. S. Government Printing Office, Washington, D. C. (1966).

Wilson, R. G., and G. R. Brewer, Ion Beams (with Applications to Ion Implantation), John Wiley and Sons, New York (1973).